

**THE INVESTIGATION OF ANTICANCER  
PROPERTIES OF (R)-4'-METHYLKLAVUZON IN  
LIVER CANCER CELLS AND LIVER CANCER  
STEM CELLS**

**A Thesis Submitted to  
The Graduate School of Engineering and Sciences of  
İzmir Institute of Technology  
in Partial Fulfillment of the Requirements for the Degree of**

**DOCTOR OF PHILOSOPHY**

**in Bioengineering**

**by  
Murat DELMAN**

**December 2017  
İZMİR**

We approve the thesis of **Murat DELMAN**

**Examining Committee Members:**

---

**Prof. Dr. Ali ÇAĞIR**

Department of Chemistry, İzmir Institute of Technology

---

**Prof. Dr. Neşe ATABEY**

Department of Medical Biology, Dokuz Eylül University

---

**Assist. Prof. Dr. Özden YALÇIN ÖZUYSAL**

Department of Molecular Biology and Genetics, İzmir Institute of Technology

---

**Assist. Prof. Dr. Gülistan MEŞE ÖZÇİVİCİ**

Department of Molecular Biology and Genetics, İzmir Institute of Technology

---

**Prof. Dr. Kemal Sami KORKMAZ**

Department of Bioengineering, Ege University

**28 December 2017**

---

**Prof. Dr. Ali ÇAĞIR**

Supervisor, Department of Chemistry,  
İzmir Institute of Technology

---

**Prof. Dr. Esra ERDAL**

Co-advisor, Department of Medical  
Biology, Dokuz Eylül University

---

**Assoc. Prof. Dr. Engin ÖZÇİVİCİ**

Head of Department of Biotechnology  
and Bioengineering

---

**Prof. Dr. Aysun SOFUOĞLU**

Dean of the Graduate School of  
Engineering and Sciences

## ACKNOWLEDGMENTS

First of all, I would like to express my deepest regards and thanks to my supervisor Prof. Dr. Ali ÇAĞIR for his professional guidance, endless patience and encouragement during writing my dissertation and his humanity during my tough times. He always allowed me to show my degree of freedom in my scientific and social area without any force. I extremely appreciate and take his perception of respect to me and all individuals as an example. I enriched my thesis through his respect and knowledge.

I, sincerely would like to thank Prof. Dr. Esra ERDAL for accepting to be my co-advisor and for providing me her research facility and materials. I appreciate Prof. Dr. Neşe ATABEY and Assist. Prof. Dr. Özden YALÇIN ÖZUYSAL for participating as a committee member and for reviewing my work.

I am thankful to Dane RUSCUKLU, Özgür YILMAZER, Evrim BALCI and Yekta GÜNAY OĞUZ at Biotechnology and Bioengineering Application and Research Center for their help and tolerance during my experiments.

I was very lucky to study with incredible people who helped me during my impossibilities and incompetence. Firstly, I am grateful to Burcu ALAÇAM, İsmail AKÇOK, Derya BOSTANBAŞ, Tuğçe KANBUR, Meltem KUTLUER, Fikrican DİLEK for being my colleague throughout my doctoral studies. I would like to express my deepest fidelity to Sanem TERCAN AVCI, Eren ŞAHİN, Soheil AKBARİ, Özge TÜNCEL, Eylem KURULGAN, Cenk DAĞLIOĞLU, Melda GÜRAY, Süleyman Can ÖZTÜRK, Elvan ÖZTÜRK for their scientific help and motivation.

I would like to express my sincere thanks to my beloved friends who I met spontaneously in my life. Ayça ZEYBEK was always next to me during my doctoral period and tough times. Gizem BOR motivated me when I was despaired without getting bored. All these people taught me to see the life through a different perspective.

I would like to thank to The Scientific and Technological Research Council of Turkey (TUBITAK) (113S464) and Izmir Institute of Technology Scientific Research Project, (BAP-2015IYTE04) for financial support of my thesis.

I want to express my thankfulness to TÜBİTAK for supporting my thesis TÜBİTAK-BİDEB (2211-C) for supporting my graduate study with a scholarship.

Finally I dedicate this thesis to my dear family, Halime and Hikmet DELMAN.

## ABSTRACT

### THE INVESTIGATION OF ANTICANCER PROPERTIES OF (*R*)-4'-METHYLKLAUZON IN LIVER CANCER CELLS AND LIVER CANCER STEM CELLS

Hepatocellular carcinoma (HCC) is the fifth most seen cancer type and the third leading cause of death from cancers. HCC is a fatal disease and HCC patients have a 5-year survival rate of 14%. Discovery and identification of mechanisms of action for new therapeutic agents are required for a better treatment of HCC. One of the most important target in cancer treatment is the epigenetic acetylation of histones. Histone deacetylases (HDAC) and sirtuins provide chromatin compaction and transcriptional repression by removing acetyl groups from histone proteins and non-histone proteins. Re-acetylation of chromatin and re-expression of tumor suppressor genes with the discovery of novel HDAC and/or sirtuin inhibitors are therapeutic targets in cancer research.

In this study, (*R*)-4'-methylklavuzon was found to be cytotoxic in HuH-7 cells with  $IC_{50}$  values of 1.25  $\mu$ M for HuH-7 parental cells, 2.5  $\mu$ M for EpCAM<sup>+</sup>/CD133<sup>+</sup> HuH-7 cells and 1.25  $\mu$ M for EpCAM<sup>-</sup>/CD133<sup>-</sup> HuH-7 cells. It was observed that (*R*)-4'-methylklavuzon causes cell cycle arrest at G1 phase at 1.00  $\mu$ M concentration in three cell populations, it induces apoptosis at 10  $\mu$ M concentration at the end of 24 hours incubation. (*R*)-4'-methylklavuzon does not inhibit Class I/II HDACs in vitro whereas it causes inhibition of endogenous HDACs and/or sirtuins inside the cells sorted by MACS and FACS at 0.10  $\mu$ M concentration. (*R*)-4'-methylklavuzon upregulates p21 expression significantly in HuH-7 cell populations to cause G1 arrest. It causes 45% inhibition in p53/MDM2 complex formation when examined with pure p53 and MDM2 proteins. Drug candidate causes 46% SIRT1 inhibition at 100  $\mu$ M concentration in vitro whereas there was no inhibition of HDAC1 enzyme at the same concentration. SIRT1 protein levels in HuH-7 parental cells were upregulated to 240% within 24 hours of incubation with 3.00  $\mu$ M of drug candidate. It was found that (*R*)-4'-methylklavuzon can also inhibit CRM1 protein providing increased retention of tumor suppressor proteins in the nucleus. p53 was overexpressed at 0.10 and 1.00  $\mu$ M concentrations within 6 and 24 hours in HepG2 cells but slightly overexpressed in HuH-7 parental cells.

## ÖZET

### (R)-4'-METİLKLAUZON'UN KARACİĞER KANSER HÜCRELERİ VE KARACİĞER KANSER KÖK HÜCRELERİ ÜZERİNDEKİ ANTI-KANSER ÖZELLİKLERİNİN İNCELENMESİ

Hepatoselüler karsinoma (HSK) beşinci en yaygın kanser türü olup kanser nedeniyle ölümlerin üçüncü en yüksek nedenidir. HSK ölümcül bir hastalık olup HSK hastalarının 5 yıllık yaşam süreleri %14'tür. Yeni terapötik ajanların keşfi HSK tedavisi için gerekmektedir. Kanser tedavisinde en önemli hedeflerden birisi histonların asetilasyonudur. Histon deasetilazlar (HDAS) ve sirtuinler asetil gruplarını histon proteinlerinden uzaklaştırarak kromatin sıkılaşmasına ve transkripsiyonel represyona sebep olurlar. Yeni HDAS/sirtuin inhibitörleri ile kromatinin tekrar asetillenerek tümör baskılayıcı genlerin tekrar eksprese edilmesi terapötik hedeflerdendir.

Bu çalışmada, (R)-4'-metilklavuzon'un HuH-7 parental hücreleri için 1.25  $\mu$ M, EpCAM<sup>+</sup>/CD133<sup>+</sup> HuH-7 hücreleri için 2,5  $\mu$ M; EpCAM<sup>-</sup>/CD133<sup>-</sup> HuH-7 hücreleri için 1.25  $\mu$ M olan IC<sub>50</sub> değerleri ile sitotoksik olduğu bulunmuştur. (R)-4'-metilklavuzon'un üç hücre popülasyonunda 1,00  $\mu$ M konsantrasyonda G1 fazında hücre döngüsünde birikmeye sebep olduğu ve 24 saatlik inkübasyonda 10  $\mu$ M konsantrasyonda apoptozu indüklediği gözlemlenmiştir. (R)-4'-metilklavuzon'un in vitro koşullarda sınıf I/II histon deasetilaz enzimlerini inhibe etmediği ancak MACS ve FACS ile ayrılmış hücrelerdeki endojen sınıf I/II histon deasetilazları ve/veya sirtuinleri 0,10  $\mu$ M konsantrasyonda hücre içinde inhibe ettiği bulunmuştur. (R)-4'-metilklavuzon, HuH-7 hücrelerinde p21 ekspresyonunu 3,3 kata kadar arttırabilmiştir. p53/MDM2 kompleks oluşumunu %45 oranında azalttığı görülmüştür. In vitro koşullarda SIRT1 enziminin 100  $\mu$ M ilaç adayı ile %46 oranında inhibe olduğu bulunmuştur. HuH-7 hücrelerindeki SIRT1 protein seviyelerinin 3,00  $\mu$ M ilaç adayı ile 24 saatlik inkübasyonunda %240 oranında artmıştır. (R)-4'-metilklavuzon'un CRM1 proteinini inhibe ederek tümör baskılayıcı proteinleri nukleus içinde tutabileceği anlaşılmıştır. 0,10  $\mu$ M ve 1,00  $\mu$ M ilaç adayı ile 6 ve 24 saat muamele edilen hücrelerdeki p53 protein seviyelerinin HepG2 hücrelerinde yüksek miktarda artış gösterdiği ancak HuH-7 hücrelerinde çok az bir artış gösterdiği bulunmuştur.

*for the salvation of 'persona' imprisoned in my mind...*

# TABLE OF CONTENTS

LIST OF FIGURES .....	xi
LIST OF TABLES .....	xvi
CHAPTER 1. INTRODUCTION .....	1
1.1. Hepatocellular Carcinoma (HCC).....	1
1.2. Cancer Stem Cells (CSCs) .....	1
1.3. Role of Cancer Stem Cells in Hepatocellular Carcinoma.....	2
1.4. Histone Deacetylases (HDACs).....	2
1.5. Role of Histone Deacetylases in Hepatocellular Carcinoma .....	3
1.6. Histone Deacetylase Inhibitors (HDACIs) .....	3
1.7. Sirtuins .....	4
1.8. Sirtuins and Cancer Stem Cells.....	6
1.8.1. Role of Sirtuins in Stem Cells.....	6
1.8.1.1. Embryonic Stem Cells and Development .....	6
1.8.1.2. Hematopoietic Stem Cells (HSCs).....	7
1.8.2. Cell Differentiation .....	7
1.8.3. Sirtuins in Stem Cell Signaling Pathways.....	8
1.8.3.1. Hedgehog Pathway.....	9
1.8.3.2. Wnt/ $\beta$ -catenin Pathway .....	9
1.8.4. Sirtuins and Cancer Stem Cells.....	10
1.8.5. Epithelial–Mesenchymal Transition (EMT) .....	11
1.9. SIRT1 .....	12
1.10. SIRT1 and Hepatocellular Carcinoma .....	13
1.10.1. Role of SIRT1 in Normal Liver Cells .....	13
1.10.2. Role of SIRT1 in Hepatocellular Carcinoma .....	13
1.10.2.1. SIRT1 Expression in Hepatocellular Carcinoma.....	13
1.10.2.2. Effect of SIRT1 on HCC Tumorigenesis.....	14
1.10.2.3. Effect of SIRT1 on Irradiation Resistance of Hepatoma Cells and Chemotherapy .....	15
1.10.2.4. Downstream Targets.....	15

1.10.2.4.1. p53.....	15
1.10.2.4.2. PTEN/PI3K/AKT.....	16
1.10.2.4.3. c-Myc.....	16
1.11. Contradiction on the Oncogenic Role of SIRT1 in HCC.....	17
1.12. Sirtuin Inhibitors.....	18
1.12.1. Selisistat.....	18
1.12.2. Nicotinamide and Its Analogs.....	18
1.12.3. Hydroxynaphthaldehyde Derivatives.....	18
1.12.4. Kinase Inhibitors.....	19
1.12.5. Sirtuin Rearranging Ligands (SirReals).....	19
1.12.6. Structural Diverse Sirtuin Inhibitors.....	19
1.13. Sirtuins as Therapeutic Targets for Cancer Stem Cells.....	20
1.14. p21 and p27 Cell Cycle Inhibitors.....	20
1.15. p53 and MDM2 Pathway.....	21
1.16. p53 and SIRT1.....	24
1.17. CRM1 and p53.....	27
1.18. ( <i>R</i> )-4'-methylklavuzon.....	30
1.19. The Aim of the Study.....	31
CHAPTER 2. MATERIALS AND METHODS.....	32
2.1. Cell Culture.....	32
2.2. Isolation of Cancer Stem Cells by Magnetic Cell Separation (MACS).....	32
2.3. Cell Viability Assay.....	33
2.4. Cell Cycle Analysis.....	34
2.5. Apoptosis Analysis.....	34
2.6. Cell Viability Assay of ( <i>R</i> )-4'-methylklavuzon Derivatives.....	35
2.7. In vitro Histone Deacetylase Enzyme Activity Measurement.....	35
2.8. Cell-based Histone Deacetylase Enzyme Activity Measurement using Cells Sorted by MACS.....	36
2.9. Isolation of Cancer Stem Cells by Fluorescence-Activated Cell Sorting (FACS).....	37



2.10. Cell-based Histone Deacetylase Enzyme Activity Measurement using Cells Sorted by (FACS) .....	37
2.11. In vitro HDAC1 Enzyme Activity Measurement .....	38
2.12. Histone Extraction and Acetylation and Methylation Analysis of H3K27 Residue by Western Blotting .....	39
2.13. In vitro SIRT1 Enzyme Activity Measurement .....	41
2.14. Quantification of Intracellular SIRT1 Levels by ELISA .....	42
2.15. Determination of p21 and p27 Expressions by qPCR .....	43
2.16. Immunofluorescence Visualization of R1OK2 Protein Localization in HepG2 and HuH-7 Cells .....	45
2.17. Immunofluorescence Visualization of p53 Protein Levels in HepG2 and HuH-7 Cells .....	46
2.18. Propidium Iodide Staining of HepG2 Cell Spheroids.....	47
2.19. Immunofluorescence Visualization of p53 Protein Levels in HepG2 Cell Spheroids.....	47
2.20. Colorimetric Determination of p53/MDM2 Complex Inhibition by ELISA .....	48
2.21. Spheroid Assay Based on Matrigel.....	49
2.22. Statistical Analysis.....	50
CHAPTER 3. RESULTS .....	51
3.1. ( <i>R</i> )-4'-methylklavuzon Inhibits Proliferation of HuH-7 Cell Populations.....	51
3.2. ( <i>R</i> )-4'-methylklavuzon Increases G1 Phase.....	53
3.3. ( <i>R</i> )-4'-methylklavuzon Induces Apoptosis .....	54
3.4. Cytotoxic Activity of ( <i>R</i> )-4'-methylklavuzon Derivatives on MIA-PaCa2 and HPDEC Cells.....	55
3.5. ( <i>R</i> )-4'-methylklavuzon Has No Inhibitory Effects on Class I/II Histone Deacetylase Enzyme Activity In Vitro.....	56
3.6. ( <i>R</i> )-4'-methylklavuzon Inhibits Endogenous Sirtuin and/or Class I/II Histone Deacetylase Enzyme Activity in HuH-7 Cell Populations Sorted by MACS.....	57

3.7. ( <i>R</i> )-4'-methylklavuzon Inhibits Endogenous Sirtuin and/or Class I/II Histone Deacetylase Enzyme Activity in HuH-7 Parental Cells and EpCAM <sup>+</sup> /CD133 <sup>+</sup> HuH-7 Cells Sorted by FACS .....	59
3.8. In vitro HDAC1 Enzyme Activity Measurement .....	61
3.9. ( <i>R</i> )-4'-methylklavuzon Upregulates H3K27 Trimethylation in Cells Sorted by FACS.....	63
3.10. ( <i>R</i> )-4'-methylklavuzon Inhibits SIRT1 Enzyme Activity In Vitro.....	65
3.11. ( <i>R</i> )-4'-methylklavuzon Upregulates Intracellular SIRT1 Protein Levels .....	66
3.12. ( <i>R</i> )-4'-methylklavuzon Upregulates p21 and p27 Gene Expressions .....	68
3.13. ( <i>R</i> )-4'-methylklavuzon Inhibits CRM1 Protein in HepG2 and HuH-7 Cells .....	71
3.14. TK126 Inhibits CRM1 Proteins in HepG2 and HuH-7 Cells .....	76
3.15. ( <i>R</i> )-4'-methylklavuzon Upregulates p53 Protein Levels in HepG2 and HuH-7 Cells .....	77
3.16. Immunofluorescence Visualization of p53 Protein Levels in HepG2 Cell Spheroids .....	80
3.17. Colorimetric Determination of p53/MDM2 Complex by ELISA .....	81
3.18. Effects of ( <i>R</i> )-4'-methylklavuzon on HuH-7 Spheroids.....	86
 CHAPTER 4. DISCUSSION.....	 91
 CHAPTER 5. CONCLUSION .....	 102
 REFERENCES.....	 104

## LIST OF FIGURES

<u>Figure</u>	<u>Page</u>
Figure 1.1. Subcellular localization of sirtuins .....	5
Figure 1.2. Roles of sirtuins in Hedgehog, Wnt/ $\beta$ -catenin, and Notch stem cell signaling pathways .....	8
Figure 1.3. Role of sirtuins in Epithelial–Mesenchymal Transition (EMT).....	11
Figure 1.4. Upstream and downstream pathways of SIRT1 .....	17
Figure 1.5. Roles of p21 and p27 in cell cycle regulation .....	21
Figure 1.6. Crystal structure of MDM2 bound to p53 .....	23
Figure 1.7. SIRT1 triggers p53 transcription-independent apoptosis.....	25
Figure 1.8. SIRT1 causes gene silencing by H3K9 deacetylation of target gene promoters.. .....	26
Figure 1.9. Nuclear export of cargo proteins is initiated by binding of CRM1 with nuclear export signal (NES) of the related protein .....	29
Figure 1.10. Structure of (R)-4'-methylklavuzon .....	31
Figure 1.11. p53 and pNBS1 expression analysis of (R)-4'-methylklavuzon .....	31
Figure 2.1. HDAC substrate which is named 'Boc-Lys(Ac)-AMC' and provided with Cell-based Histone Deacetylase (HDAC) Enzyme Activity Kit. ....	36
Figure 2.2. Reaction mechanism of Fluor de Lys-SIRT1 substrate by HDAC1 enzyme .....	39
Figure 2.3. Reaction mechanism of Fluor de Lys-SIRT1 substrate by SIRT1 enzyme .....	42
Figure 3.1. Time and concentration dependent cytotoxic activity of (R)-4'-methylklavuzon on HuH-7 parental cells .....	51
Figure 3.2. Time and concentration dependent cytotoxic activity of (R)-4'-methylklavuzon on EpCAM <sup>+</sup> /CD133 <sup>+</sup> HuH-7 cells .....	52
Figure 3.3. Time and concentration dependent cytotoxic activity of (R)-4'-methylklavuzon on EpCAM <sup>-</sup> /CD133 <sup>-</sup> HuH-7 cells .....	52
Figure 3.4. Comparative cytotoxic activity of (R)-4'-methylklavuzon HuH-7 cell population .....	53
Figure 3.5. Time and dose dependent effects of (R)-4'-methylklavuzon on cell cycle of HuH-7 cells .....	53

Figure 3.6. Time and dose dependent apoptotic effects of ( <i>R</i> )-4'-methylklavuzon on HuH-7 cell populations. ....	54
Figure 3.7. The structures of novel 4'-alkyl substituted ( <i>R</i> )-4'-methylklavuzon derivatives .....	55
Figure 3.8. In vitro effects of ( <i>R</i> )-4'-methylklavuzon on class I/II histone deacetylase enzymes isolated from HuH-7 parental, EpCAM <sup>+</sup> /CD133 <sup>+</sup> HuH-7 cells and EpCAM <sup>-</sup> /CD133 <sup>-</sup> HuH-7 cells .....	56
Figure 3.9. Inhibitory effects of ( <i>R</i> )-4'-methylklavuzon on endogenous histone deacetylase enzymes in HuH-7 cell populations .....	57
Figure 3.10. Comparative scheme of cell-based HDAC assay and cell viability assay for HuH-7 parental cells .....	58
Figure 3.11. Comparative scheme of cell-based HDAC assay and cell viability assay for EpCAM <sup>+</sup> /CD133 <sup>+</sup> HuH-7 cells .....	58
Figure 3.12. Comparative scheme of cell-based HDAC assay and cell viability assay for EpCAM <sup>-</sup> /CD133 <sup>-</sup> HuH-7 cells .....	59
Figure 3.13. Inhibitory effects of ( <i>R</i> )-4'-methylklavuzon on endogenous histone deacetylase enzymes in HuH-7 cell populations. ....	59
Figure 3.14. Comparative graph of cell-based HDAC assay and cell viability assay for HuH-7 parental cells .....	60
Figure 3.15. Comparative graph of cell-based HDAC assay and cell viability assay for EpCAM <sup>+</sup> /CD133 <sup>+</sup> HuH-7 cells .....	60
Figure 3.16. Comparative graph of cell-based HDAC assay and cell viability assay for EpCAM <sup>-</sup> /CD133 <sup>-</sup> HuH-7 cells .....	61
Figure 3.17. Inhibitory effect of ( <i>R</i> )-4'-methylklavuzon on HDAC1 enzyme .....	62
Figure 3.18. Inhibitory effect of TK126 on HDAC1 enzyme .....	62
Figure 3.19. Effects of ( <i>R</i> )-4'-methylklavuzon on methylation and acetylation status of H3K27 residue in HuH-7 parental cells at the end of 24 and 48 hour of incubation .....	63
Figure 3.20. Effects of ( <i>R</i> )-4'-methylklavuzon on methylation status of H3K27 residue in HuH-7 parental cells and EpCAM <sup>+</sup> /CD133 <sup>+</sup> HuH-7 cells sorted by FACS after 72 hours of drug treatment. ....	64

Figure 3.21. Effects of ( <i>R</i> )-4'-methylklavuzon on acetylation status of H3K27 residue in HuH-7 cell populations sorted by MACS after 72 hours of drug treatment.....	64
Figure 3.22. Inhibitory effect of ( <i>R</i> )-4'-methylklavuzon on SIRT1 enzyme activity .....	65
Figure 3.23. Inhibitory effect of TK126 on SIRT1 enzyme activity .....	66
Figure 3.24. Effect of ( <i>R</i> )-4'-methylklavuzon on SIRT1 enzyme levels within 24 hours .....	67
Figure 3.25. Comparative analysis of cell-based HDACs/sirtuins assay and intracellular SIRT1 ELISA.....	68
Figure 3.26. Agarose gel images of p21 and p27 PCR products .....	68
Figure 3.27. Time dependent fold changes of p21 expression in HuH-7 parental cells after incubation with ( <i>R</i> )-4'-methylklavuzon treatment.....	69
Figure 3.28. Time dependent fold changes of p27 expression in ( <i>R</i> )-4'-methylklavuzon treated HuH-7 parental cells .....	70
Figure 3.29. Concentration dependent p21 expression for 72 hours in ( <i>R</i> )-4'-methylklavuzon treated HuH-7 cell populations (HuH-7 Parental, EpCAM <sup>+</sup> /CD133 <sup>+</sup> and EpCAM <sup>-</sup> /CD133 <sup>-</sup> ).....	70
Figure 3.30. Concentration dependent p27 expression for 72 hours in ( <i>R</i> )-4'-methylklavuzon treated HuH-7 cell populations (HuH-7 Parental, EpCAM <sup>+</sup> /CD133 <sup>+</sup> and EpCAM <sup>-</sup> /CD133 <sup>-</sup> ).....	71
Figure 3.31. Immunofluorescence imaging of RIOK2 proteins in HuH-7 parental cells after drug candidate treatment .....	72
Figure 3.32. Spinning disc confocal microscopy imaging of RIOK2 proteins in HuH-7 parental cells after ( <i>R</i> )-4'-methylklavuzon treatment by immunofluorescence staining.....	73
Figure 3.33. Immunofluorescence imaging of RIOK2 proteins in HepG2 cells after drug candidate treatment .....	74
Figure 3.34. Spinning disc confocal microscopy imaging of RIOK2 proteins in HepG2 cells after ( <i>R</i> )-4'-methylklavuzon treatment by immunofluorescence staining.....	75
Figure 3.35. Immunofluorescence imaging of RIOK2 proteins in HuH-7 parental cells after TK126 treatment.....	76

Figure 3.36. Immunofluorescence imaging of RIOK2 proteins in HepG2 cells after TK126 treatment .....	77
Figure 3.37. Immunofluorescence imaging of p53 upregulation in HepG2 cells after (R)-4'-methylklavuzon treatment.....	78
Figure 3.38. Immunofluorescence imaging of p53 upregulation in HuH-7 parental cells after (R)-4'-methylklavuzon treatment .....	79
Figure 3.39. Microscope images of (R)-4'-methylklavuzon treated HepG2 spheroids stained with DAPI, PI and p53 antibody at the end of 24 hours of incubation. ....	80
Figure 3.40. Total protein optimization of HuH-7 cell lysate .....	81
Figure 3.41. Effect of (R)-4'-methylklavuzon on pure p53/MDM2 complex .....	82
Figure 3.42. Levels of p53/MDM2 complex in HuH-7 cells incubated with various concentrations of (R)-4'-methylklavuzon for 6 hours .....	83
Figure 3.43. Levels of p53/MDM2 complex in HuH-7 cells incubated with various concentrations of (R)-4'-methylklavuzon for 24 hours .....	84
Figure 3.44. Levels of p53/MDM2 complex in HuH-7 cells incubated with various concentrations of (R)-4'-methylklavuzon for 24 hours .....	85
Figure 3.45. Microscope images (4X) of HuH-7 parental cell spheroids in matrigel at the end of 48 hours of incubation with (R)-4'-methylklavuzon .....	86
Figure 3.46. Microscope images (40X) of HuH-7 parental cell spheroids in matrigel at the end of 48 hours of incubation with (R)-4'-methylklavuzon. ....	87
Figure 3.47. Microscope images (4X) of EpCAM <sup>+</sup> /CD133 <sup>+</sup> HuH-7 cell spheroids in matrigel at the end of 48 hours of incubation with (R)-4'- methylklavuzon. ....	88
Figure 3.48. Microscope images (40X) of EpCAM <sup>+</sup> /CD133 <sup>+</sup> HuH-7 cell spheroids in matrigel at the end of 48 hours of incubation with (R)-4'- methylklavuzon. ....	89
Figure 3.49. Microscope images (4X and 40X) of spheroids formed with HuH-7 parental and EpCAM <sup>+</sup> /CD133 <sup>+</sup> HuH-7 cells at the end of 48 hours of incubation with (R)-4'-methylklavuzon .....	90
Figure 4.1. Multiple sequence alignment of eight sirtuins showing highly conserved residues (red) and conserved residues (green).....	93

Figure 4.2. Docking studies of ( <i>R</i> )-4'-methylklavuzon and TK126 to the active site of SIRT1.....	94
Figure 4.3. Proximity of cysteine amino acids to the ( <i>R</i> )-4'-methylklavuzon .....	94

## LIST OF TABLES

<b><u>Table</u></b>	<b><u>Page</u></b>
Table 1.1. Localizations, substrates and biological functions of SIRT1 .....	6
Table 1.2. Functions and mechanisms of action of sirtuins in stem cells.....	7
Table 1.3. Important cargo proteins of CRM1.....	28
Table 1.4. Differential subcellular localizations of proteins in human cancers.....	30
Table 2.1. p21 ve p27 PCR Mixture .....	44
Table 2.2. p21 ve p27 PCR Conditions .....	44
Table 2.3. p21 ve p27 qPCR Conditions .....	44
Table 2.4. Matrigel Suspension .....	49
Table 3.1. Calculated IC <sub>50</sub> values of ( <i>R</i> )-4'-methylklavuzon derivatives on MIA-PaCa2 and HPDEC cells .....	55
Table 3.2. Amount of inhibition for p53/MDM2 complex formation by ( <i>R</i> )-4'- methylklavuzon treated pure p53 and MDM2 proteins. ....	82
Table 3.3. p53/MDM2 complex status in 6-hours drug treated HuH-7 cells .....	83
Table 3.4. p53/MDM2 complex status in 24-hours drug treated HuH-7 cells .....	84
Table 3.5. p53/MDM2 complex status in 48-hours drug treated HuH-7 cells .....	85



# CHAPTER 1

## INTRODUCTION

### 1.1. Hepatocellular Carcinoma (HCC)

Primary liver cancers can be categorized as either hepatoblastoma, hepatocellular carcinoma (HCC), angiosarcoma or cholangiocarcinoma (CCA). The most common of these is HCC, which accounts for nearly 80% of all liver cancer cases. HCC is the fifth most common cancer and third leading cause of cancer-related deaths worldwide. 600,000 new HCC cases that occur each year are from developing countries. Risk factors including exposure to hepatitis viruses, vinyl chloride, tobacco, foodstuffs contaminated with aflatoxin B1 (AFB1), heavy alcohol intake, nonalcoholic fatty liver disease, diabetes, obesity, diet, coffee, oral contraceptives, and hemochromatosis. There are some applications such as partial liver resection and liver transplantation among treatment options. But a few cases are considered to be suitable for such applications. Signal inhibitors such as Sorafenib, trans-arterial chemoembolisation and percutaneous ethanol injection do not ameliorate the prognosis of the disease (Llovet et al. 2008). Novel therapeutic agents and methods are required to be developed for HCC treatment without recurrence.

### 1.2. Cancer Stem Cells (CSC)

Tissue cells and stem cells remain in the niche for a certain time. But stem cells are provided for a long period of time for regeneration or growth of the tissue. Mutations which may cause transformation in their genome can occur during this long period. Such mutations alter the regulation of Wnt, Notch, Hedgehog pathways that are responsible for normal stem cell renewal and also alter the regulation of PTEN, TP53 that are tumor suppressors. As a result of these mutations, related cells transform into cancer stem cells obtaining uncontrolled self renewal ability and becoming more resistant against therapeutic agents (Signore et al. 2011).

### **1.3. Role of Cancer Stem Cells in Hepatocellular Carcinoma**

Initial evidence that CSCs might contribute to the development of HCC came from a side population (SP) cells study with stem-like characteristics from the HCC cell lines: HuH-7 and PLC5 (Chiba et al. 2006). CD133<sup>+</sup> cells separated from HuH-7 and PLC5 cultures as well as from primary tumor samples from SCID mice possessed higher tumorigenicity and clonogenicity than CD133<sup>-</sup> cells. These CD133<sup>+</sup> CSCs were resistant to chemotherapeutic agents (Doxorubicin and 5-Fluorouracil) due to the upregulation of ATP-binding cassette (ABC) superfamily transporters through the activation of Akt/PKB and Bcl-2 cell survival pathways (Ma et al. 2008b). Epithelial cell adhesion molecule (EpCAM) was also found to have prognostic value. The combination of EpCAM<sup>+</sup> and AFP<sup>+</sup> markers was predicted poor survival, in contrast to EpCAM<sup>-</sup>/AFP<sup>-</sup> which was associated with good prognosis (Yamashita et al. 2008).

### **1.4. Histone Deacetylases (HDACs)**

HDACs catalyze the removal of an acetyl group from the  $\epsilon$ -amino group of lysine side chains of the core nucleosomal histones (H2A, H2B, H3 and H4), thereby reconstituting the positive charge on the lysine. The active site of HDACs consists of a cylindrical pocket, covered by hydrophobic and aromatic amino acids where the side chain of lysine residue fits when deacetylation takes place. The family of HDACs comprises four classes: class I, II and IV are zinc-dependent amidohydrolases, whereas class III requires NAD<sup>+</sup> for the deacetylation reaction.

Overexpression of specific HDACs has been observed in many types of cancer and often correlates with poor prognosis (Spiegel et al. 2012). HDAC1 is overexpressed in gastric, pancreas, colorectal, prostate and hepatocellular cancers and it is related with a severe prognosis. It is shown that HDAC1 is embryonic lethal when suppressed as a result of increased p21 expression followed by decreased proliferation (Lagger et al. 2002).

## **1.5. Role of Histone Deacetylases in Hepatocellular Carcinoma**

It has been found that HDAC1 is essential for epithelial-mesenchymal transition which is triggered by TGF $\beta$ 1 and cell migration in hepatocytes. It is considered that invasive properties of HCC cells is provided by high levels of HDAC1 which increases epithelial-mesenchymal transition in invasive HCC cells (Lei et al. 2010). High levels of HDAC1, 2, 3 and ki-67 compared to normal healthy tissue were also reported (Quint et al. 2011). It has been found that inhibition of HDAC1 decreases the levels of  $\beta$ -catenin in nucleus, the levels of CCND1 and EGFR which are responsible for proliferation (Cheng et al. 2011). According to a recent study, deletion of HDAC3 resulted in an increase in acetylation of lysine 9 and 14 of histone 3, lysine 5 and 12 of histone 4 causing hepatocellular carcinoma (Bhaskara et al. 2010).

High levels of SIRT1 in HCC tissues compared to healthy tissues and correlation of expression levels of SIRT1 in advanced tumors were reported. The repression of HCC cell proliferation by decreasing the SIRT1 expressions was demonstrated by Choi and coworkers (Choi et al. 2011).

It has been shown that TSA and SAHA which are HDAC inhibitors, cause apoptosis on hepatoma cells depending on the time and dose (Carlisi et al. 2010). Moreover, induction of apoptosis in HuH-7, PLC/PRF/5, Hep3b and HepG2 cell lines with TSA and SAHA by an increase in acetylation of histone 3 was detected (Yang et al. 2010).

## **1.6. Histone Deacetylase Inhibitors (HDACIs)**

There are three chemotherapeutic agents approved by FDA as a HDAC inhibitor called vorinostat, romidepsin (Grant et al. 2007) and belinostat which are approved for the treatment of patients with relapsed or refractory peripheral T-cell lymphoma (PTCL) (Mottamal et al. 2015). It has been reported that HDACIs show more toxicity against transformed cells compared to normal cells with an unknown mechanism. It is considered that HDACIs show their effect by increased levels of reactive oxygen species or decreased levels of DNA repair proteins (RAD50, RAD51, MRE11) (Lee et al. 2010). Additionally, mechanism of HDACIs can be listed as modification of acetylation status of gene promoters, relaxation of chromatin by

neutralisation of acidic charges on histone proteins, overexpression of transcription, inhibition of deacetylation of some transcription factors such as p53, NF- $\kappa$ B, E2F1, STAT1, STAT3, YY1, acetylation of chaperone proteins (Hsp90), DNA repair proteins (Ku70), tubulin proteins, arrest at G1/S by increasing p21 expression and decreasing cyclin expression, decrease in angiogenesis by repressing pro-angiogenic factors (VEGF, HIF1 $\alpha$ , TNF- $\alpha$ , IL-1). Besides these mechanisms, HDACs activate intrinsic mitochondrial pathway by increasing pro-apoptotic proteins (Noxa, Puma) and decreasing anti-apoptotic proteins (Bcl-2, Bcl-XL, XIAP, Mcl-1). Moreover, HDACs overexpress death receptors (DR4, DR5, Fas) which are responsible for extrinsic pathways.

It is known that approximately all the HDACs cause an arrest at G1/S. This situation is explained by the induction of CDKN1A (p21<sup>WAF1/CIP1</sup>) independent from p53 and hypophosphorylation of retinoblastoma (Rb). HDACs are considered to be used in combination with topoisomerase II inhibitors and proteasome inhibitors due to their various working mechanisms. All together, NF- $\kappa$ B activation, disruption of aggresome function and initiation of proteotoxic stress in the cell are also aimed by using HDACs. Besides these mechanisms, repression of cyclin D and cyclin A genes are considered to cause an arrest at cell cycle by loss of CDK2, CDK4 function and hypophosphorylation of Rb. Arrest at G1/S cycle is explained by repression of CTP synthase and thymidylate synthase which are responsible for DNA synthesis and decrease in levels of c-Myc while TGF- $\beta$  signal increases by HDACs. Function of transcription factors such as p53, E2F1, STAT1, STAT3 and NF- $\kappa$ B is directly related with their acetylation and deacetylation status and all those proteins are hyperacetylated with HDAC inhibitors.

## 1.7. Sirtuins

Sirtuins are a conserved enzyme family that require nicotinamid dinucleotide (NAD) for deacetylase activity (North and Verdin 2004; Sauve and Youn 2012). They have important roles in senescence (Tissenbaum and Guarente 2001; Wood et al. 2004), longevity (Gan and Mucke 2008), DNA repair (Lombard et al. 2008), transcriptional silencing (Tissenbaum and Guarente 2001), apoptosis (Cohen et al. 2004; Wang et al. 2006) and metabolic enzyme regulation (Schwer and Verdin 2008). Sirtuins are

categorized as Class III histone deacetylases due to their dependence on  $\text{NAD}^+$  as a cofactor for protein deacetylation. Deacetylation reaction occurs in two steps that include consumption of  $\text{NAD}^+$  and production of NAM, 1-O-acetyl-ADP-ribose (1-OAADPR) and deacetylated substrate (Haigis and Guarente 2006). The catalytic activity of sirtuins varies in addition to deacetylation such as removing myristoyl (Feldman et al. 2013), palmitoyl (Jiang et al. 2013), crotonyl (Bao et al. 2014), glutaryl (Tan et al. 2014) and succinyl (Du et al. 2011) from the  $\epsilon$ -amino group of acylated lysine residues due to their unique  $\text{NAD}^+$ -dependent mechanism.

Sirtuins are categorized into 5 classes (I, II, III, IV and U) according to phylogenetic analyses. Mammalian sirtuins (SIRT1–7) are classified into classes I–IV whereas sirtuins of gram-positive bacteria are classified into class U (Frye et al. 2000).

Moreover, the mammalian sirtuins show different subcellular localization and catalytic activity. C- and N-terminal residues ends of sirtuins contain specific localization sequences determining the subcellular localization of the sirtuin isotypes (Tanno et al. 2007, North et al. 2007).

For instance, SIRT1 and SIRT2 can shuttle between nucleoplasm and cytoplasm in a cell cycle and cell-type-dependent manner (Tanno et al. 2007, North et al. 2007). Despite the presence of this mechanism, SIRT1 locates mainly in nucleus whereas SIRT2 locates primarily in cytosol (Figure 1.1).

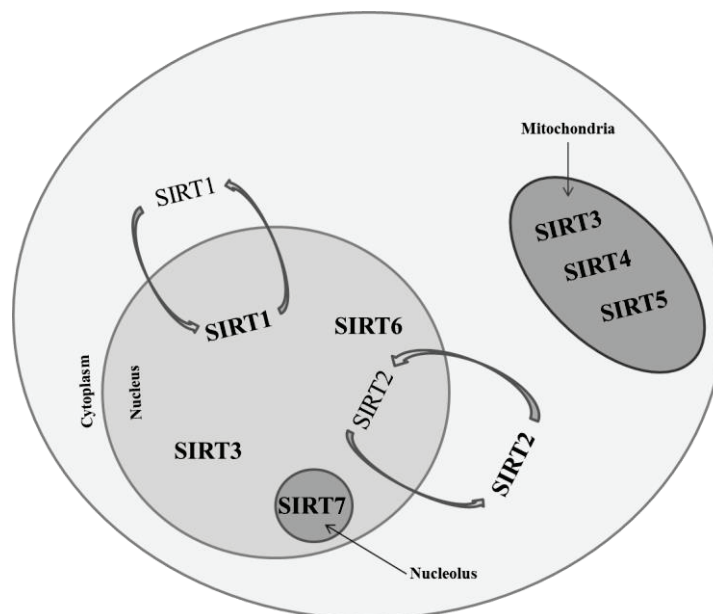


Figure 1.1. Subcellular localization of sirtuins.  
(Adapted from Schiedel et al. 2017)

## 1.8. Sirtuins and Cancer Stem Cells

Aging and cancer are related with each other and associated with stem cell function. Sirtuins are thought to be stress-responsive enzymes altering the acetylome for cellular adaptations.

### 1.8.1. Role of Sirtuins in Stem Cells

#### 1.8.1.1. Embryonic Stem Cells and Development

Embryonic stem cells (ESCs) contain higher levels of histone acetylation than differentiated cells (Efroni et al. 2008). Thus, sirtuins are strictly linked to development and differentiation of ESCs.

SIRT1 levels was found at higher levels in ESCs before its downregulation by miRNAs during differentiation (Saunders et al. 2010). SIRT1 is considered to maintain stemness of ESCs and to play a role in developmental programs upon differentiation of ESCs (Table 1.1, Table 1.2). Environmental conditions determine whether SIRT1 functions during differentiation or not. Under normal conditions, SIRT1 disruption does not affect differentiation but under oxidative stress, SIRT1 maintains stemness by nuclear translocation of p53 providing Nanog expression (Han et al. 2008; Calvanese et al. 2010).

Table 1.1. Localizations, substrates and biological functions of SIRT1 (Adapted from Schidel et al. 2017)

Isotype	Class	Localization	Cellular Substrate	Interaction partner	Enzymatic activity	Biological functions
SIRT1	I	Nucleus, Cytoplasm	Histone H1 (K26), histone H3 (K9, K14, K56), histone H4 (K16), KDAC1, p53, p73, NF-κB (p65), p300, PCAF, FOXO1, FOXO3, FOXO4, PGC1α, HIF1α, HIF2α, HSF1, HIV Tat, BCL6, AceCS1, LXR, TORC1, FXR, eNOS, APE1, MEF2, Notch1, Ku70, XPA, WRN, NBS1, LKB1, HMGCS1, c-MYC, SATB1, KAP1, Atg 5/7/8, androgene receptor, SUV39H1, BMAL1, PER2, DNMT1, hMOF, TIP60, cortactin, PARP1, SREBP-1C, RFX-5, TDG, FOXA2, IRF-1, HMGB1, PGAM1, PML, CRABP1, TopBP1, Smad7, CRTCL	AROS, DBC1, DJ-1	Deacetylation	Apoptosis, metabolism, cell cycle, tumorigenesis, tumor suppression, neuroprotection, stress response, longevity, cell migration, circadian control, viral transcription, insulin signaling

SIRT1 is a member of Polycomb repressive complex 4 (PRC4), that is responsible for developmental genes repression in ESCs (Kuzmichev et al. 2005) and binding to the promoters of development-associated genes in ESCs. Overexpression or enzymatic activation of SIRT1 by resveratrol enhance the efficiency of induced pluripotent stem cells (iPSC) generation, whereas downregulation of SIRT1 shows the opposite effect. This mechanism is associated with deacetylation of p53 and increased Nanog expression (Lee et al. 2012).

### 1.8.1.2. Hematopoietic Stem Cells (HSCs)

In vivo studies with SIRT1<sup>-/-</sup> mice showed that SIRT1 regulates stemness in Hematopoietic stem cells (HSCs) positively. The mechanism underlying hematopoietic cell stemness is reactive oxygen species (ROS) elimination, FOXO activation, and inhibition of p53. Moreover, FOXO3 mediates homeostatic control by SIRT1 in HSCs (Matsui et al. 2012).

Table 1.2. Functions and mechanisms of action of sirtuins in stem cells

Sirtuin	Action	Mechanism	Cells
SIRT1	Maintenance of stemness	Nanog expression is maintained by mitochondrial translocation of p53	ESC
SIRT1	Maintenance of stemness	Developmental genes are repressed by PRC4 component	ESC
SIRT1	Maintenance of stemness	ROS elimination, FOXO activation and inhibition of p53	HSC
SIRT1	Promotes differentiation	Notch-Hes1 signaling is blocked interaction with N-CoR	NSC
SIRT2	Promotes differentiation	GSK3 $\beta$ is negatively regulated	ESC
SIRT3	Maintenance of stemness	Required for HSC self-renewal at old age	HSC
SIRT6	Promotes differentiation	Acetylation of H3K56 and H3K9 at Oct4 and Sox2 promoters are regulated	ESC
SIRT6	Maintenance of stemness	Wnt target genes are repressed by interacting with LEF1 and deacetylating histone 3	HSC
SIRT7	Maintenance of stemness	UPR <sup>mt</sup> and NRF1 are regulated	HSC

### 1.8.2. Cell Differentiation

It was found that SIRT1 can suppress differentiation in iPSCs. SIRT1 levels decrease and miRNA-34a levels, which is a SIRT1 inhibitor, increase during neural stem cell generation from mouse iPSCs. Moreover, enzymatic inhibition of SIRT1 by

nicotinamide (NAM) increases the generation of neural stem cells (NSCs) and mature nerve cells (Hu et al. 2014a).

### 1.8.3. Sirtuins in Stem Cell Signaling Pathways

Such pathways like Hedgehog, Wnt and Notch are main regulators of stem cell self-renewal and differentiation. Epigenetic regulations like DNA methylation and histone modifications (Toh et al. 2017) control these pathways strictly. Sirtuins, mainly SIRT1, interact with some of the members of these signaling networks (Figure 1.2).

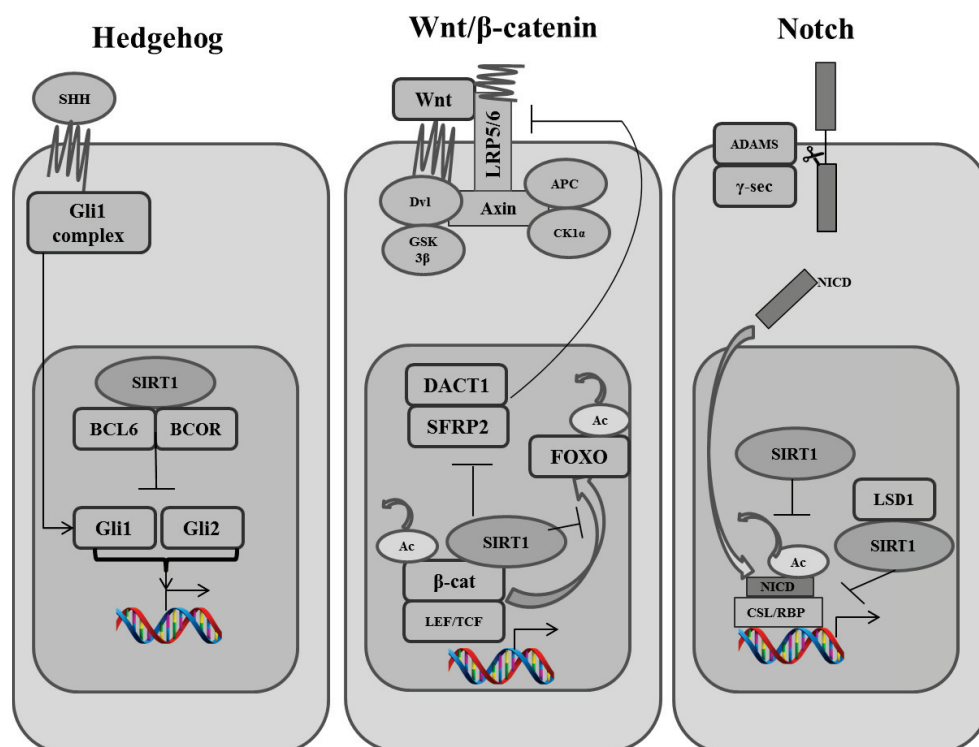


Figure 1.2. Roles of sirtuins in Hedgehog, Wnt/ $\beta$ -catenin and Notch stem cell signaling pathways. SHH, Sonic Hedgehog;  $\beta$ -cat,  $\beta$ -catenin; Dvl, Disheveled; GSK3 $\beta$ , glycogen synthase kinase-3 $\beta$ ; ADAMS, a disintegrin and metalloproteases; APC, adenomatous polyposis coli; CK1 $\alpha$ , casein kinase 1 $\alpha$ ; CSL/RBP, CBF1 Suppressor of Hairless LAG-1/recombination signal binding protein for immunoglobulin  $\kappa$ J region; LEF/TCF, lymphoid enhancer factor/T-cell factor; LSD1, lysine demethylase 1A; LRP5/6, low-density lipoprotein-related proteins 5 and 6; NICD, Notch intracellular domain;  $\gamma$ -sec,  $\gamma$ -secretase. (Adapted from O'Callaghan et al. 2017)



SIRT1 suppresses Sonic Hedgehog effectors Gli1 and Gli2 by an interaction with BCL6 and BCOR. SIRT1 increases Wnt/ $\beta$ -catenin signaling as a result of  $\beta$ -catenin and FOXO transcription factors by deacetylation and SFRP2 and DACT1 suppression. SIRT2 is responsible for inhibition of  $\beta$ -catenin signaling and downregulation of Wnt target genes expression. SIRT6 suppresses Wnt target genes by an interaction with LEF1 and histone 3 deacetylation. SIRT1 destabilizes the NICD by deacetylation and interacts with LSD1 for repression of Notch target genes.

### **1.8.3.1. Hedgehog Pathway**

The Hedgehog pathway is responsible for adult tissue homeostasis and organ patterning during embryogenesis (Matsui et al. 2016). When Sonic Hedgehog (Shh) binds to the Patched receptor, transmembrane protein Smoothed provides the release and nuclear translocation of Gli transcription factors for Hedgehog target gene expressions. It was found that SIRT1 is an *in vivo* negative regulator of this pathway in neuron precursors. SIRT1 epigenetically represses Gli1 and Gli2 which have roles in the expression of genes required for normal cerebellar development. This mechanism also acts as a tumor suppressor in medulloblastoma including activated Hedgehog pathway. It is hypothesized that activation of BCL6/BCOR/SIRT1 complex may be a therapeutic target in Sonic Hedgehog-dependent tumors (Tiberi et al. 2014).

### **1.8.3.2. Wnt/ $\beta$ -catenin Pathway**

The canonical Wnt pathway is responsible for proliferation and alterations in epigenetic control which are related with a variety of cancers (Toh et al. 2017). Research show that SIRT1 might promote Wnt/ $\beta$ -catenin signaling in both normal progenitor and cancer cells by mainly activation of  $\beta$ -catenin. SIRT1 deacetylates  $\beta$ -catenin and causes nuclear accumulation of  $\beta$ -catenin and upregulation of transcription of Wnt/ $\beta$ -catenin target genes in both adipogenesis and osteogenesis (Feng et al. 2016, Zhou et al. 2016b).

### 1.8.4. Sirtuins and Cancer Stem Cells

Deregulation of epigenetics in cancer cause aberrantly activated or suppressed stem cell signaling pathways. Thus, sirtuins are considered to play a role in generation of a cancer cell population that are able to display self-renewal and differentiation causing tumor growth. It is also speculated that CSCs and normal stem cells of the corresponding tissue contain distinct stem cell programs which provides unique roles for sirtuins in CSCs.

In vitro and in vivo SIRT1 expression was found to be upregulated in various cancer stem cells such as glioma (Lee et al. 2015), breast (Ma et al. 2015), colorectal (Chen et al. 2014b) and leukemia (Li et al. 2012, 2014). Furthermore, SIRT1 provides both oncogenic transformation and maintenance of stemness in glioma cells (Lee et al. 2015). Thus, high levels of SIRT1 were found in CD133<sup>+</sup> glioma stem cells compared to CD133<sup>-</sup> non-stem cells. Consequently, SIRT1 knockdown increases the radiosensitivity of CD133<sup>+</sup> cells both in vitro and in vivo (Chang et al. 2009)

Upregulation of SIRT1 and down regulation of its regulator miR-34a were characterized in CD44<sup>+</sup>/CD24<sup>-</sup> breast cancer stem cells (BCSCs). Downregulation of SIRT1 and overexpression of miR-34a decreased tumorsphere formation and expression of CSC markers including ALDH1 and Nanog (Ma et al. 2015).

SIRT1 was also found at higher levels in colorectal cancer cells colocalizing with the colorectal CSC marker CD133. SIRT1 knockdown reduces CD133<sup>+</sup> cell population, sphere formation and tumorigenicity in vivo. Additionally, stem cell markers such as OCT4, NANOG, and TERT expressions are also decreased (Chen et al. 2014b). SIRT1 expression was found at higher levels in Nanog<sup>+</sup> liver CSCs but decreases during differentiation. Furthermore, SIRT1 was shown to play an important role in maintenance of liver CSCs self-renewal by epigenetic regulation of the SOX2 promoter (Liu et al. 2016). It is obvious that SIRT1 is crucial for the maintenance of CSCs. Besides unknown downstream mechanisms, loss of SIRT1 provides decreased sphere formation, reduced expression of CSC markers and increased sensitivity to treatment.

### 1.8.5. Epithelial–Mesenchymal Transition (EMT)

Epithelial cells change their cytoskeleton structure, lose apical–basal polarity and cell–cell adhesion during EMT obtaining increased cell mobility. Activation of EMT programs are related to stem-like traits on both normal and neoplastic cells (Mani et al. 2008).

SIRT1 positively regulates EMT in prostate cancer by its deacetylase function. SIRT1 binds to the E-cadherin promoter by the zinc finger transcription factor ZEB1. It causes transcriptional repression of E-cadherin by preventing RNA polymerase II binding as a result of histone 3 deacetylation. Thus, SIRT1 knockdown decreases prostate cancer cell migration and metastasis (Byles et al. 2012). Additionally, SIRT1 silences the E-cadherin promoter in pancreatic cancer by an interaction with Twist and methyl-CpG binding domain protein-1 (MBD1) (Xu et al. 2013). EMT in pancreatic cancer cells is a result of upregulation of SIRT1 whereas SIRT1 inhibition induces mesenchymal–epithelial transition (Figure 1.3) (Deng et al. 2009).

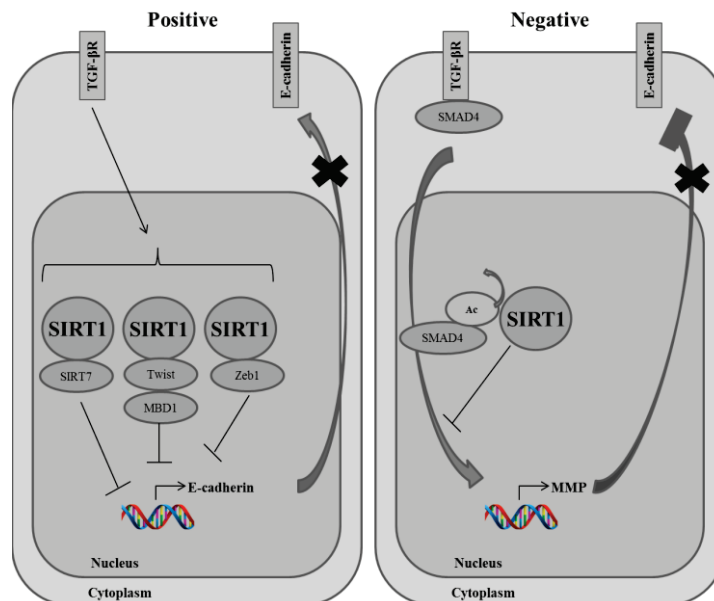


Figure 1.3. Role of sirtuins in Epithelial–Mesenchymal Transition (EMT). Positive: TGF-β signaling increases SIRT1 levels. SIRT1 binds to the E-cadherin promoter in a complex with Zeb1 and represses E-cadherin expression. Alternatively, SIRT1 silences E-cadherin promoter in a complex with Twist and MBD1. Negative: Deacetylation of Smad4 by SIRT1 inhibits TGF-β signaling. Consequently, MMP transcription and E-cadherin degradation is decreased. (Adapted from O’Callaghan et al. 2017)

Reduction of EMT in both transformed primary human mammary epithelial cells and kidney epithelial cells is explained by repression in TGF- $\beta$  signaling pathway as a result of Smad4 deacetylation by SIRT1 (Simic et al. 2013). In various cancer cells such as oral squamous cell carcinoma, lung cancer, and ovarian cancer, SIRT1 was identified as an EMT repressor (Sun et al. 2013a,b; Chen et al. 2014a).

## 1.9. SIRT1

SIRT1 is the most studied member of the sirtuin family. SIRT1 can deacetylate both nuclear and cytoplasmic substrates due to its subcellular localization. It was showed that SIRT1 can directly regulate transcription via histones H1 (Vaquero et al. 2004), H3 (Vaquero et al. 2004, Suter et al. 2012, Das et al. 2009) and H4 (Vaquero et al. 2004, 2007) deacetylation and indirectly via NF- $\kappa$ B (Kauppinen et al. 2013), FOXO1 (Yang et al. 2005), FOXO4 (van der Horst et al. 2004), HIF1 $\alpha$  (Lim et al. 2010) and HIF2 $\alpha$  (Dioum et al. 2009) deacetylation. SIRT1 deacetylates H1K26, H3K9, H3K14, H3K56, H4K16, HDAC1K89, HDAC1220, HDAC1K432, HDAC1K438, HDAC1K439, HDAC1K441, P300K1020,P300K2014, c-MycK323, E2F1K117, E2F1K120, E2F1K125,  $\beta$ -cateninK49,  $\beta$ -cateninK345, retinoblastomaK873, retinoblastomaK874.

Tumor suppressor genes like SFRP1 and SFRP2 are silenced as a result of SIRT1- dependent deacetylation of H4K16Ac. It was found that inhibition of SIRT1 by pharmacologic compounds or RNAi reactivates transcription of these tumor suppressor genes in breast cancer cell lines indicating potentials of SIRT1 inhibition.

Besides cancer research, SIRT1 knockdown reduces viral transcription in HPV- and HIV-infected cell lines (Pagans et al. 2005). SIRT1 is responsible in apoptosis by deacetylation of the tumor suppressor proteins p53 (Vaziri et al. 2001), p73 and Ku70 (Jeong et al. 2007). Tumor suppressive roles of some SIRT1 inhibitors are a result of p53-hyperacetylation (Heltweg et al. 2006, Lain et al. 2008).

SIRT1 regulates both pro- and antiapoptotic effects identified as “the SIRT1 paradox”. Deacetylation and activation of the transcriptional corepressor KAP1 by SIRT1 is an example of antiapoptotic effect of SIRT1. KAP1 is a member of nonhomologous end-joining (NHEJ) which is a DNA double-strand break repair pathway (Lin et al. 2015). On the other hand, SIRT1 mediated deacetylation of NF- $\kappa$ B

sensitizes cells to TNF $\alpha$ -induced apoptosis (Yeung et al. 2004). As a conclusion, tumor promoter or tumor suppressor roles of SIRT1 is dependent on the cellular context (Deng et al. 2009). Besides its role in cancer progression or suppression, SIRT1 is also responsible for development or neuroprotective effects on neurodegenerative diseases like Huntington's disease (Jeong et al. 2012, Jiang et al. 2012), Alzheimer's disease (Qin et al. 2006) and Parkinson's disease (Donmez et al. 2012).

## **1.10. SIRT1 and Hepatocellular Carcinoma**

SIRT1 was found to be involved in hepatic lipid and glucose metabolism by deacetylation of specific transcription factors and enzymes (Chang et al. 2014).

### **1.10.1. Role of SIRT1 in Normal Liver Cells**

SIRT1 was shown to contribute to circadian control in vitro and in vivo (Asher et al. 2008). It was found that SIRT1 is associated with the CLOCK:BMAL1 chromatin complex, which are two important circadian transcription factors and SIRT1 activity is regulated in a circadian manner together with histone 3 and BMAL1 acetylation levels. Thus, hepatic-specific SIRT1-deficient mice shows circadian rhythm dysfunction and augmented histone 3 and BMAL1 acetylation (Asher et al. 2008, Nakahata et al. 2008). Contrarily, SIRT1 enzymatic activation reduced period gene 2 (Per2) expression which is a circadian clock gene that expresses repressors in CLOCK:BMAL1-mediated nuclear transcription by Histone 3 acetylation depression at Per2 gene promoters (Bellet et al. 2013).

### **1.10.2. Role of SIRT1 in Hepatocellular Carcinoma**

#### **1.10.2.1. SIRT1 Expression in Hepatocellular Carcinoma**

SIRT1 was found to be expressed at very low levels in normal liver cells, whereas it is expressed at significantly higher levels in liver tumor cells. Overexpression

of SIRT1 was found in nine HCC cell lines (HuH-7, HepG2, Hep3B, HKC1-4, HKC1-2, SNU-449, SNU-423, SK-Hep-1, PLC5) (Simone et al. 2011).

SIRT1 protein levels were detected at higher levels in human HCC carcinoma tissues compared to adjacent nontumor liver tissues. Contrarily, expressions of the other sirtuin family members (SIRT2-7) were detected as equal or lower levels compared to SIRT1 levels in HCC cell lines (exceptions: SIRT5 and SIRT7 in Hep3B and HepG2; SIRT6 in Hep3B) (Simone et al. 2011, Portmann et al. 2013).

Moreover, positive correlation between the expression levels of SIRT1 protein and tumor grades was reported and SIRT1 is overexpressed frequently in high-stage HCC tumors (grades 3–4) (Chen et al. 2012). Statistical analysis revealed that high expression levels of SIRT1 protein were detected frequently in tumors of younger patients and female patients (Simone et al. 2011). Consequently, SIRT1-positive HCC patients have a lower 10-year survival rate than those having SIRT1-negative HCC (Chen et al. 2012, Choi et al. 2011).

Interestingly, average SIRT1 messenger RNA (mRNA) between HCC tissues and nontumorous liver parenchyma was found to be similar and constant (Simone et al. 2011, Bae et al. 2014). Thus, upregulated SIRT1 protein levels was not a result of mRNA levels but a consequence of post-transcriptional mode (Bae et al. 2014). Furthermore, overexpression of SIRT1 in HCC might be caused by decreased protein degradation rather than the increase of mRNA translation (Chen et al. 2012).

### **1.10.2.2. Effect of SIRT1 on HCC Tumorigenesis**

Mutational analyses showed that only wild-type SIRT1 induces HCC cell proliferation and colony formation whereas SIRT1 deacetylase domain mutant doesn't induce the proliferation. It suggests that deacetylation function of SIRT1 is necessary for HCC progression (Chen et al. 2012).

The role of SIRT1 in EMT might be the key point to promote HCC cell metastasis. SIRT1 activation in human hepatoma SMMC-7721 cells resulted in epithelial marker (E-cadherin) downregulation whereas of mesenchymal marker (vimentin) and EMT-associated transcriptional factors (Snail and Twist) upregulation causing cell invasion and migration (Hao et al. 2014). This data shows that SIRT1 is

crucial for HCC tumorigenesis and its inhibition is a new strategy to ameliorate hepatocellular carcinoma prognosis.

### **1.10.2.3. Effect of SIRT1 on Irradiation Resistance of Hepatoma Cells and Chemotherapy**

It was found that SIRT1 inhibition has an effect on HCC cell resistance against chemotherapy and irradiation. Sorafenib is the first FDA approved multikinase inhibitor that targets RAS/RAF kinases and involved in tumor signaling and vasculature (Lowinger et al. 2002, Mann et al. 2001, Wilhelm et al. 2006). It was demonstrated that single-agent sorafenib prolong survival in patients with advanced HCC (Llovet et al. 2008, Yau et al. 2009, Abou-Alfa et al. 2011). Although this treatment, SIRT1-overexpressing SK-Hep1 cells show resistance to sorafenib (Chen et al. 2012).

Interestingly, resveratrol showed its antiproliferative and apoptosis-promoting effects only in p53-positive HepG2 cells which could trigger the p53-induced apoptosis process normally (Huang et al. 1999). In contradiction to effects of SIRT1 knockdown on inducing apoptosis via p53 pathway, overexpression of SIRT1 in p53-positive HepG2 cells induced the expression levels of p21, that is the most important p53 target (Kuo et al. 2002, Huang et al. 1999, Shih et al. 2002). This data revealed that p53-positive HepG2 cells had bypassed signaling from the deacetylation activity of SIRT1 antagonizing the proliferation promotion reactions generated by SIRT1 overexpression. Consequently, it is consisted with the previous result showing that SIRT1 overexpression promoted proliferation of normal L02 cells rather than malignant HepG2 cells.

### **1.10.2.4. Downstream Targets**

#### **1.10.2.4.1. p53**

p53 is the most studied target of SIRT1. p53 acetylation which is induced by DNA damage affects its activation and sequence specific DNA binding. p53 deacetylation diminishes p53-dependent cell growth arrest and apoptosis indicating that acetylation is crucial for p53 to function as a tumor suppressor (Gu et al. 1997, Tang et

al. 2008). SIRT1 removes acetyl group from C-terminal Lys382 residue of p53 downregulating its acetylation level and transcriptional activity (Vaziri et al. 2001).

Oncogenesis induced by SIRT1 mainly depends on the mutant p53 rather than wild-type p53 in hepatocellular carcinoma. Wild-type p53 has alternatives to prevent the inhibiting effects of SIRT1 overexpression by its deacetylation activity.

It was found that AMP-activated protein kinase (AMPK) which is an important factor in normal and malignant cells regulates deacetylation of p53 by SIRT1. AMPK phosphorylates and inactivates SIRT1 via binding to the deacetylase domain of SIRT1 (Thr344) loci providing p53 transcription, acetylation and apoptosis in HCC cells (Lee et al. 2012). On the other hand, SIRT1 overexpression decreases AMPK phosphorylation levels in HCC cells through a wild-type p53-dependent mechanism (Zhang et al. 2015). Consequently, AMPK-SIRT1-p53 loop might have regulatory effects in HCC.

#### **1.10.2.4.2. PTEN/PI3K/AKT**

PTEN/PI3K/AKT signaling pathway is activated in HCC facilitating cell proliferation, differentiation, migration and apoptosis. It was found that SIRT1 has oncogenic roles associated with PTEN/PI3K/AKT (Psyrris et al. 2012). PTEN which is a phosphatase and tensin homologue, is inactivated in HCC to induce phosphatidylinositol-3-kinase (PI3K) function which works in phosphorylation and inactivation of AKT. SIRT1 overexpression deacetylates PTEN and prohibits its activity to trigger PI3K/AKT-induced mitotic entry, growth and proliferation of HCC cells (Wang et al. 2012). Consequently, tumorigenesis of hepatocellular carcinoma which is induced by SIRT1 depends on the PTEN/PI3K/AKT signaling pathway.

#### **1.10.2.4.3. c-Myc**

SIRT1 is also associated with oncogene c-Myc which increases protein expression and deacetylase activity of SIRT1 (Menssen et al. 2012). Conversely, SIRT1 upregulates transcriptional activity and stability of c-Myc in fibroblasts (Menssen et al. 2012, Mao et al. 2011). It was found that SIRT1 and c-Myc constitute a positive



feedback loop regulate each other in both mice or human liver tumors (Figure 1.4) (Jang et al. 2012).

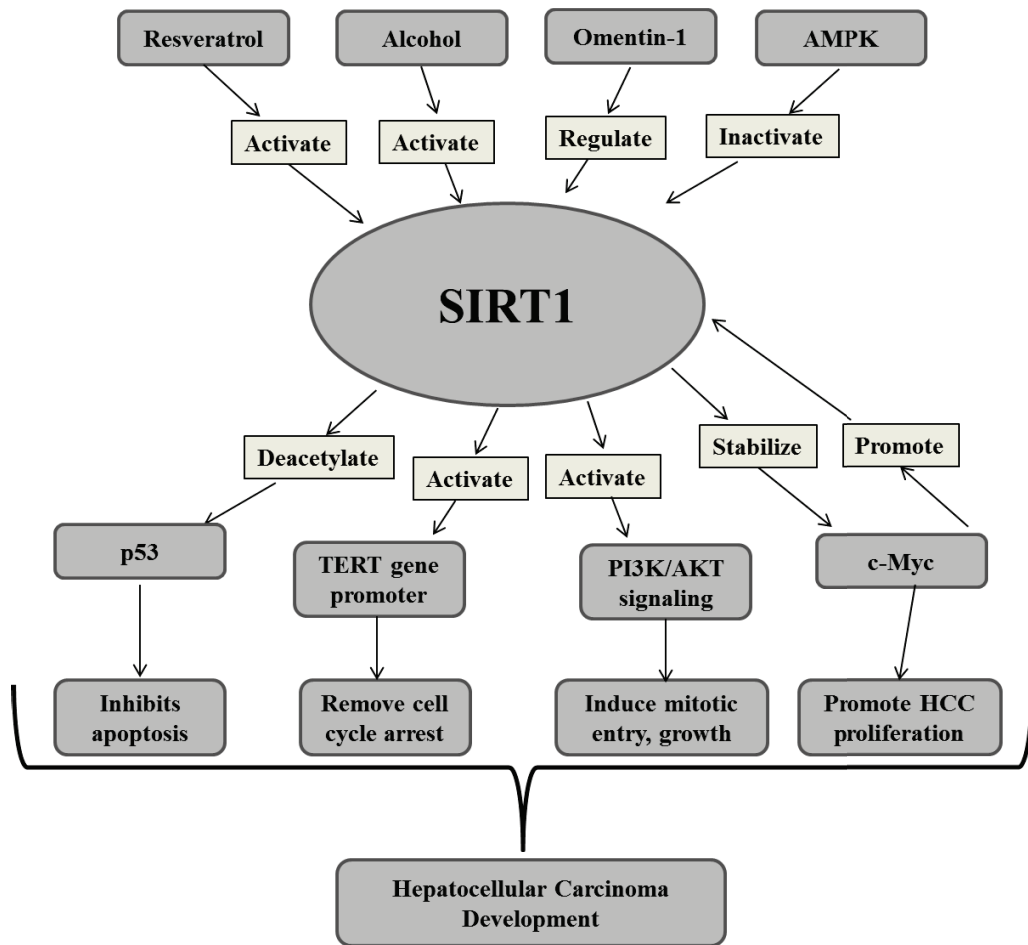


Figure 1.4. Upstream and downstream pathways of SIRT1. (Adapted from Wu et al. 2015)

### 1.11. Contradiction on the Oncogenic Role of SIRT1 in HCC

The exact function of SIRT1 in HCC tumorigenesis is controversial. Tumor suppressor role of SIRT1 was observed in SIRT1-deficient mice researches (Cheng et al. 2003). Moreover, in 42/263 clinical HCC samples, SIRT1 expression was decreased indicating its tumor suppressor role via DNA damage response and genome integrity (Wang et al. 2008).

SIRT1 subcellular localization varies from cell to cell. It was demonstrated that only the nuclear SIRT1 promotes HCC development whereas cytoplasmic SIRT1 is considered as a tumor suppressor (Song et al. 2014). Additionally, cytoplasmic SIRT1 functions to increase cell apoptosis via caspases instead of SIRT1 deacetylase activity

that is crucial in liver normal metabolism and for SIRT1 promoter role in HCC (Jin et al. 2007).

## **1.12. Sirtuin Inhibitors**

### **1.12.1. Selisistat**

The only SIRT1 inhibitor which has reached clinical trials is called selisistat which is an indole having carboxamide moiety which mimics the amide group of nicotinamide. It is a selective SIRT1 inhibitor with an  $IC_{50}$  value of 98 nM, which has completed phase I and II clinical trials for the treatment of Huntington's disease (Reilmann et al. 2014, Sussmuth et al. 2015, Westerberg et al. 2015).

### **1.12.2. Nicotinamide and Its Analogs**

Nicotinamide, is the endogenous inhibitor of all sirtuin isotypes (Luo et al. 2001, Bitterman et al. 2002) and it is formed as a result of both deacylation and ADP-ribosylation. It has an ability to inhibit human sirtuins with  $IC_{50}$  values ranging from 1.00 to 100  $\mu$ M based on its physiological concentrations.

### **1.12.3. Hydroxynaphthaldehyde Derivatives**

A hydroxynaphthaldehyde derivative called sirtinol which is a dual SIRT1/2 inhibitor (Yee et al. 2015) was identified by high-throughput phenotypic screen. Sirtinol was found to inhibit various classes of enzymes in vitro via aggregation or precipitation. In addition, sirtinol acts as an iron chelator in vitro in cultured leukemia cells. Another derivative cambinol can also inhibit both SIRT1 and SIRT2 (Yee et al. 2015) and was shown as a first sirtuin inhibitor to have anticancer effects in a xenograft mouse model (Heltweg et al. 2006). One of the most potent cambinol analog has an  $IC_{50}$  value of 1.00  $\mu$ M (Medda et al. 2009) to inhibit SIRT2.

#### **1.12.4. Kinase Inhibitors**

An idea suggesting adenosine mimesis of kinase inhibitors may also act on NAD<sup>+</sup>-dependent enzymes, revealed potential sirtuin inhibitors from several kinase inhibitor libraries. Hyperacetylation of the tubulin network was shown in A549 human lung adenocarcinoma cells as a result of treatment with molecule called Ro-31-8220 (Trapp et al. 2006). The first photoswitchable sirtuin inhibitor was discovered by combining sirtuin inhibiting bisindolylmaleimides with the photochromic diarylmaleimides. The “open” photoisomere of the molecule for SIRT2 inhibition was shown in cells (Falenczyk et al. 2014).

The compound GW5074 was attributed as c-Raf kinase inhibitor before its sirtuin inhibitory effects were found (Lackey et al. 2000). Derivatives of GW5074 based on its indolinone scaffold inhibit sirtuin isotypes SIRT1-3. Cellular effects of the kinase-derived sirtuin inhibitors should be evaluated not solely by sirtuin inhibition but also by indirect kinase inhibition.

#### **1.12.5. Sirtuin Rearranging Ligands (SirReals)**

In a library screening SirReal2 was discovered as highly potent and SIRT2-selective inhibitor leading to discovery of a new class of SIRT2 selective inhibitors. It was found that SirReal2 and other SirReal analogs have a unique inhibition mode causing structural rearrangement of the active site of SIRT2 upon ligand binding. Thus, these inhibitors are called as “sirtuin rearranging ligands” (SirReals). In cancer cell lines, lead structure was reported to increase tubulin acetylation via SirReal2 action (Rumpf et al. 2015).

#### **1.12.6. Structural Diverse Sirtuin Inhibitors**

Suramin which is a polyanionic naphthylurea and an antiprotozoal agent was found as a potent SIRT1 inhibitor (Howitz et al. 2003) after 100 years of its first discovery. Suramin analogs were reported to inhibit SIRT1 with an IC<sub>50</sub> value of 93 nM

and SIRT2 with an  $IC_{50}$  value of 407 nM (Trapp et al. 2007). Suramin also binds to SIRT5 according to co-crystallization assays (Schuetz et al. 2007).

Tenovins are also another type of sirtuin inhibitors. Lead structures tenovin-1 and its analog tenovin-6 inhibit SIRT1 and SIRT2 in a similar range. In addition to their tubulin and p53 hyperacetylation ability, they can also suppress the growth of xenograft tumors in mice.

### **1.13. Sirtuins as Therapeutic Targets for Cancer Stem Cells**

Sirtuin inhibition is a new area of potential therapeutic anticancer strategy. There are two classes of sirtuin inhibitors. First class contains nicotinamide (NAM) and thioacyllysine-containing compounds which are mechanism-based inhibitors. The other class contains indole derivatives as well as tenovin and its analogues, sirtinol and its analogues, splitomicin and its derivatives, which function with a noncovalent binding to the sirtuin active site and blocking of substrate binding (Heltweg et al. 2006, Ota et al. 2006, Lara et al. 2009, Rotili et al. 2012b).

Decrease in sirtuin activity was demonstrated as an important way for specifically targeting CSCs that are resistant to standard therapy. In vivo treatment of Tenovin-6 (a small-molecule inhibitor of SIRT1 and SIRT2) resulted in loss of imatinib-resistant chronic myeloid leukemia (CML)  $CD34^+$  stem cells. This result was achieved basically by SIRT1 inhibition providing elevated acetylated and total p53 levels (Li et al. 2012). Elimination of  $CD133^+$  ALL stem cells, decrease  $ALDH^+$  cells and tumorsphere formation in uveal melanoma cell lines by Tenovin-6 treatment was demonstrated (Jin et al. 2015, Dai et al. 2016).

### **1.14. p21 and p27 Cell Cycle Inhibitors**

Cyclin dependent kinase inhibitors are important elements in cell cycle checkpoints. They prevent replication and inheritance of damaged DNA to daughter cells by directing it to be repaired or directing cells to death. p21 is regulated by the tumor suppressor p53 and it is an effector molecule of p53. p53 binds to the promoter of p21 and activates it when needed. When p53 is inactivated, p21 expression levels are

decreased. Although p21 is regulated with p53 there are many p53-independent pathways such as MYC for its regulation. The function of p21 is also regulated by post-translational modifications. For instance, when Thr145 which is a nuclear localisation signal of p21 is phosphorylated p21 is transported to cytoplasm where it is inactivated.

p27 protein levels are higher during senescence and reduced during G1 and S phases of the cell cycle. p27 protein levels are decreased by proteolysis after they are labelled by phosphorylation for degradation. One of the proteolytic pathways of p27 is mediated by cyclin-E-CDK2 after phosphorylation of Thr187. After this event, p27 interacts with SKP2-dependent E3 ligase complex which is responsible for its degradation. Besides this mechanism, phosphorylation of Tyr88 can lead to Thr187 phosphorylation causing p27 degradation at the G1-S transition. Ser10 is the other phosphorylation site for p27. When Ser10 is phosphorylated during G1 phase, p27 is exported from nucleus and inactivated like p21 (Abukhdeir and Park 2009) (Figure 1.5).

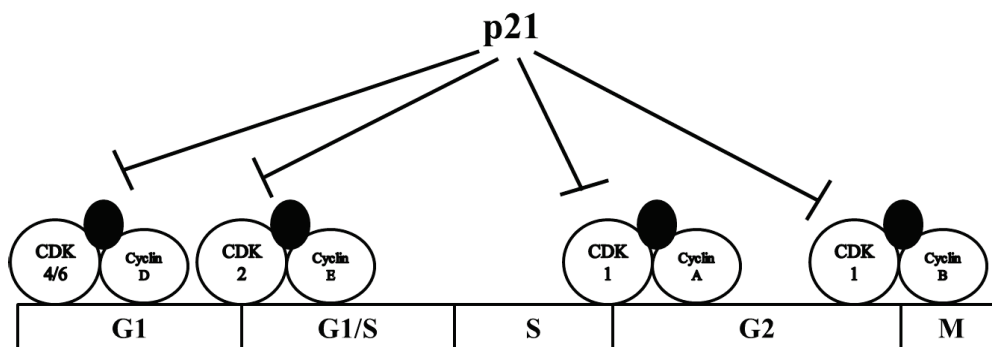


Figure 1.5. Roles of p21 and p27 in cell cycle regulation. (Adapted from Dutto et al. 2014)

### 1.15. p53 and MDM2 Pathway

Tumor suppressor p53 is a transcription factor which has important roles in cell cycle, apoptosis, DNA repair, senescence, angiogenesis, cellular metabolism and immune system (Teodoro et al. 2007, Fridman et al. 2003, Vousden et al. 2002). The function of p53 is inactivated in 50% of cancer cases due to mutations and deletions. In cancer cells, p53 which is not mutated is inactivated by its primary inhibitor murine double minute 2 (MDM2, in humans: HDM2). MDM2 is an oncoprotein and it was discovered with its higher expression in transformed mouse cell lines (Feki et al. 2004, Momand et al. 1992, Fakharzadeh et al. 1991-2000).

p53 binds to promoter of MDM2 gene and upregulates its expression. MDM2 directly binds to p53 and inhibits its expression with different mechanisms such as (1) inhibition of transactivation of p53 directly, (2) exports p53 to the outside of nucleus, (3) proteasomal degradation of p53 by E3 ubiquitin ligase activity (Freedman et al. 1999, Juven 1999, Wu 1993). Disruptions in the balance between p53/MDM2 forms malign tumors in healthy cells. For instance, overexpression of MDM2 accelerates tumor formation by causing growth in the cells and results in decreased therapeutic response (Bond et al. 2004, Oliner et al. 1992, Zhou et al. 2000, Rayburn et al. 2005, Momand et al. 1998, Gunther et al. 2000, Bond et al. 2005, Capoulade et al. 1998, Momand et al. 2000).

The acetylation level of p53 is increased in vivo significantly as a result of environmental stresses. It is shown that the stability of p53 is increased by acetylation (Ito et al. 2001). p53 is acetylated and ubiquitinated in the same residues in its carboxyl termini. This mechanism created an idea that states modifications compete for the same residues (Ito et al. 2001, Rodriguez et al. 2000). It is found that Sir2a (SIRT1) enzyme is resistant to Trichostatin A and dependent to NAD. It represses transcriptional activity of p53 by deacetylation (Luo et al. 2000, Juan et al. 2000, Luo et al. 2001). It is hypothesized that Sir2a (SIRT1) is responsible for rapid inactivation of the function of p53 when target genes of p53 is unnecessary.

The inhibition of MDM2 and p53 interaction has developed novel strategies for cancer treatment. It is found that the interaction between MDM2 and p53 is formed between 120 amino acids in MDM2 N-termini and transactivation region in p53 N-termini (Chen et al. 1993, Picksley et al. 1994). The MDM2-p53 interaction molecularly forms between Phe19, Trp23 and Leu26 amino acids which places in a hydrophobic region in MDM2 as illustrated in Figure 1.6. This hydrophobic region enables to design novel small molecules which are not peptide based to re-activate p53 protein. It is found that peptide based molecules would not be beneficial due to their insufficient penetration through cell membrane.

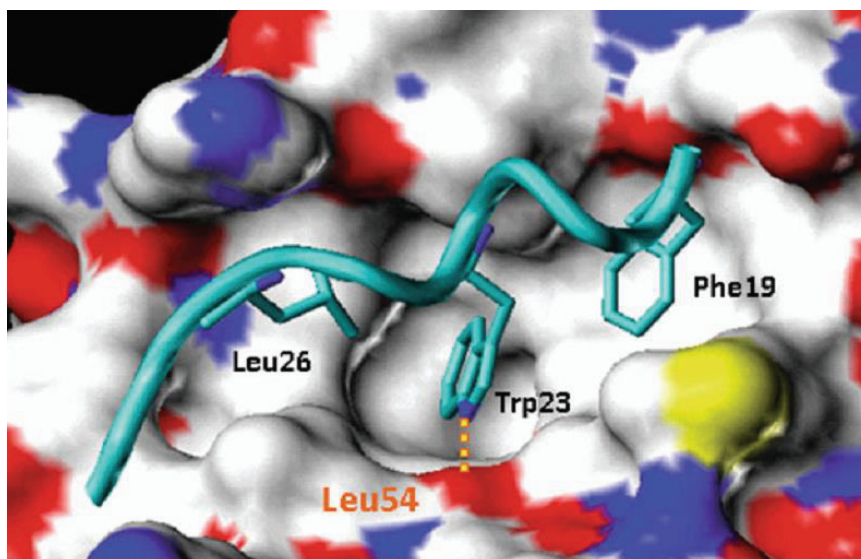


Figure 1.6. Crystal structure of MDM2 bound to p53

The most specific inhibitor developed is nutlins by Hoffman-La Roche laboratories. It is found that compound RG7112 which was developed by modifications on nutlins bind to MDM2 with a  $K_d$  value of 10.7 nM. The compound RG7112 is the first MDM2 inhibitor which was accepted for phase I clinical trials. It is reported that small molecule MDM2 inhibitors which are not peptide based are more than 1000 times potent compared to natural p53 peptides. Nutlins and the other MDM2 inhibitors show different cellular responses in both healthy cells and cancer cells (Vassilev et al. 2004, Shangary et al. 2008). In healthy cells, p53 activation causes cell cycle arrest but doesn't induce cell death. In some of cancer cell lines, p53 activation results in both cell cycle arrest and cell death. This situation shows that existence of wild type p53 is important for cancer cells but cell death can not be triggered by only this feature with MDM2 inhibitors.

MDM2 binds to p73, E2F-1, HIF-1a and Numb proteins with the same region (Lau et al. 2008, Ambrosini et al. 2007, LaRusch et al. 2007, Colaluca et al. 2008). MDM2 inhibitors that can bind to this region can inhibit binding of these abovementioned proteins to MDM2. It is found that Nutlin-3 inhibits the interaction between MDM2 and p73 (Lau et al. 2008), E2F-1 (Ambrosini et al. 2007) and HIF-1a (La Rusch et al. 2007).

Ito et al. found that acetylation interferes with ubiquitination mechanism and controls stability of p53. They also showed that MDM2 and HDAC1 forms a complex and manages acetylation status of p53 revealing the relation between ubiquitination and

acetylation. This relation is formed by overlapping lysine amino acids in p53 protein. It is shown that MDM2 selectively binds to HDAC1. It is found that simultaneously expressed MDM2 and HDAC1 with low levels don't have significant effects on the acetylation status of p53. It is concluded that MDM2 and HDAC1 works simultaneously for p53 deacetylation.

The activity of HDAC1 with decreased expressions can be triggered by MDM2 existence. This situation indicates that MDM2 coordinates HDAC1 and p53 protein complex. It is found that MDM2 controls the activity of HDAC1 to p53. According to this hypothesis, deacetylase activity of HDAC1 is increased by increased expressions of MDM2 by p53.

HDAC1 is not the only factor that is responsible for regulation of p53 acetylation. There are evidence for deacetylation of p53 in the cytoplasm more than HDAC1 which mostly functions in nucleus. The most important of this evidence is NAD-dependent and Trichostatin A-resistant Sir2a (SIRT1).

### **1.16. p53 and SIRT1**

SIRT1 deacetylates both histone proteins such as H1, H3 and H4 and also non-histone proteins including p53, FOXO, Ku70, p300, Rb, E2F1, NF- $\kappa$ B, p73 and PGC-1 $\alpha$  (Brooks et al. 2009, Deng et al. 2009). SIRT1 has a role in the two types of known p53-mediated apoptotic pathways, p53 transcription-dependent apoptosis and p53 transcription-independent apoptosis. The first mechanism includes apoptosis-related target genes like BAX, PUMA, and NOXA. p53 transcription-independent apoptosis requires interaction between mitochondrial p53 and antiapoptotic BCL proteins to initiate the release of cytochrome c from the mitochondrial intramembrane (Erster et al. 2004).

It is considered that SIRT1 can redirect p53 from the cytosol to the mitochondria under increased ROS conditions resulting in transcription-independent p53-induced apoptosis (Figure 1.7). It seems that activity levels of SIRT1 might regulate cell fate by p53 deacetylation. It is known that SIRT1 deacetylation can block nuclear translocation providing increased cytosolic p53 accumulation resulting in p53 translocation to mitochondria. Thus, SIRT1 can block p53 transcription-dependent apoptosis and increase p53-mediated transcription-independent apoptosis.



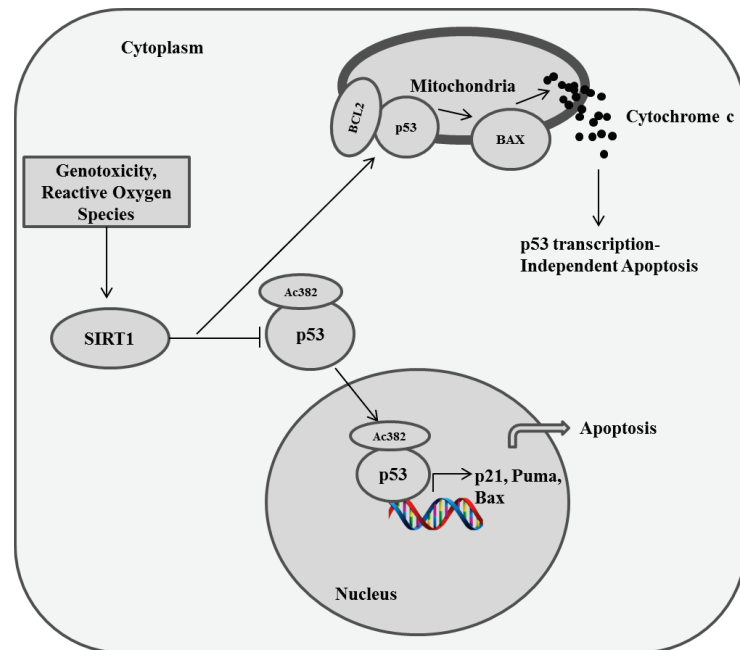


Figure 1.7. SIRT1 triggers p53 transcription-independent apoptosis. In mouse embryonic stem cells, intracellular ROS increases cytoplasmic SIRT1 protein. SIRT1 binds and deacetylates p53 at K379 (human K382) and prevents nuclear translocation of p53. Deacetylated p53 translocates onto the mitochondrial outer-membrane and provides the release of proapoptotic BCL protein BAX as a result of interaction with anti-apoptotic BCL proteins including BCL2, BCLx1. Activated BAX provides the release of cytochrome c from mitochondria to cytoplasm initiating transcription-independent apoptosis. (Adapted from O'Callaghan et al. 2017)

It is shown that SIRT1 knockout mice have p53 hyperacetylation. Moreover, inhibition of SIRT1 activity using sirtinol causes senescence-like cell growth arrest including decreased Ras-MAPK signaling in various human cancer cells (Cheng et al. 2003). Reduction in SIRT1 levels triggers acetylation of p53 resulting in cell cycle arrest, DNA repair and apoptosis. It is found that tenovins inhibit deacetylase activity of SIRT1 and SIRT2 significantly increasing acetylation level of p53K382, histoneH4K16 and tubulinK40.

SIRT1 is responsible for repression of p53-dependent transactivation in tumors. p53 binds to SIRT1 promoter and represses SIRT1 transcription (Yi et al. 2010). In conclusion, p53 is a member of this feedback circuit either to regulate SIRT1 expression and the p53 response. SIRT1 deacetylates H3K9 of target gene promoters such as p21, GADD45, PCNA causing gene silencing and deacetylated chromatin formation (Figure 1.9).

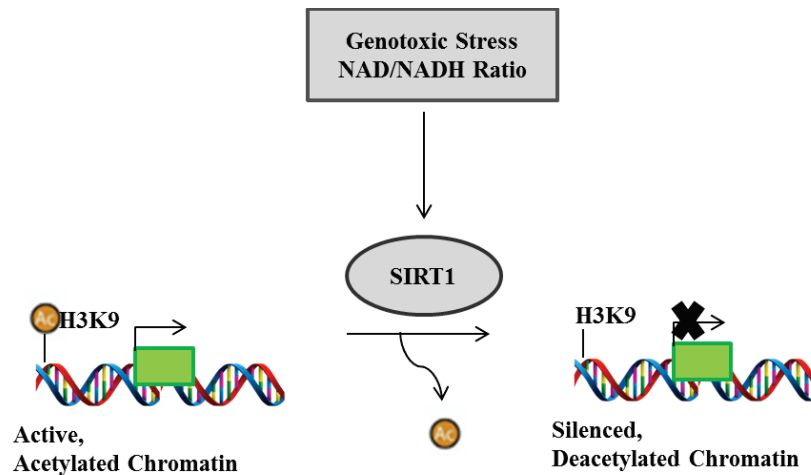


Figure 1.8. SIRT1 causes gene silencing by H3K9 deacetylation of target gene promoters.

SIRT1 is responsible of deacetylation of different substrates like histones (H4, H3 and H1) and non-histone proteins. These non-histone substrates can be a) histone modifying enzymes (p300, SUV39H1, PCAF and TIP60), b) transcription factors (p53, nuclear factor (NF- $\kappa$ B), p73, forkhead transcription factors FOXO1, FOXO3a, Myc, hypoxia-inducible transcription factors (HIF)-1a and HIF2-a), c) cell signaling modifiers and enzymes (AKT), d) DNA repair modulators (Ku70, WRN, NBS1, APE1), e) regulators of metabolism, circadian clock (PGC-1a, PER2) (Houtkooper et al. 2012, Saunders et al. 2007).

SIRT1 provides both constitutive heterochromatin (CH) and facultative heterochromatin (FH) formation. SIRT1 induces methyl-transferases activity promoting the methylation of CpG islands (Yao et al. 2014). Lack of SIRT1 prevents both heterochromatin marks (H3K79me3) to spread and heterochromatin protein 1 (HP1) to localize (Vaquero et al. 2004). Inhibition of SIRT1 reactivates silenced tumor suppressor genes in cancer cell without loss of promoter hypermethylation (Pruitt et al. 2006).

DNA signaling and repair are also regulated by SIRT1. In the repair mechanism of single strand breaks (SSBs), the nucleotide excision repair (NER) pathway is regulated by SIRT1. SIRT1 also deacetylates several DNA repair factors like X-ray repair cross complementing gene 4 protein (XRCC4p) (Gao et al. 2000); Ku70 (Jeong et al. 2009); Werner's Syndrome protein (WRN) (Li et al. 2008). SIRT1 has a function in binding and modifying of Nijmegen breakage syndrome protein (NBS1) which is a

regulatory component of the MRE11-Rad51-NBS (MRN) nuclear complex that senses the early stages of double strand break (DSB) (Yuan et al. 2007, Yuan et al. 2007).

SIRT1 translocates p53 from cytosol to the mitochondria under increased ROS conditions. p53 accumulation in mitochondria triggers transcription-independent apoptosis. In conclusion, oxidative stress determines cell fate through SIRT1-mediated p53 deacetylation (Yi et al. 2010).

Overexpression of SIRT1 is found in human hepatocellular carcinoma (HCC). Only SIRT1 is overexpressed in human HCC cell lines (Hep3B, HepG2, HuH-7, HLE, HLF, HepKK1, skHep1) among other sirtuin family members compared with normal hepatocytes.

Inhibition of SIRT1 activity promotes cytostatic effect, impaired proliferation, an increased differentiation markers expression and cellular senescence. In vivo studies revealed that knockdown of SIRT1 provides 50% fewer animals developing tumors and treatment with a sirtuin inhibitor called cambinol provides overall lower tumor burden.

HCC cells express poorly differentiated markers glypican (GPC3) and  $\alpha$ -fetoprotein (AFP) and lack of the epithelial marker E-cadherin (CDH1). Loss of SIRT1 result in a decrease in AFP and GPC3 and an increase in E-cadherin (CDH1) mRNA expression levels.

In vivo bioluminescent imaging revealed that 80% of control mice develops tumors after day 11 whereas 33% of mice that are SIRT1 knocked down formed tumor up to 30 days. Repression in tumor cell growth in HCC animal models as a result of SIRT1 inhibition was an achievement to propose SIRT1 as a novel target for cancer therapy. All indicated HCC cell lines wild-type (HepG2), null (Hep3B) or mutated (HuH-7), regardless of their p53 status, overexpresses SIRT1 and their proliferations were inhibited after SIRT1 inhibition (Portmann et al. 2013).

### **1.17. CRM1 and p53**

Nuclear exporter chromosome region maintenance 1 (CRM1, also known as exportin 1 or XPO1) protein is the mediator of over 230 identified cargos including proteins and RNAs (Xu et al. 2012). CRM1 is also characterized as a ubiquitous nuclear export receptor protein of the karyopherin- $\beta$  family, which is responsible for the export of specific NES containing cargo proteins from nucleus to cytoplasm (Fornerod et al.

1997, Fukuda et al. 1997, Ossareh-Nazari et al. 1997). Overexpression of CRM1 and its influence on poor prognosis of the malignancies were characterized in solid tumors (e.g. pancreatic, ovarian, cervical, renal carcinomas, osteosarcomas and gliomas) (Noske et al. 2008, Huang et al. 2009, Shen et al. 2009, van der Watt et al. 2009, Yao et al. 2009, Inoue et al. 2013) and hematological malignancies (e.g., chronic myeloid/lymphoid leukemia (CML/CLL), acute myeloid/lymphoid leukemia (AML/ALL), mantle cell lymphomas (MCL) and multiple myeloma (MM)) (Sakakibara et al. 2011, Lapalombella et al. 2012, Ranganathan et al. 2012, Etchin et al. 2013a, 2013b; Kojima et al. 2013, Schmidt et al. 2013, Walker et al. 2013, Zhang et al. 2013, Tai et al. 2014, Yoshimura et al. 2014).

CRM1 exports some important tumor suppressors (e.g., p53, p73 and FOXO1), anti-apoptotic proteins (e.g., NPM and AP-1) and growth regulator/pro-inflammatory proteins (e.g., p21, p27, Rb, BRCA1, IκB and APC) as shown in the Table 1.3 below, which is a brief summary of the database: <http://prodata.swmed.edu/LRNes/> (Kau et al. 2004, Turner et al. 2012, Xu et al. 2012).

Table 1.3. Important cargo proteins of CRM1

AMPK $\alpha$ 2	E2F1	HPV11 E1	p21Cip1	PARP-10	Snail
BMAL1	Foxo3	HPV16 E7	p28GANK	PCNA	Sox10
BRCA1	Foxa2	hRio2	p37 protein of ASFV	PDK-1	SOX9
BRCA2	HDAC1	hTERT	p38 (p40)	Rev	STAT1
COP1	HDAC4	I $\kappa$ B $\alpha$	p53	SIRT1	STAT3
Cyclin B1	HDAC5	I $\kappa$ B $\epsilon$	p73	SIRT2	survivin
Cyclin D1	HDM2	MAPKAP kinase 2 (MK2)	PAK4	Smad4	Topoisomerase II-alpha
E2F-4	HIV-REV	NANOG	PAK5	Smurf1	Topoisomerase II-beta

It is considered that CRM1 inhibitors can block the aberrant export of related proteins and RNAs from nucleus into cytoplasm providing increased nuclear retention of tumor-suppressors and transcriptional factors resulting in death of cancer cells (Figure 1.9).

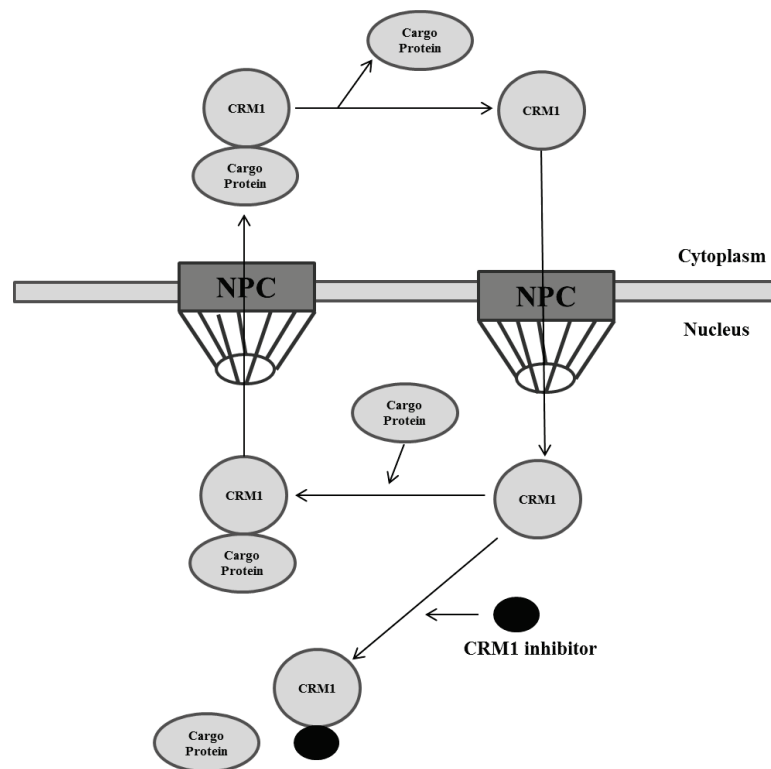


Figure 1.9. Nuclear export of cargo proteins is initiated by binding of CRM1 with nuclear export signal (NES) of the related protein.

CRM1, as other nuclear import receptors like importin-7, is positively regulated by MYC and negatively regulated by p53 (Golomb et al. 2012) affecting ribosomal biogenesis. There are some CRM1 inhibitors that inactivate cysteine 528 including ratjadone analogs, synthetic leptomyacin B derivatives and selective inhibitors of nuclear export (SINE).

Goniothalamine is a styryl lactone and extracted from plants of the genus *Goniothalamus* (Jewers et al. 1974, Gademann et al. 2011). Goniothalamine is known as inhibitor of nucleocytoplasmic transport above the concentration of 500 nM, which was showed by immunostaining of Rio2 in HeLa cells. It has a cytotoxicity with an  $IC_{50}$  of  $\sim 1.50 \mu\text{M}$  in breast cancer cells (Wach et al. 2010).

Topoisomerase converts supercoiled structure of DNA into a relaxed form by making strand breaks. Type I topoisomerases form single strand breaks while type II form double stranded breaks. Retaining topoisomerases in the nucleus is crucial to form double stranded DNA breaks in a cancer cell (Champoux et al. 2001).

Drug resistance during successful chemotherapy is a major problem in cancer therapy. Some of the resistances are caused by export of topoisomerases from nucleus to the cytoplasm. Topoisomerase II $\alpha$  should be retained in the nucleus to form

permanent double stranded breaks. Combination of CRM1 inhibitors with chemotherapeutics can resensitize cancer cells to related drug molecule (Yu et al. 1997, Turner et al. 2012, El-Tanani et al. 2016).

Table 1.4. Differential subcellular localizations of proteins in human cancers

Protein	Function	Cancer	Normal Localization	Mislocation
FOXO	Transcription factor	Various types of cancer	Nucleus	Cytoplasm
$\beta$ -catenin	Wnt signaling	Colorectal cancer	Cytoplasm	Nucleus
p53	Transcription factor	Various types of cancer	Nucleus	Cytoplasm
BARD1	BRAC1 interacting protein	Breast cancer	Cytoplasm	Nucleus
BRAC1	DNA repair	Breast cancer	Cytoplasm	Nucleus
NF- $\kappa$ B	Transcription factor	Various types of cancer	Cytoplasm	Nucleus
p21WAF1	Cell cycle inhibitor	CML, ovarian, breast	Nucleus	Cytoplasm
p27KIP	Cell cycle inhibitor	AML, breast	Nucleus	Cytoplasm
RUNX3	Transcription factor	Gastric cancer	Nucleus	Cytoplasm
Rb	E2F binding protein	Various types of cancer	Nucleus	Cytoplasm
HIF-1 $\alpha$	Transcription factor	Breast, prostate cancer	Cytoplasm	Nucleus
PTEN	Phosphatase	Various types of cancer	Nuc/Cyto	Cytoplasm
BCR-ABL	Kinase	CML	Nuc/Cyto	Cytoplasm

Wild-type p53 can be inactivated by abnormal cytoplasmic localization (Yu et al. 1997, Turner et al. 2012) although its total functions including DNA binding ability remain intact. It can be activated by relocating the protein into the nucleus. p53 is a NLS and NES signals containing protein and can be mediated via importin- $\alpha/\beta$  and CRM1 (Hill et al. 2014).

### 1.18. (R)-4'-methylklavuzon

It was synthesized by Ali Çağır's group in 2009 (Figure 1.10) and its cytotoxic effects was demonstrated on PC3 and MCF-7 cell lines (Kasaplar et al. 2009). Its intracellular working mechanism was studied on HTC116 p53<sup>+/+</sup> and HTC116 p53<sup>-/-</sup> cell lines by performing cell cycle and apoptosis assays and it was found that there was G1 arrest and induction of apoptosis depending on the dose on HTC116 p53<sup>+/+</sup>. It has been shown that (R)-4'-methylklavuzon increases expression of p53 gene in HTC116 p53<sup>+/+</sup> cells at a concentration of 100 nM as seen in Figure 1.11. It has been observed that pNBS1 (phosphorylated Nijmegen Breakage Syndrome) which is responsible for

repair of double stranded DNA breaks was upregulated in p53<sup>-/-</sup> whereas it was downregulated in p53<sup>+/+</sup> cells. It is hypothesized that DNA breaks are formed and cells are directed to apoptosis (Metz 2013).

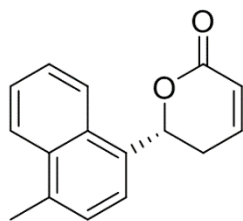


Figure 1.10. Structure of (*R*)-4'-methylklavuzon

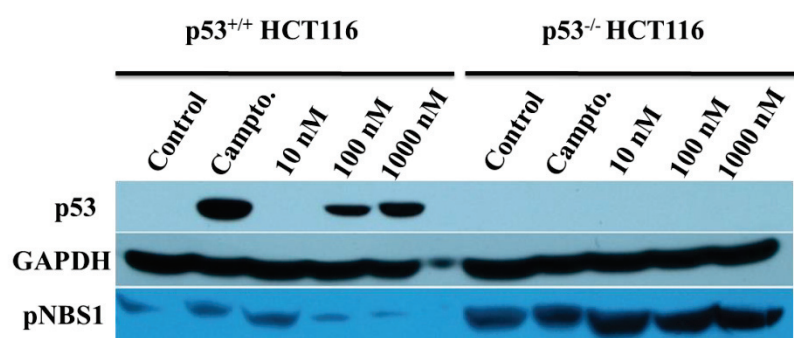


Figure 1.11. p53 and pNBS1 expression analysis of (*R*)-4'-methylklavuzon

## 1.19. The Aim of the Study

In this study, anti-cancer properties of (*R*)-4'-methylklavuzon were investigated for the treatment of liver cancer. Effects of the (*R*)-4'-methylklavuzon was tested on both hepatocellular carcinoma cells (HuH-7 parental) and hepatic cancer stem cells (HuH-7 EpCAM<sup>+</sup>/CD133<sup>+</sup>) that are enriched from the parental cells.

Inhibitory effects of (*R*)-4'-methylklavuzon against Class I/II histone deacetylases and sirtuins were also investigated. Consequences like decreased cell viability, arrest in G1 phase, inhibition of HDACs/sirtuins, upregulation of p21 gene expression and increased acetylation/methylation of histone proteins as a result of HDACs/sirtuin inhibition were aimed to be shown.

Secondary aim of this thesis was to show upregulation of p53 protein levels in HuH-7 and HepG2 cells. Moreover CRM1 and MDM2 inhibitory properties of (*R*)-4'-methylklavuzon were determined in HuH-7 and HepG2 cells.

## CHAPTER 2

### MATERIALS AND METHODS

#### 2.1. Cell Culture

Cells were kindly provided by Prof. Dr. Esra ERDAL from Izmir International Biomedicine and Genome Institute. Cell populations (HuH-7 parental, EpCAM<sup>+</sup>/CD133<sup>+</sup>, EpCAM<sup>-</sup>/CD133<sup>-</sup> and HepG2) were cultivated in DMEM (Dulbecco's Modified Eagle Medium) containing 10% FBS, 1% penicillin-streptomycin, 1% L-Glutamine, 1% Non-Essential Amino Acid Solution in a humidified 5% CO<sub>2</sub> incubator at 37°C.

#### 2.2. Isolation of Cancer Stem Cells by Magnetic Cell Separation (MACS)

A commercial kit from Miltenyi Biotec. was used to isolate cancer stem cells from HuH-7 parental cells based on the surface markers called CD133 and EpCAM using specific antibodies. EpCAM<sup>+</sup>/CD133<sup>+</sup> cell population which is accepted as cancer stem cells in HuH-7 cell line was separated from EpCAM<sup>-</sup>/CD133<sup>-</sup> cell population via magnetic cell separation method.  $10 \times 10^7$  cells were suspended in 500  $\mu$ l MACS Buffer (5% Fetal Bovine Serum and 2 mM EDTA in PBS) and filtered primarily with 100  $\mu$ m filter (BD Falcon, 352360) and then 40  $\mu$ m filter (BD Falcon, 352340).

Filtered cells were centrifuged at +4°C and 2500 rpm followed by resuspension in 300  $\mu$ l MACS buffer and combined with 100  $\mu$ l FcR blocking reagent (Miltenyi, 130-059-901) to prevent nonspecific bindings. EpCAM-FITC antibody (anti-EpCAM-FITC, miltenyi 130-080-301) was added in a ratio of 1/10 (v/v) in total and incubated at +4°C for 10 minutes in the dark. After antibody labelling, cells were washed twice with MACS buffer and centrifuged at 2500 rpm and +4°C to remove unbound antibodies. EpCAM labelled cells were suspended in 300  $\mu$ l MACS buffer and 40  $\mu$ l of anti-FITC (anti-FITC microbead, miltenyi 130-048-701) magnetic beads were added into 400  $\mu$ l



mixture in total. Cells were incubated with magnetic beads at +4°C for 12 minutes in the dark and were washed twice with MACS buffer.

The cell suspension was applied onto positive separating columns (Miltenyi, 130-042-401) followed by the immobilization of labelled cells in the column while unlabelled cells flow through the column. EpCAM<sup>-</sup> cells were applied to negative separating columns (Miltenyi, 130-042-901) to separate them from all the remaining EpCAM<sup>+</sup> cells. Cells in the positive selection column were obtained by turning the magnetic field off and washing steps. Same procedures were applied for CD133 surface marker using specific antibody (anti-CD133-APC, miltenyi 130-090-826) and micro bead (anti-APC microbead, miltenyi 130-090-855 ). At the end of the experiment, EpCAM<sup>+</sup>/CD133<sup>+</sup> and EpCAM<sup>-</sup>/CD133<sup>-</sup> cell populations were obtained. Percentages of EpCAM and CD133 expressions of three cell populations (parental, EpCAM<sup>+</sup>/CD133<sup>+</sup> and EpCAM<sup>-</sup>/CD133<sup>-</sup> ) were analyzed by using using flow cytometer (FACS Canto II, BD) for purity check. Cells sorted by MACS were used in cell viability, cell cycle analysis, apoptosis analysis and p21/p27 gene expression analysis. Percentage of positivity in EpCAM<sup>+</sup>/CD133<sup>+</sup> was 85.9% and negativity was 5.3%. Percentage of positivity and negativity in parental cells was 10.6% and 52.8%, respectively. Percentage of positivity and negativity in EpCAM<sup>-</sup>/CD133<sup>-</sup> cells was 12.4% and 42.9%, respectively.

### **2.3. Cell Viability Assay**

2000 cells were inoculated into each well of 96-well plate and incubated overnight. Cells were treated with 20, 10, 5.00, 2.50, 1.25, 0.625 and 0.10 µM of (*R*)-4'-methylklavuzon for 24, 48 and 72 hours. The control cells were treated with only DMSO at 1% final concentration as drug treated cells received. After the incubation, cells were treated with MTT (3-(4,5-Dimethylthiazol-2-yl)-2,5-Diphenyltetrazolium Bromide) reagent (Sigma, M5655) and incubated for 4 hours at 37°C in a humidified 5% CO<sub>2</sub> incubator. After 4 hours, plates were centrifuged for 10 minutes at 1800 rpm and supernatant was discarded. 100 µl/well of DMSO was added and plates were shaken orbitally for 15 minutes. Absorbance measurement was performed at 570 nm by using an automatic plate reader (Thermo, Varioskan). All experiments were repeated thrice in triplicates.

## 2.4. Cell Cycle Analysis

60,000 cells/well were inoculated into 6-well plates and incubated overnight. 10, 1.00 and 0.10  $\mu\text{M}$  of (*R*)-4'-methylklavuzon were applied to the cells and incubated for 24, 48 and 72 hours. The control cells were treated with only DMSO at 1% final concentration as drug treated cells received. After incubations, cells were harvested, washed with PBS and centrifuged at 800 rpm for 10 minutes. Cell pellet was resuspended in 1 ml of ice-cold PBS. Ice-cold absolute ethanol was added onto the pellet suspension dropwise while vortexing. Cells were fixed at  $-20^{\circ}\text{C}$  for 24 hours. After fixation, cells were centrifuged at 1200 rpm for 10 minutes, washed with PBS and centrifuged again. Pellet was resuspended in 200  $\mu\text{l}$  of 0.1% Triton X-100 in PBS and was treated with 20  $\mu\text{L}$  of RNaseA (200  $\mu\text{g}/\text{ml}$ ) and incubated at  $37^{\circ}\text{C}$  under 5%  $\text{CO}_2$  for 30 minutes. After incubation, 20  $\mu\text{L}$  of propidium iodide (1  $\text{mg}/\text{ml}$ ) was added into cell suspensions and incubated for 15 minutes at room temperature. Cell cycles were analyzed by a collection of 10000 events using flow cytometer (BD FACS Canto II, BD) and ModFit LT statistics software. All experiments were repeated thrice in triplicates.

## 2.5. Apoptosis Analysis

Effects of (*R*)-4'-methylklavuzon on apoptosis were investigated using Annexin V-FITC commercial kit (Biovision, K101-100). 60,000 cells/well were inoculated into 6-well plate and incubated overnight. Cells were treated with 10, 1.00 and 0.10  $\mu\text{M}$  of (*R*)-4'-methylklavuzon for 24, 48 and 72 hours. The control cells were treated with only DMSO at 1% final concentration as drug treated cells received. After incubations, cells were harvested, washed with PBS and centrifuged at 800 rpm for 5 minutes at  $+4^{\circ}\text{C}$ . Cell pellet was resuspended in 250  $\mu\text{L}$  of binding buffer provided with the kit. 2.5  $\mu\text{L}$  of Annexin V-FITC and 2.5  $\mu\text{L}$  of propidium iodide were added to that suspension and incubated for 5 minutes in the dark. Apoptosis analysis was performed by a collection of 10000 events using flow cytometer (BD FACS Canto II, BD). All experiments were repeated thrice in triplicates.

## 2.6. Cell Viability Assay of (*R*)-4'-methylklavuzon Derivatives

2000 cells were inoculated into each well of 96-well plate and incubated overnight. Cells were treated with 20, 10, 5.00, 2.50, 1.25, 0.625 and 0.10  $\mu\text{M}$  of (*R*)-4'-methylklavuzon derivatives for 24, 48 and 72 hours. The control cells were treated with only DMSO at 1% final concentration as drug treated cells received. After the incubation, cells were treated with MTT (3-(4,5-Dimethylthiazol-2-yl)-2,5-Diphenyltetrazolium Bromide) reagent (Sigma, M5655) and incubated for 4 hours at 37°C in 5% CO<sub>2</sub> incubator. After 4 hours, plates were centrifuged for 10 minutes at 1800 rpm and supernatant was discarded. 100  $\mu\text{l}$ /well of DMSO was added and plates were shaken orbitally for 15 minutes. Absorbance measurement was performed at 570 nm by using an automatic plate reader (Thermo, Varioskan). All experiments with MIA-PaCa2 cells were repeated thrice in triplicates and all experiments with HPDEC cells were repeated thrice in duplicate.

## 2.7. In vitro Histone Deacetylase Enzyme Activity Measurement

Inhibitory effects of (*R*)-4'-methylklavuzon on histone deacetylases in hepatocellular carcinoma cells were investigated by using a commercial kit based on fluorescence measurement (Cayman, Flour De Lys, 10011563). The basic mechanism includes addition of an acetylated lysine to protein sample that has HDAC activity and measurement of deacetylated lysine after treatment with the solution provided with the kit. Fluorescence was measured at 360 nm excitation wavelength and 460 nm emission wavelength with a plate reader (Thermo, Varioskan). Class I and Class II HDAC activity was analyzed using this kit. Entire protocol includes nucleus isolation, protein isolation from nucleus, analysing samples with positive control that is recombinant HDAC1 and Trichostatin A (TSA) molecule. Results were analyzed by using the standard curve plotted on a graph. Protein samples isolated from cell populations were treated with 81, 27, 9.00, 3.00, 1.00, 0.50 and 0.10  $\mu\text{M}$  of (*R*)-4'-methylklavuzon. All experiments were repeated in triplicates.

## 2.8. Cell-based Histone Deacetylase Enzyme Activity Measurement using Cells Sorted by MACS

Inhibitory effects of (*R*)-4'-methylklavuzon on endogenous histone deacetylases inside the hepatocellular carcinoma cells were investigated using a commercial kit called cell-based HDAC activity assay kit (Cayman, 600150). According to the protocol, 10,000 cells/well were inoculated into the black 96-well plates and incubated overnight. Cells were treated with 5.00, 3.00, 1.00, 0.50, 0.25 and 0.10  $\mu\text{M}$  concentrations of (*R*)-4'-methylklavuzon. The control cells were treated with only DMSO at 1% final concentration as drug treated cells received. After drug treatment, plate was centrifuged at 500 g for 5 minutes. Medium was removed and 200  $\mu\text{L}$  of assay buffer was added and plate was centrifuged again at 500 g for 5 minutes. HDAC substrates called Boc-Lys(Ac)-7-Amino-4-Methylcoumarin (Boc-Lys(Ac)-AMC) (Figure 2.1) for samples and Trichostatin A (TSA) for positive controls were added to the plate and incubated for 2 hours at 37°C under 5% CO<sub>2</sub>.

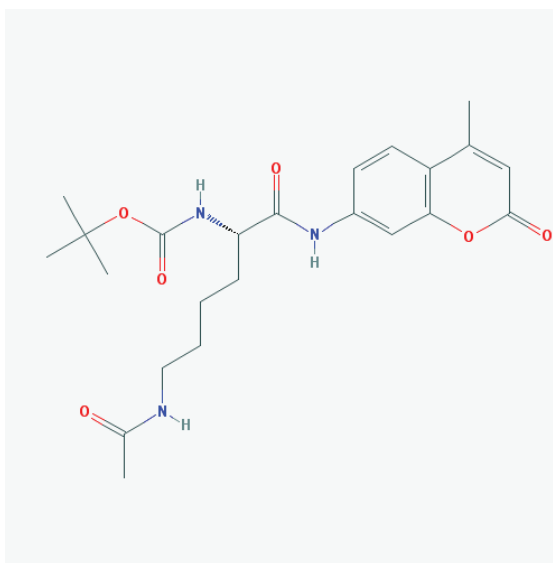


Figure 2.1. HDAC substrate which is named ‘Boc-Lys(Ac)-AMC’ and provided with Cell-based Histone Deacetylase (HDAC) Enzyme Activity Kit.

Lysis/Developer solution was added into each well and fluorescence measurement was carried out at 360 excitation wavelength and 460 emission wavelength by using a plate reader (Thermo, Varioskan). Results were analyzed using standard curve plotted on a graph. All experiments were repeated in triplicates.

## **2.9. Isolation of Cancer Stem Cells by Fluorescence-Activated Cell Sorting (FACS)**

A minimum of  $60 \times 10^6$  cells were harvested with trypsin and centrifuged at 1500 rpm for 5 minutes. Pellet was washed with 10 ml of sterile FACS buffer (1 mM EDTA, 25 mM HEPES, 1% FBS in 1X PBS). Cells were filtered with firstly 100  $\mu\text{m}$  filter (BD Falcon, 352360) followed by 40  $\mu\text{m}$  filter (BD Falcon, 352340) to obtain single cells. Cells were counted by using hemacytometer after filtration and centrifuged at 1500 rpm for 5 minutes and labelled with EpCAM (anti-EpCAM-FITC, miltenyi 130-080-301) and CD133 antibody antibody (anti-CD133-APC, miltenyi 130-090-826) (1:11 dilution) including FcR blocking reagent (Miltenyi, 130-059-901) to prevent nonspecific bindings. Cells were incubated with antibodies at  $+4^\circ\text{C}$  for 10 minutes in the dark. After incubation, cells were washed with FACS buffer and centrifuged at 1500 rpm for 5 minutes to remove unbound antibodies. Cells were aliquoted as  $20 \times 10^6$  cells in 2 ml FACS buffer and 0.5  $\mu\text{M}$ /1 ml DAPI (4.4  $\mu\text{l}$  from 80  $\mu\text{g}/\mu\text{l}$  stock) was added to quantify dead cells. EpCAM<sup>+</sup>/CD133<sup>+</sup> and EpCAM<sup>-</sup>/CD133<sup>-</sup> cells were sorted using flow cytometer (FACS Aria III, BD). Cells sorted by FACS were used in cell-based HDAC enzyme activity assay and trimethylation analysis of H3K27. Percentage of positive cells were analyzed as 97% according to the selected gating.

## **2.10. Cell-based Histone Deacetylase Enzyme Activity Measurement using Cells Sorted by (FACS)**

Inhibitory effects of (*R*)-4'-methylklavuzon on endogenous histone deacetylases inside the hepatocellular carcinoma cells were investigated using a commercial kit called cell-based HDAC activity assay kit (Cayman, 600150). According to the protocol, 10,000 cells/well were inoculated into the black 96-well plates and incubated overnight. Cells were treated with 5.00, 3.00, 1.00, 0.50, 0.25 and 0.10  $\mu\text{M}$  concentrations of (*R*)-4'-methylklavuzon. The control cells were treated with only DMSO at 1% final concentration as drug treated cells received. After drug treatment, plate was centrifuged at 500 g for 5 minutes. Medium was removed and 200  $\mu\text{L}$  of assay buffer was added and plate was centrifuged again at 500 g for 5 minutes. HDAC substrates called Boc-Lys(Ac)-7-Amino-4-Methylcoumarin (Boc-Lys(Ac)-AMC) (Figure 2.1) for samples and Trichostatin A (TSA) for positive controls were added to

the plate and incubated for 2 hours at 37°C under 5% CO<sub>2</sub>. Lysis/Developer solution was added into each well and fluorescence measurement was carried out at 360 excitation wavelength and 460 emission wavelength by using a plate reader (Thermo, Varioskan). Results were analyzed using standard curve plotted on a graph. All experiments were repeated in triplicates.

## 2.11. In Vitro HDAC1 Enzyme Activity Measurement

Inhibitory effects of (*R*)-4'-methylklavuzon on HDAC1 enzyme were investigated using a commercially available fluorescence based HDAC1 Fluorometric Drug Discovery Kit (Enzo, Fluor De Lys, BML-AK511). The HDAC1 Fluorimetric Drug Discovery Kit is based on the combination of the Fluor de Lys®-“SIRT1” (p53 379-382) Substrate and Developer II.

The assay procedure has two steps. First, the Fluor de Lys®-“SIRT1” Substrate, which contains an acetylated lysine side chain, is incubated with HDAC1 enzyme. Deacetylation of the substrate sensitizes the substrate and in the second step, treatment with the Fluor de Lys® Developer II produces a fluorophore. Despite the substrate's name (it was first developed as a SIRT1 substrate), Fluor de Lys®-“SIRT1” is an excellent substrate for HDAC1 ( $K_m = 19.3 \mu\text{M}$ ). Trichostatin A (TSA) was used as a positive control.

Inhibitory effect of (*R*)-4'-methylklavuzon on HDAC1 enzyme was tested by combining 7.5 unit/well enzyme with 1.00  $\mu\text{M}$ , 50  $\mu\text{M}$  and 100  $\mu\text{M}$  of drug candidate. HDAC1 was pre-treated with the drug candidate for 2 minutes before addition of substrate. Enzyme and (*R*)-4'-methylklavuzon was incubated for 1 hour at 37°C in the presence of 20  $\mu\text{M}$  Fluor de Lys Substrate. After incubation, developer solution that is supplied with the kit was added and incubated for 45 minutes at room temperature.

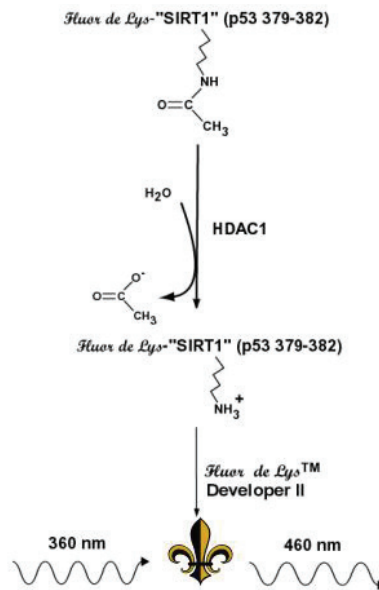


Figure 2.2. Reaction mechanism of Fluor de Lys-SIRT1 substrate by HDAC1 enzyme

Fluorescence was measured at 360 nm excitation wavelength and 460 nm emission wavelength with a plate reader (Thermo, Varioskan) (Figure 2.2). Results were analyzed by using the standard curve plotted on a graph. All experiments were repeated thrice in triplicates.

## 2.12. Histone Extraction and Acetylation and Methylation Analysis of H3K27 Residue by Western Blotting

$5 \times 10^5$  Cells/well were seeded in tissue culture petri dishes and incubated overnight. (R)-4'-methylklavuzon was applied to the cells at various concentrations and incubated for 72 hours. The control cells were treated with only DMSO at 1% final concentration as drug treated cells received. Histone proteins were isolated from three cell populations after (R)-4'-methylklavuzon treatment to analyze acetylation and trimethylation status of histone 3 lysine 27 by western blotting. Briefly, cells were washed with ice-cold PBS and scraped from cell culture dishes then centrifuged at 3000 g and +4°C for 10 minutes. Pellets were washed with ice-cold PBS containing 5 mM sodium butyrate. Cell pellets were lysed by suspending in ice-cold triton extraction buffer (TEB) containing 0.5% Triton X-100, 2 mM PMSF, 0.02% NaN<sub>3</sub> in a ratio of  $1 \times 10^7$  cells/ml for 10 minutes. Lysates were centrifuged at 2000 rpm and +4°C for 10 minutes then supernatant was discarded and pellets were resuspended in TEB and centrifuged again. Pellets were resuspended in 0.2 N HCl in a ratio of  $4 \times 10^7$  cells/ml

and incubated +4°C for 16 hours by gentle mixing. After HCl treatment, histone proteins were centrifuged at 2000 rpm and +4°C for 10 minutes then supernatant was incubated with a final concentration of 33% trichloroacetic acid (TCA) on ice for 30 minutes with gentle mixing. Mixture was centrifuged at 16000 g and +4°C for 10 minutes and pellet was washed with ice-cold ethanol and centrifuged again at 16000 g and +4°C for 10 minutes. Acetone treatment was repeated and pellet was dried for 20 minutes. Dried pellet was dissolved in 100 µl distilled water. Protein concentration was determined with BCA Protein Assay (Pierce, 23227). 3.0 µg/well histone proteins were mixed with 1X final concentration of 2X loading buffer (Novex Sample Buffer) containing 10% β-mercaptoethanol and boiled at 95°C for 5 minutes. After boiling, samples were placed on ice for a while and loaded into wells filled with tris-glycine running buffer (25 mM Tris, 250 mM glycine, 0.1% SDS). Samples were run in stacking gel at 70 V until they reach the running gel and they were run in running gel for 4 hours. Samples were transferred to PVDF membrane at 300 mA for 3 hours. Membrane was blocked with 6% skimmed milk and TBS buffer containing 0.5% Tween-20 by shaking for 1 hour at room temperature to prevent unspecific bindings during blotting. Membranes were incubated with anti-H3K27ac (1:500 diluted, Millipore, 07-360) and anti-H3K27me3 (1:1000 diluted, Millipore, 07-449) primer antibodies at +4°C for 16 hours by gentle shaking. After antibody incubation, membranes were washed with TBS-T buffer for 5 minutes for four times. Secondary antibodies (Pierce, 1858414) were prepared as 1:2500 dilutions in TBS-T (0.025%) buffer containing 3% skimmed milk and membranes were incubated with secondary antibodies at room temperature for 1 hour by gentle shaking. After antibody incubation, membranes were washed with TBS-T buffer for 5 minutes for four times. Histone proteins were detected using Supersignal West Pico Chemiluminescent kit (Pierce, 34080). Histone proteins (histone 3, histone 2A, histone 2B, histone 4) were used as a control of equal loading. Assays were performed in duplicate.



## 2.13. In Vitro SIRT1 Enzyme Activity Measurement

Inhibitory effect of (*R*)-4'-methylklavuzon on SIRT1 enzyme was investigated using a commercially available fluorescence based SIRT1 Fluorometric Drug Discovery Kit (Enzo, Fluor De Lys, BML-AK555). The SIRT1 Fluorescent Activity Assay is based on the combination of Fluor de Lys®-SIRT1 Substrate/Developer II. The Fluor de Lys®-SIRT1 Substrate is a peptide containing amino acids 379-382 of human p53 (Arg-His-Lys-Lys(Ac)). The assay's fluorescence signal is generated in proportion to the deacetylation of the Lys-382 which is a known in vivo target of SIRT1 activity. The assay procedure has two steps. First, the Fluor de Lys®-SIRT1 Substrate, which contains the p53 (Arg-His-Lys-Lys) ( $\epsilon$ -acetyl), is incubated with human recombinant SIRT1 together with the cosubstrate  $\text{NAD}^+$ . Deacetylation of Fluor de Lys®-SIRT1 sensitizes the substrate and in the second step, treatment with the Fluor de Lys® Developer II produces a fluorophore (Figure 2.3). As a positive control, resveratrol and suramin were used as activator and inhibitor of SIRT1, respectively.

Inhibitory effect of (*R*)-4'-methylklavuzon on SIRT1 enzyme was tested by combining 1 unit/well enzyme with 50  $\mu\text{M}$  and 100  $\mu\text{M}$  of drug candidate. SIRT1 was pre-treated with drug candidate for 2 minutes before addition of substrate. Enzyme and (*R*)-4'-methylklavuzon were incubated for 1 hour at 37°C in the presence of 50  $\mu\text{M}$  Fluor de Lys Substrate and 500  $\mu\text{M}$   $\text{NAD}^+$ . After incubation, developer solution which is supplied with the kit was added and incubated for 45 minutes at room temperature.

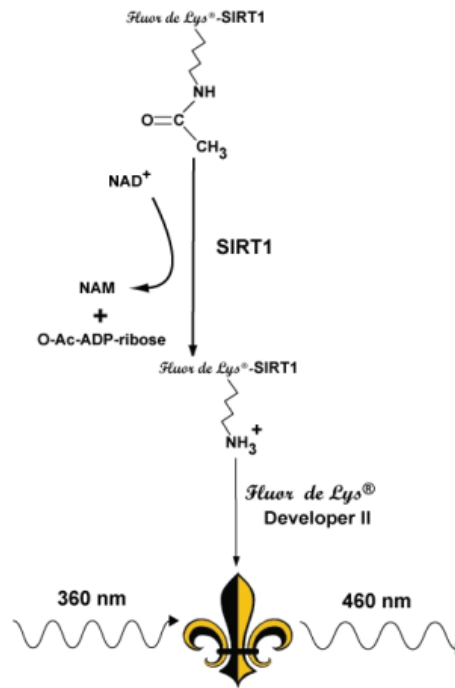


Figure 2.3. Reaction mechanism of Fluor de Lys-SIRT1 substrate by SIRT1 enzyme

Fluorescence was measured at 360 nm excitation wavelength and 460 nm emission wavelength with a plate reader (Thermo, Varioskan). Results were analyzed by using the standard curve plotted on a graph. All experiments were repeated thrice in triplicates.

## 2.14. Quantification of Intracellular SIRT1 Levels by ELISA

Effects of (*R*)-4'-methylklavuzon on intracellular SIRT1 levels in HuH-7 parental cells were investigated using a commercially available Sirtuin 1 (human) (IntraCellular) ELISA Kit (Adipogen). SIRT1 level measurement is based on a sandwich Enzyme Linked-Immunosorbent Assay (ELISA) and a monoclonal antibody specific for SIRT1 is pre-coated onto the 96-well microtiter plate.  $5 \times 10^5$  Cells/well were seeded in tissue culture petri dishes and incubated overnight. (*R*)-4'-methylklavuzon was applied to the cells at 5.00, 3.00 and 1.00  $\mu$ M concentrations and incubated for 24 hours. The control cells were treated with only DMSO at 1% final concentration as drug treated cells received. Total protein was isolated from three cell populations after (*R*)-4'-methylklavuzon treatment. Protein concentration was determined with BCA Protein Assay (Pierce, 23227). Cell lysate containing 44  $\mu$ g of proteins was optimized to be

used in ELISA assay and 44 µg of proteins in cell lysate was treated with monoclonal antibody which is pre-coated and after extensive washing, SIRT1 was recognized by the addition of a purified polyclonal antibody specific for SIRT1. After removal of excess polyclonal antibody, HRP conjugated anti-rabbit IgG was added and peroxidase activity was quantified using the substrate 3,3',5,5'-tetramethylbenzidine (TMB) at 450 nm on a plate reader (Thermo, MultiSkan). All experiments were repeated thrice in triplicates.

## 2.15. Determination of p21 and p27 Expressions by qPCR

Gene expressions that are responsible in cell cycle were investigated after (*R*)-4'-methylklavuzon treatment of the cells. Parental cells were treated with 1.00 µM and 3.00 µM of drug candidate for 24, 48 and 72 hours. EpCAM<sup>+</sup>/CD133<sup>+</sup> and EpCAM<sup>-</sup>/CD133<sup>-</sup> cells were incubated with drug candidate for 72 hours. Total RNA was isolated from each cell population by using GeneJet RNA Purification Kit (Thermo Scientific, K0731) and mRNA molecules were converted to cDNA molecules by using RevertAid First Strand cDNA Synthesis Kit (Thermo Scientific, K1622). qPCR reactions were performed in Roche LightCycler 480 II using Power SYBR Green PCR Master Mix (Life Technologies, 4367659). Glyceraldehyde-3-phosphate dehydrogenase (GAPDH) was used as internal control. p21 and p27 expressions were normalized using GAPDH expressions. Primer sets (Sentromer DNA Technologies, Istanbul) that were used for real-time PCR analysis are listed below;

p21-F: 5'- CCATGTGGACCTGTCACTGT -3'

p21-R: 5'- GAGAAGATCAGCCGGCGTTT -3'

p27-F: 5'- AAGAAGCCTGGCCTCAGAAG -3'

p27-R: 5'- TCCATTCCATGAAGTCAGCGAT -3'

GAPDH-F: 5'-CCAGCAAGAGCACAAGAGGAA-3'

GAPDH-R: 5'-GGTCTACATGGCAACTGTGAGG-3'

p21 and p27 expressions were analyzed using commercial kits based on SYBR Green according to the optimized PCR mixture and conditions. All experiments were repeated thrice in triplicates.

Optimized PCR mixture and conditions are shown in Tables 2.1 – 2.3.

Table 2.1. p21 ve p27 PCR Mixture

<b>Components</b>	<b>Volume (µl)</b>
dH <sub>2</sub> O	14.65
Buffer (including KCl)	2.00
25 mM MgCl <sub>2</sub>	1.20
10 mM dNTP mixture	0.40
10 µM Forward Primer	0.50
10 µM Reverse Primer	0.50
Template	0.50
Taq DNA Polymerase	0.25

Table 2.2. p21 ve p27 PCR Conditions

<b>Conditions</b>		
Initial Denaturation	95°C 3 minutes	1 X
Denaturation	95°C 30 seconds	
Annealing	58°C 30 seconds	40 X
Elongation	72°C 45 seconds	
Final Extension	72°C 5 minutes	1 X

Table 2.3. p21 ve p27 qPCR Conditions

<b>Conditions</b>		
Initial Denaturation	95°C 5 minutes	1 X
Denaturation	95°C 10 seconds	
Annealing	62°C 20 seconds	45 X
Elongation	72°C 30 seconds	

## **2.16. Immunofluorescence Visualization of RIOK2 Protein Localization in HepG2 and HuH-7 Cells**

Primary antibody (Anti-RIOK2 antibody [5D11] Mouse monoclonal, cat: ab131635) and secondary antibody (Goat Anti-Mouse IgG H&L (Alexa Fluor® 488), cat: ab150113) for RIOK2 were purchased from Abcam.  $25 \times 10^3$  HepG2 cells and  $25 \times 10^3$  HuH-7 cells were seeded in 24-well plates separately and cultured at 37°C under 5% CO<sub>2</sub> for 24 hours. After incubation, cells were treated with indicated drug concentrations and incubation times. At the end of the treatment, cells were washed with 1X Phosphate buffered saline (PBS) three times and fixed with 4% paraformaldehyde in 1X PBS at +4°C for 20 minutes. Cells were rinsed three times with PBS and permeabilized in 0.5% Triton-X-100 for 12 minutes at room temperature. Cells were rinsed three times with 1X PBS and incubated in blocking solution (5% bovine serum albumin in 0.1% Tween-20/PBS) for 1 hour at room temperature to prevent non-specific binding of the primary antibody. Cells were rinsed three times with 1X PBS and incubated with anti-RIOK2 antibody [5D11] mouse monoclonal (1:150 dilution) in 1X PBS containing 0.1% Tween-20 and 1% bovine serum albumin overnight at +4°C. Cells were rinsed with 1X PBS three times each for 10 minutes. Cells were incubated with secondary antibody Goat Anti-Mouse IgG H&L (Alexa Fluor® 488) (1:200 dilution) in 1X PBS containing 0.1% Tween-20 and 1% bovine serum albumin overnight at +4°C. Cells were rinsed with 1X PBS three times each for 10 minutes and incubated with 4,6-diamidino-2-phenylindole (DAPI) in distilled water to counterstain double-stranded DNA in nuclei for 10 minutes at room temperature followed by washing with distilled water for three times. Cells were covered with 1X PBS and visualized for 3.6 seconds exposure time under fluorescence microscope (CKX41, Olympus) equipped with a LUCPlanFLN 40X/0.6 objective (Olympus) and SC100 digital camera (Olympus). Cells were also visualized under spinning disc confocal microscope (Olympus, IX71) equipped with 100X objective (Olympus) and laser source (Andor). The data obtained from fluorescence microscope was analyzed with cellSens software and data obtained from spinning disc confocal microscope was analyzed with ImageJ software. Images are representative of three independent experiments. All experiments were repeated thrice in triplicates.

## **2.17. Immunofluorescence Visualization of p53 Protein Levels in HepG2 and HuH-7 Cells**

Primary antibody (p53 (7F5) Rabbit mAb, cat: 2527) and secondary antibody (Anti-Rabbit IgG (H+L), F(ab')<sub>2</sub> Fragment (Alexa Fluor® 488 Conjugate), cat: 4412) for p53 were purchased from Cell Signaling (Danvers, MA, USA). 25×10<sup>3</sup> HepG2 cells (containing wild-type p53) and 25×10<sup>3</sup> HuH-7 cells (containing p53 with a missense mutation) were seeded in 24-well plates separately and cultured at 37°C under 5% CO<sub>2</sub> for 24 hours. After incubation, cells were treated with indicated drug concentrations and incubation times. At the end of the treatment, cells were washed with 1X Phosphate buffered saline (PBS) three times and fixed with 4% paraformaldehyde in 1X PBS at +4°C for 20 minutes. Cells were rinsed three times with PBS and permeabilized in 0.5% Triton-X-100 for 12 minutes at room temperature. Cells were rinsed three times with 1X PBS and incubated in blocking solution (5% bovine serum albumin in 0.1% Tween-20/PBS) for 1 hour at room temperature to prevent non-specific binding of the primary antibody. Cells were rinsed three times with 1X PBS and incubated with monoclonal primary antibody p53 (7F5) Rabbit mAb (1:1600 dilution) in 1X PBS containing 0.1% Tween-20 and 1% Bovine serum albumin overnight at +4°C. Cells were rinsed with 1X PBS three times each for 10 minutes. Cells were incubated with secondary antibody Anti-Rabbit IgG (H+L), F(ab')<sub>2</sub> Fragment (Alexa Fluor® 488 Conjugate) (1:1000 dilution) in 1X PBS containing 0.1% Tween-20 and 1% Bovine serum albumin at room temperature for two hours. Cells were rinsed with 1X PBS three times each for 10 minutes and incubated with 4,6-diamidino-2-phenylindole (DAPI) in distilled water to counterstain double-stranded DNA in nuclei for 10 minutes at room temperature followed by washing with distilled water for three times. Cells were covered with 1X PBS and visualised for 1.24 seconds and/or 3.6 seconds exposure time under fluorescence microscope (CKX41, Olympus) equipped with a LUCPlanFLN 40X/0.6 objective (Olympus) and SC100 digital camera (Olympus). The data was analyzed with cellSens software. Images are representative of three independent experiments. All experiments were repeated thrice in triplicates.

## 2.18. Propidium Iodide Staining of HepG2 Cell Spheroids

Perfecta3D<sup>®</sup> hanging drop 96 well plates (polystyrene (untreated), sterile)(Sigma, HDP1096) were used to form spheroids. Trays were filled with sterilized distilled water to maintain humidity. 8000 HepG2 cells/well in 40  $\mu$ l of growth medium were inoculated into each hanging drop well to create drops that hang from wells containing cell suspensions. After 24 hours of incubation, 10  $\mu$ l medium was removed and 15  $\mu$ l of fresh medium was added. Cells were incubated for an additional 24 hours to form spheroids. Spheroids with similar morphology and size were chosen to set up experiments. Spheroids were treated with final concentrations at 0.10, 1.00, 10 and 20  $\mu$ M of (*R*)-4'-methylklavuzon and 10  $\mu$ M of TK126 and also 50  $\mu$ M of Goniiothalamine by adding 5  $\mu$ l of 10X drug concentration in medium into 45  $\mu$ l of medium containing spheroids. After 24 hours of incubation, while spheroids were still in the hanging drops, spheroids were directly stained with a final concentration of 50  $\mu$ g/ml Propidium Iodide at 37°C under 5% CO<sub>2</sub> incubator for 1 hour. After staining, they were directly visualized in the hanging drop under fluorescence microscope (CKX41, Olympus) equipped with a LUCPlanFLN 4X objective (Olympus) and SC100 digital camera (Olympus). The data was analyzed with cellSens software.

## 2.19. Immunofluorescence Visualization of p53 Protein Levels in HepG2 Cell Spheroids

Perfecta3D<sup>®</sup> hanging drop 96 well plates (polystyrene (untreated), sterile)(Sigma, HDP1096) were used to form spheroids. Trays were filled with sterilized distilled water to maintain humidity. 8000 HepG2 cells/well in 40  $\mu$ l of growth medium were inoculated into each hanging drop well to create drops that hang from wells containing cell suspensions. After 24 hours of incubation, 10  $\mu$ l medium was removed and 15  $\mu$ l of fresh medium was added. Cells were incubated for an additional 24 hours to form spheroids. Spheroids with similar morphology and size were chosen to set up experiments. Spheroids were treated with final concentrations at 0.10, 1.00, 10 and 20  $\mu$ M of (*R*)-4'-methylklavuzon and 10  $\mu$ M of TK126 and also 50  $\mu$ M of Goniiothalamine by adding 5  $\mu$ l of 10X drug concentration in medium into 45  $\mu$ l of medium containing spheroids. After 24 hours of incubation with indicated molecules, spheroids were pulled

down by adding excess medium from the top of wells, which decreases drop stability causing a descent onto a conventional 96 well plate, in which related wells were already filled with same medium not to disrupt spheroid morphology due to the sudden descent of the spheroid. After placement of the spheroid in conventional 96 well plate, medium was removed and spheroids were rinsed with 1X PBS three times. Fixation was carried out with 4% paraformaldehyde for 4 hours at +4°C. After fixation, spheroids were rinsed with 1X PBS three times and permeabilized with 0.5% Triton-X-100 for 1 hour at room temperature. After removal of the permeabilization solution by three times 1X PBS washing, spheroids were blocked with 5% bovine serum albumin in 0.1% Tween 20 in PBS for 1 hour at room temperature. Spheroids were rinsed with 1X PBS three times and immunolabelled with monoclonal primary p53 (7F5) Rabbit antibody (Cell Signalling, 2527) in 1X PBS containing 0.1% Tween 20 and 1% Bovine serum albumin at +4°C for overnight. Primary antibody was removed and spheroids were rinsed with 1X PBS three times. Spheroids were immunolabelled with secondary antibody (Anti-Rabbit IgG (H+L), F(ab')<sub>2</sub> Fragment, Alexa Fluor® 488 Conjugate, Cell Signaling, 4412) at +4°C for overnight. After entire immunolabelling, spheroids were rinsed with 1X PBS three times and counter-stained with DAPI for DNA staining. Spheroids were covered with 1X PBS and visualized for 3.6 second exposure time under fluorescence microscope (CKX41, Olympus) equipped with a LUCPlanFLN 4X, 20X and 40X objective (Olympus) and SC100 digital camera (Olympus). The data was analyzed with cellSens software.

## **2.20. Colorimetric Determination of p53/MDM2 Complex Inhibition by ELISA**

ImmunoSet® p53/MDM2 complex ELISA development set (Enzo Life Sciences, ADI-960-070) was used for determination of p53/MDM2 complex isolated from human cell lysates. Entire procedure includes microplate coating, reagent preparation, performing the assay and calculation of the data. 96-well plate was coated with p53 capture antibody (1:250 dilution) in coating buffer (10 mM sodium phosphate, 15 mM NaCl, pH 7.4) overnight at room temperature and after removal of coating solution, it was blocked with blocking buffer (10 mM sodium phosphate, 15 mM NaCl, 1.0% BSA, pH 7.4) for at least 1 hour at room temperature. p53 human standard and



MDM2 human standard were reconstituted in 250  $\mu$ l dH<sub>2</sub>O separately and combined for complex formation and incubated for 1 hour at room temperature. This stock p53/MDM2 complex standard solution had 1  $\mu$ g/ml of p53 concentration and 0.32  $\mu$ g/ml of MDM2 concentration. During the assay, assay buffer (100 mM sodium phosphate, 150 mM NaCl, 1.0% BSA, 0.1% Tween-20, pH 7.4) was added into control wells. Standards and samples were added in a proper design. Microplate was incubated at room temperature for 1 hour with a gentle shaking. After incubation, wells were washed four times with 300  $\mu$ l of wash buffer (10 mM sodium phosphate, 15 mM NaCl, 0.1% Tween-20, pH 7.4). After washing, MDM2 detection antibody (1:250 dilution) was added and incubated for 1 hour at room temperature with a gentle shaking. After incubation, wells were washed four times with 300  $\mu$ l of wash buffer and SA-HRP conjugate (1:1000 diluted) was added and incubated for 30 minutes at room temperature in dark with a gentle shaking. After incubation, wells are washed four times with 300  $\mu$ l of wash buffer and TMB substrate is added and incubated for 30 minutes in dark at room temperature. Reaction was ended by adding 1 N HCl. Optical density is read at 450 nm wavelength. Results were analyzed using p53/MDM2 standard curve.

## 2.21. Spheroid Assay Based on Matrigel

48-well plates were coated with 3.76 mg/ml poly-HEMA (Sigma, P3932) in 95% ethanol for overnight in 37°C incubator and then washed with 1X PBS twice. Cells were harvested with trypsin and centrifuged at 2500 rpm for 5 minutes. 1000 cells/48 well were inoculated with 2.5 mg/ml matrigel (Corning, 354234). Cells, matrigel and DMEM medium are prepared on ice shown in Table 2.4 below.

Table 2.4. Matrigel Suspension

Material	Volume ( $\mu$ l)
Matrigel	277.7 (stock: 9.9 mg/ml)
Cell suspension	100
DMEM	722.3

250  $\mu$ l from this cell suspension was inoculated into 4 different wells. Plates were centrifuged at 1000 g for 10 minutes at room temperature and incubated under 37°C and 5% CO<sub>2</sub> incubator. 350  $\mu$ l DMEM was added after one day. Cells were incubated for four days and 84  $\mu$ l DMEM was added just before drug treatment. Spheroids are treated with only 1% DMSO as control, 12.5  $\mu$ M and 62.5  $\mu$ M of (*R*)-4'-methylklavuzon for 72 hours. Microscopic images were obtained in 24, 48 and 72 hours by using inverted microscope (Olympus).

## **2.22. Statistical Analysis**

Statistical analyses were performed with One-way ANOVA Dunnett's multiple comparison test using GraphPad Prism version 5 (GraphPad Software, San Diego, CA, USA). All drug treated samples were compared versus control groups with Dunnett's multiple comparison test. All the data was presented as mean  $\pm$  SD. P values less than 0.05 were considered statistically significant.

## CHAPTER 3

### RESULTS

#### 3.1. (*R*)-4'-methylklavuzon Inhibits Proliferation of HuH-7 Cell Populations

2000 cells/well were inoculated in 96-well plates and were treated with (*R*)-4'-methylklavuzon with the concentrations of 20, 10, 5.00, 2.50, 1.25, 0.625 and 0.10  $\mu\text{M}$  and incubated for 24, 48 and 72 hours. After treatment, cell viability was analyzed using MTT method.

Time and dose dependent cytotoxic effects of (*R*)-4'-methylklavuzon are shown in Figures 3.1 – 3.4. Statistical analysis was performed with one-way ANOVA test and p-value was obtained as  $p < 0.05$ .

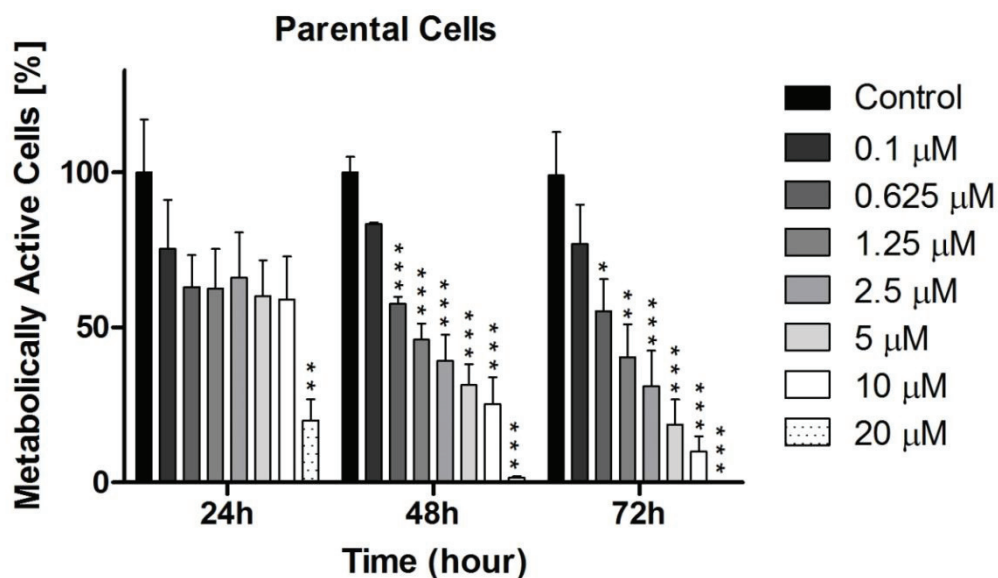


Figure 3.1. Time and concentration dependent cytotoxic activity of (*R*)-4'-methylklavuzon on HuH-7 parental cells. Statistical analysis was performed with one-way ANOVA and p values are  $< 0.001$  in \*\*\*,  $< 0.01$  in \*\* and  $< 0.05$  in \* indicating that results are statistically significant.

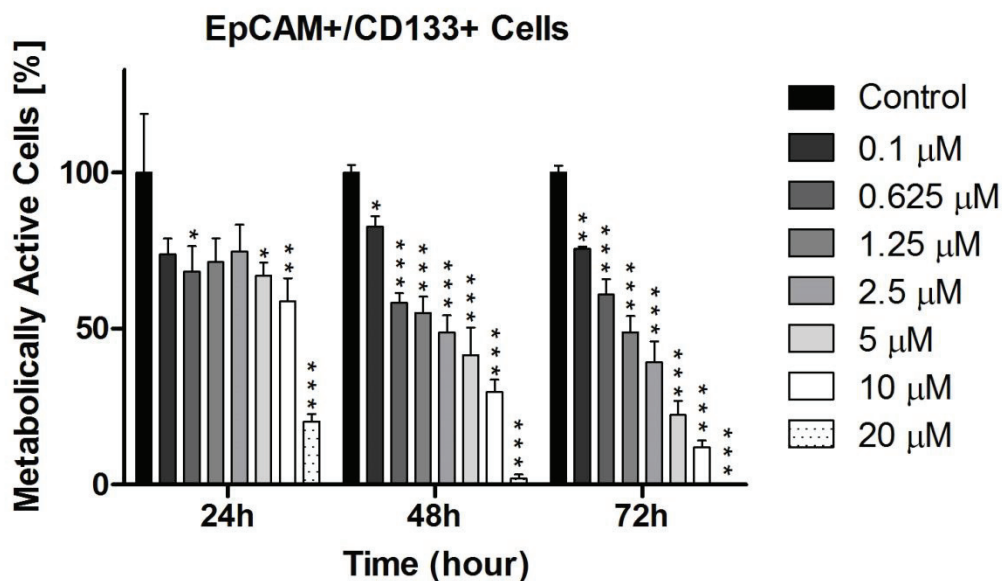


Figure 3.2. Time and concentration dependent cytotoxic activity of (R)-4'-methylklavuzon on EpCAM<sup>+</sup>/CD133<sup>+</sup> HuH-7 cells. Statistical analysis was performed with one-way ANOVA and p values are < 0.001 in \*\*\*, < 0.01 in \*\* and < 0.05 in \* indicating that results are statistically significant.

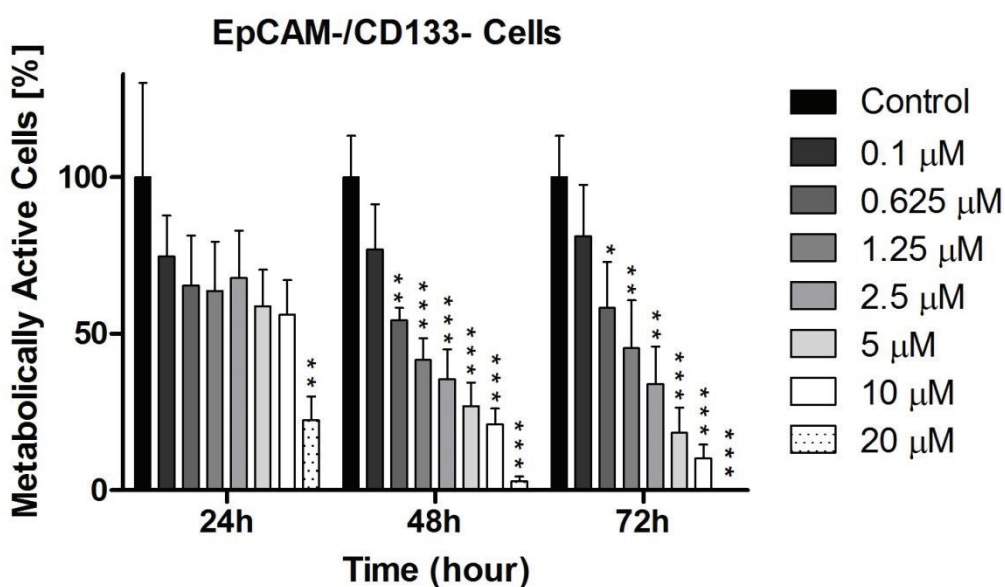


Figure 3.3. Time and concentration dependent cytotoxic activity of (R)-4'-methylklavuzon on EpCAM<sup>-</sup>/CD133<sup>-</sup> HuH-7 cells. Statistical analysis performed with one-way ANOVA and p values are < 0.001 in \*\*\*, < 0.01 in \*\* and < 0.05 in \* indicating that results are statistically significant.

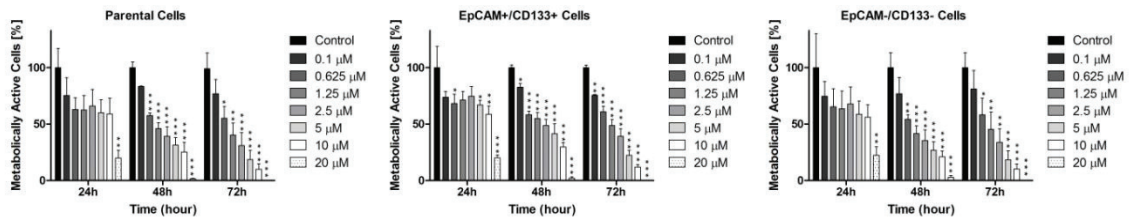


Figure 3.4. Comparative cytotoxic activity of (*R*)-4'-methylklavuzon HuH-7 cell populations. Statistical analysis was performed with one-way ANOVA and p values are < 0.001 in \*\*\*, < 0.01 in \*\* and < 0.05 in \* indicating that results are statistically significant.

### 3.2. (*R*)-4'-methylklavuzon Increases G1 Phase

60,000 cells/well were inoculated into 6-well plates and treated with (*R*)-4'-methylklavuzon with the concentrations of 10.00, 1.00 and 0.10  $\mu\text{M}$  for 24, 48 and 72 hours. Time and dose dependent effects of the drug candidate are shown in the Figure 3.5. It was found that 1.00  $\mu\text{M}$  of (*R*)-4'-methylklavuzon caused 20% increase in G1 phase ratio at the end of 48 hours of incubation, whereas 10  $\mu\text{M}$  of drug candidate caused 20% increase in G2 phase ratio in all cell populations within 48 hours.

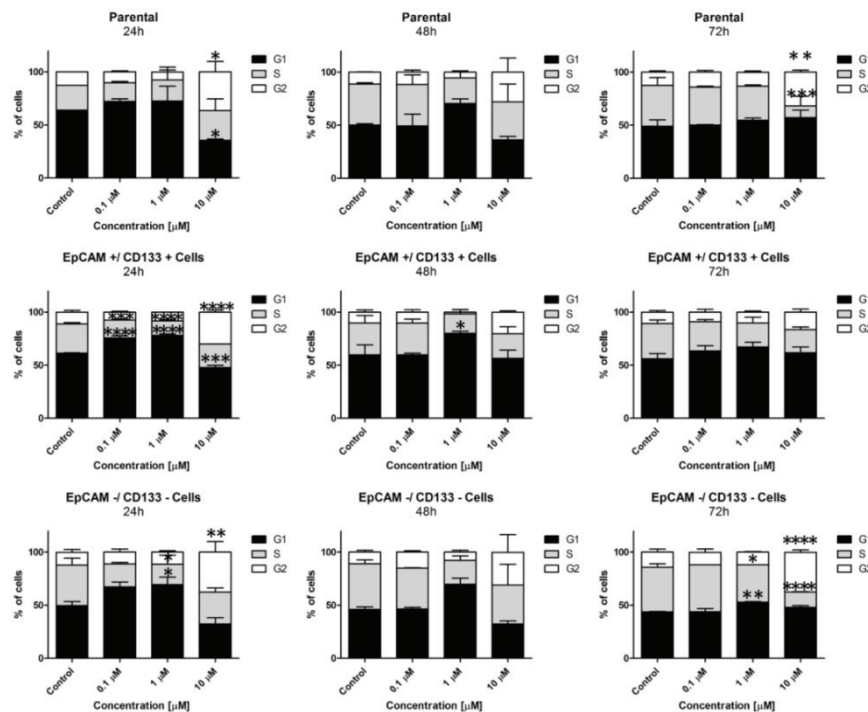


Figure 3.5. Time and dose dependent effects of (*R*)-4'-methylklavuzon on cell cycle of HuH-7 cells. Statistical analysis was performed with two-way ANOVA and p values are < 0.0001 in \*\*\*\*, < 0.001 in \*\*\*, < 0.01 in \*\* and < 0.05 in \* indicating that results are statistically significant.

### 3.3. (*R*)-4'-methylklavuzon Induces Apoptosis

60,000 cells/well were inoculated into 6-well plates and treated with (*R*)-4'-methylklavuzon with the concentrations of 10, 1.00 and 0.10  $\mu\text{M}$  for 24, 48 and 72 hours. Time and dose dependent effects of the drug candidate are shown in the Figure 3.6.

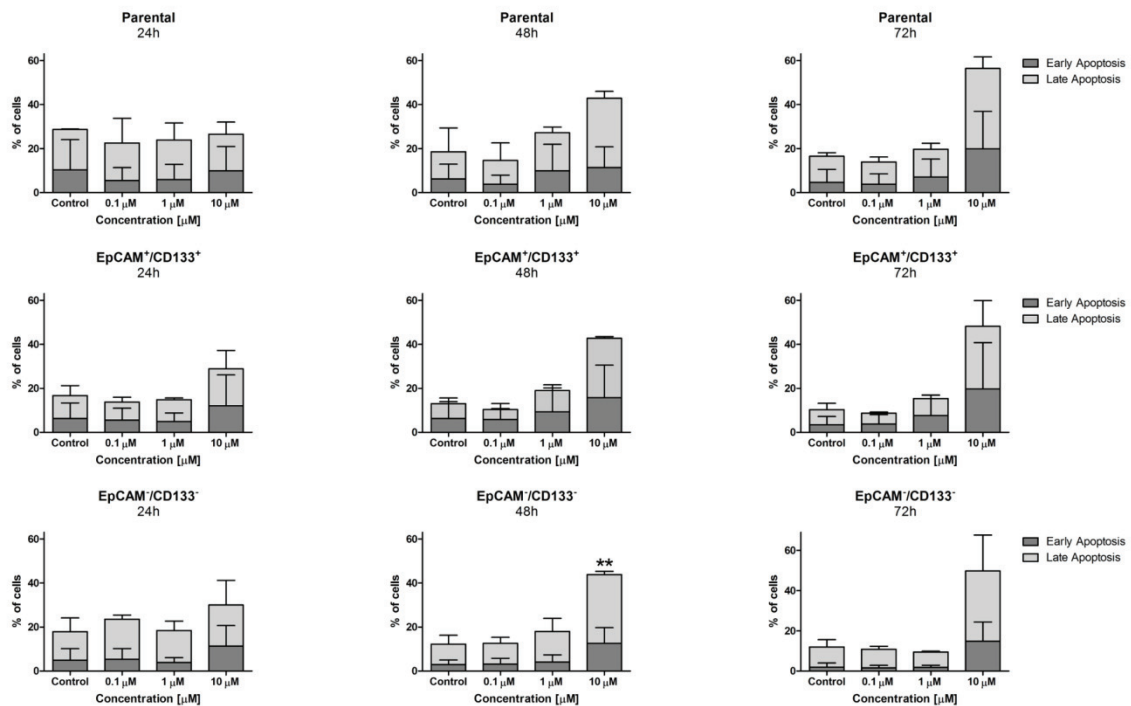


Figure 3.6. Time and dose dependent apoptotic affects of (*R*)-4'-methylklavuzon on HuH-7 cell populations. Statistical analysis was performed with two-way ANOVA and p values < 0.01 in \*\* indicating that results are statistically significant.

It was found that 10  $\mu\text{M}$  of (*R*)-4'-methylklavuzon causes approximately 20% increment in late apoptosis at the end of 72 hours of incubation. No significant data was obtained at 1.00 and 0.10  $\mu\text{M}$  concentrations within all incubation times.

### 3.4. Cytotoxic Activity of (R)-4'-methylklavuzon Derivatives on MIA-PaCa2 and HPDEC Cells

Cytotoxic activities of novel racemic (R)-4'-methylklavuzon derivatives (Figure 3.7) which were obtained from the substitution of different alkyl groups at 4'-position of (R)-4'-methylklavuzon were analyzed on MIA-PaCa2 (pancreatic cancer cells) and HPDEC (Human Pancreatic Duct Epithelial Cells) by MTT cell viability assay.

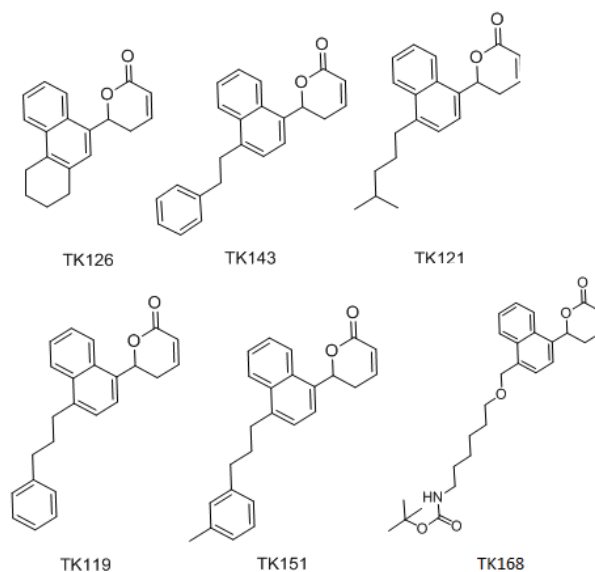


Figure 3.7. The structures of 4'-alkyl substituted (R)-4'-methylklavuzon derivatives

It was found that novel molecules have similar cytotoxic effect on both cancer cells and healthy cells without any selective property as shown in Table 3.1.

Table 3.1 Calculated IC<sub>50</sub> values of (R)-4'-methylklavuzon derivatives on MIA-PaCa2 and HPDEC cells

Compounds	MIA-PaCa2 ( $\mu\text{M}$ )	HPDEC ( $\mu\text{M}$ )
TK126	$0.16 \pm 0.03$	$0.15 \pm 0.04$
TK143	$2.20 \pm 0.11$	$2.58 \pm 0.49$
TK121	$4.09 \pm 0.20$	$4.50 \pm 0.48$
TK119	$3.21 \pm 0.39$	$4.45 \pm 0.39$
TK151	$1.40 \pm 0.69$	$1.50 \pm 0.69$
TK168	$2.52 \pm 0.48$	-

### 3.5. (*R*)-4'-methylklavuzon Has No Inhibitory Effects on Class I/II Histone Deacetylase Enzyme Activity In Vitro

Nuclear proteins were isolated according to a manual protocol recommended in In vitro HDAC Fluorometric Activity Assay Kit (Cayman, 10011563) for determination of the effects of (*R*)-4'-methylklavuzon on class I and II histone deacetylase enzymes. Protein concentrations were determined by Bradford Assay.

Amount of proteins to be tested were optimized and 4  $\mu\text{g}$  nuclear proteins/well (96-well plate) were used for (*R*)-4'-methylklavuzon treatment. 4  $\mu\text{g}$  nuclear proteins were treated with the (*R*)-4'-methylklavuzon concentrations of 81, 27, 9.00, 3.00, 1.00, 0.50, 0.10  $\mu\text{M}$  in triplicates. In vitro effects of the drug candidate are shown in the Figure 3.8.

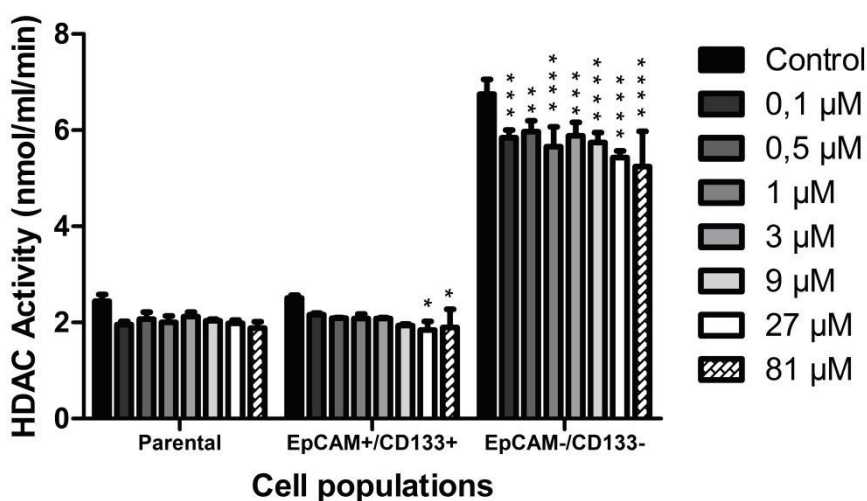


Figure 3.8. In vitro effects of (*R*)-4'-methylklavuzon on class I/II histone deacetylase enzymes isolated from HuH-7 parental, EpCAM<sup>+</sup>/CD133<sup>+</sup> HuH-7 cells and EpCAM<sup>-</sup>/CD133<sup>-</sup> HuH-7 cells. Statistical analysis was performed with two-way ANOVA and p values are < 0.0001 in \*\*\*\*, < 0.001 in \*\*\*, < 0.01 in \*\* and < 0.05 in \* indicating that results are statistically significant.



### 3.6. (*R*)-4'-methylklavuzon Inhibits Endogenous Sirtuin and/or Class I/II Histone Deacetylase Enzyme Activity in HuH-7 Cell Populations Sorted by MACS

10,000 cells/well were inoculated into black 96-well plate and treated with (*R*)-4'-methylklavuzon with the concentrations of 5.00, 3.00, 1.00, 0.50, 0.25 and 0.10  $\mu\text{M}$  for 24 hours in triplicates. Enzymatic inhibitions after drug treatment are shown in Figure 3.9.

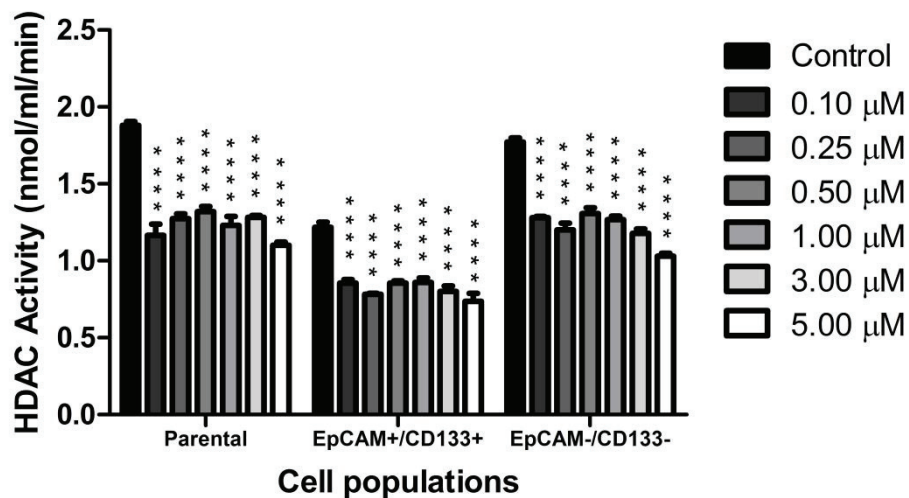


Figure 3.9. Inhibitory effects of (*R*)-4'-methylklavuzon on endogenous histone deacetylase enzymes in HuH-7 cell populations. Statistical analysis was performed with two-way ANOVA and p values are  $< 0.001$  in \*\*\*\* indicating that results are statistically significant.

Correlation of HDAC inhibition with cell viability is illustrated in Figures 3.10 – 3.12.

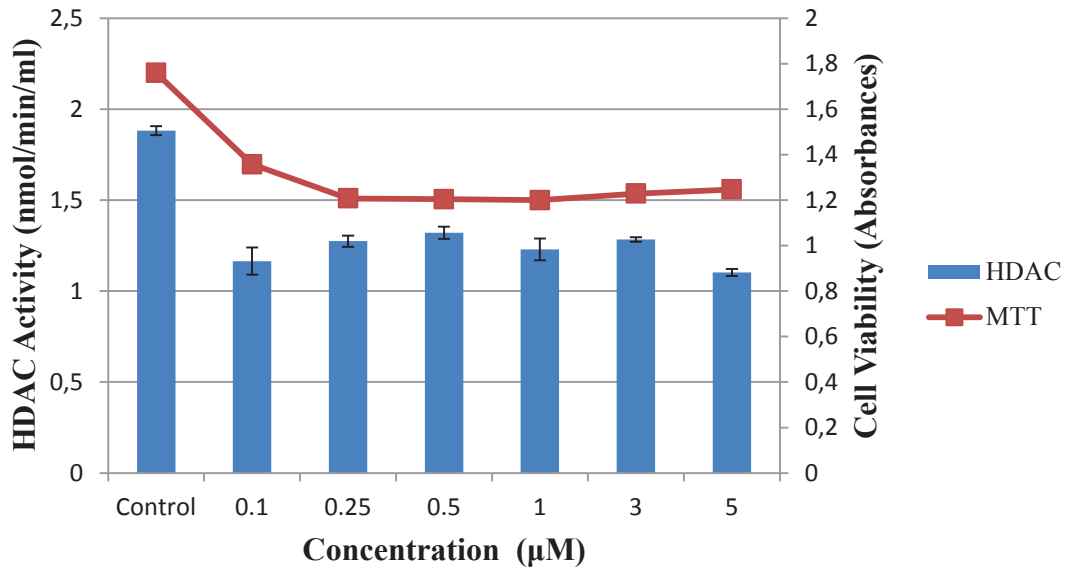


Figure 3.10. Comparative scheme of cell-based HDAC assay and cell viability assay for HuH-7 parental cells

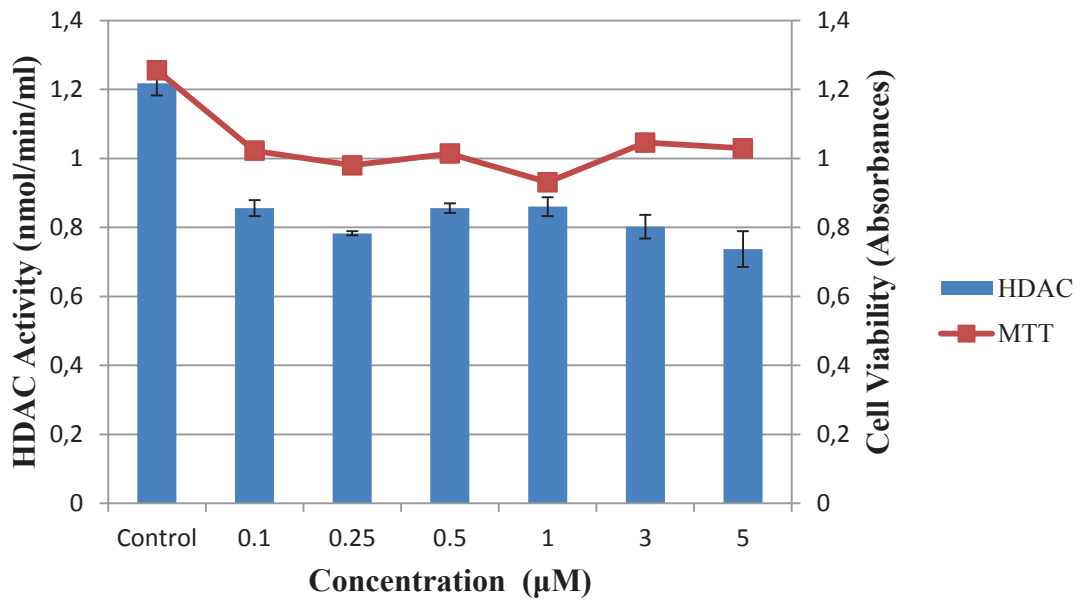


Figure 3.11. Comparative scheme of cell-based HDAC assay and cell viability assay for EpCAM<sup>+</sup>/CD133<sup>+</sup> HuH-7 cells

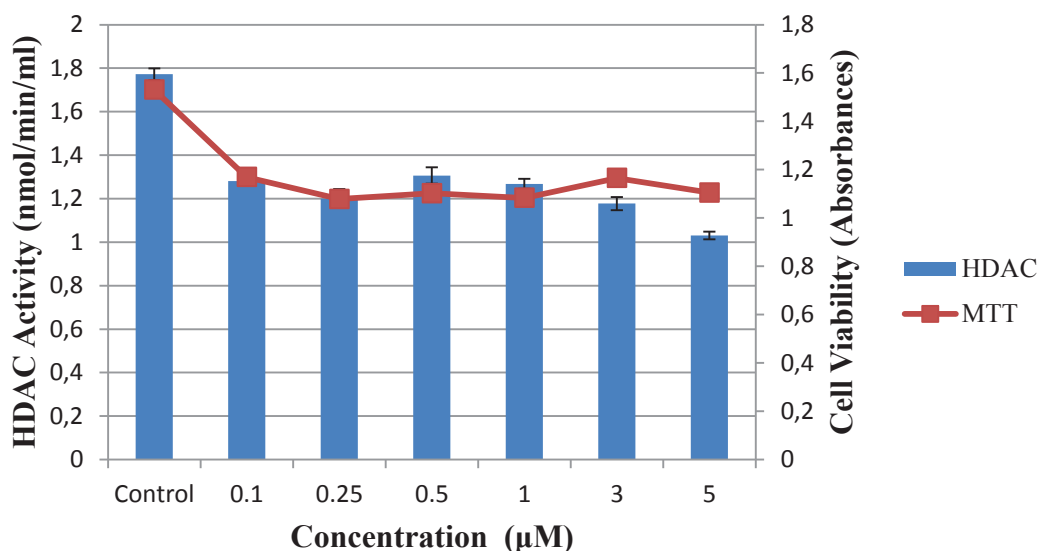


Figure 3.12. Comparative scheme of cell-based HDAC assay and cell viability assay for EpCAM<sup>-</sup>/CD133<sup>-</sup> HuH-7 cells

### 3.7. (*R*)-4'-methylklavuzon Inhibits Endogenous Sirtuin and/or Class I/II Histone Deacetylase Enzyme Activity in HuH-7 Parental Cells and EpCAM<sup>+</sup>/CD133<sup>+</sup> HuH-7 Cells Sorted by FACS

10,000 cells/well were inoculated into black 96-well plate and treated with (*R*)-4'-methylklavuzon at the concentrations of 5.0 and 1.0 µM for 24 hours in triplicates. Enzymatic inhibitions after drug treatment are shown in Figure 3.13.

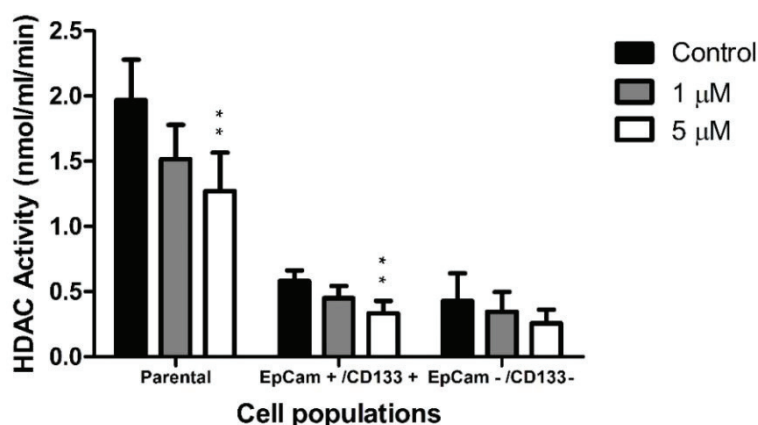


Figure 3.13. Inhibitory effects of (*R*)-4'-methylklavuzon on endogenous histone deacetylase enzymes in HuH-7 cell populations. Statistical analysis performed with one-way ANOVA and p values are < 0.05 in \*\* indicating that results are statistically significant.

Correlation of HDAC inhibition with cell viability is illustrated in Figures 3.14 – 3.16.

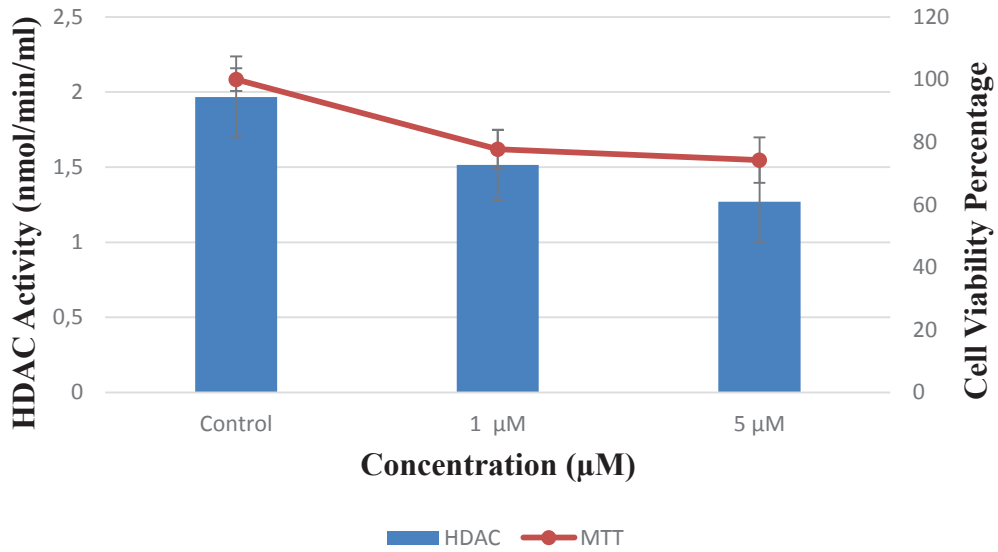


Figure 3.14. Comparative graph of cell-based HDAC assay and cell viability assay for HuH-7 parental cells.

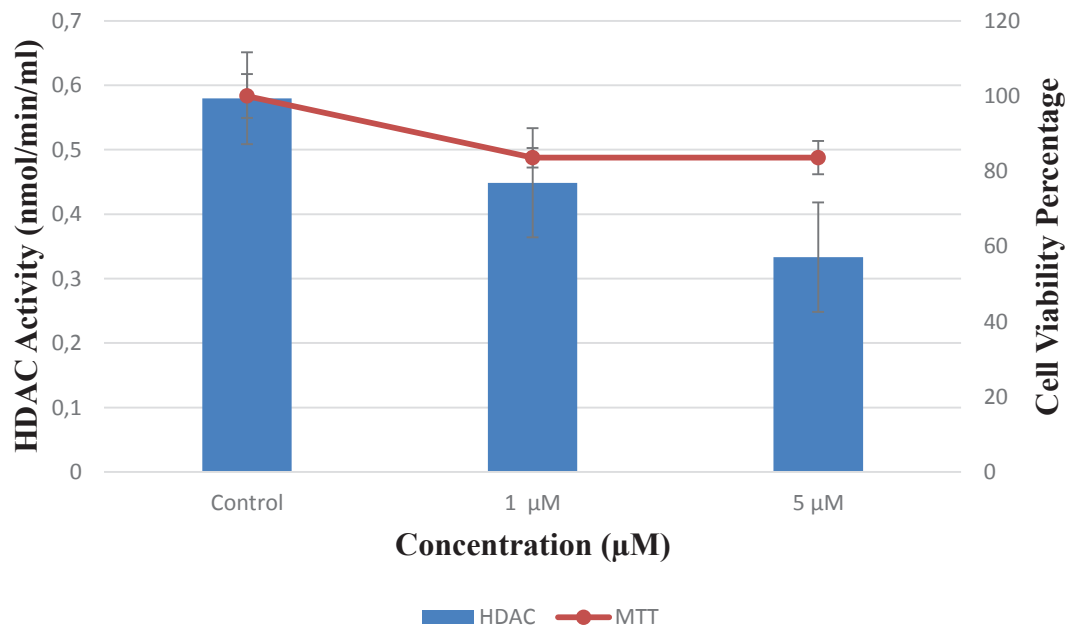


Figure 3.15. Comparative graph of cell-based HDAC assay and cell viability assay for EpCAM<sup>+</sup>/CD133<sup>+</sup> HuH-7 cells.

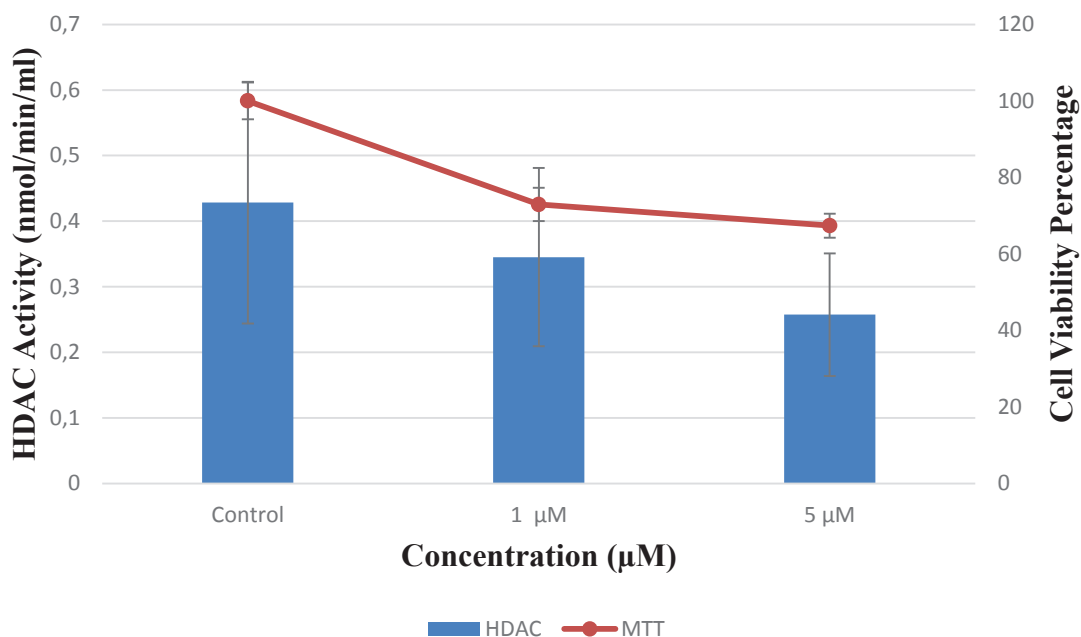


Figure 3.16. Comparative graph of cell-based HDAC assay and cell viability assay for EpCAM<sup>+</sup>/CD133<sup>+</sup> HuH-7 cells.

### 3.8. In Vitro HDAC1 Enzyme Activity Measurement

Inhibitory effect of (*R*)-4'-methylklavuzon on HDAC1 enzyme was tested by combining 7.5 unit/well enzyme with 1.00 µM, 50 µM and 100 µM of drug candidate. HDAC1 was pre-treated with the drug candidate for 2 minutes before addition of substrate. Enzyme and (*R*)-4'-methylklavuzon was incubated for 1 hour at 37°C in the presence of 20 µM Fluor de Lys Substrate. After incubation, developer solution that is supplied with the kit was added and incubated for 45 minutes at room temperature. HDAC1 enzymatic activities after drug treatment are shown in Figure 3.17.

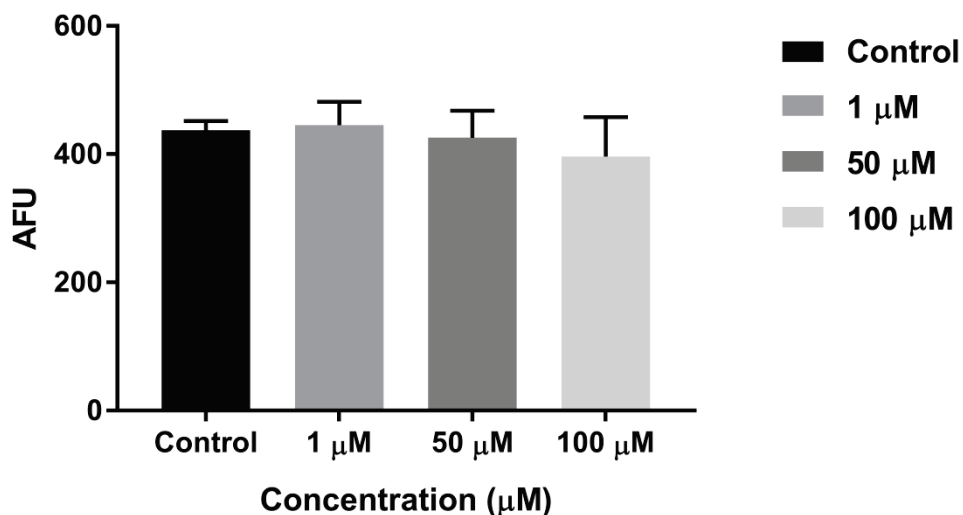


Figure 3.17. Inhibitory effect of (*R*)-4'-methylklavuzon on HDAC1 enzyme. Statistical analysis was performed with one-way ANOVA using Tukey's multiple comparisons test and no statistically significant differences were found.

Inhibitory effect of TK126 on HDAC1 enzyme was also tested as explained above. It was found that TK126 does not inhibit HDAC1 enzyme similar to (*R*)-4'-methylklavuzon. HDAC1 enzymatic activity for TK126 treatment at 100 μM concentration is shown in Figure 3.18.

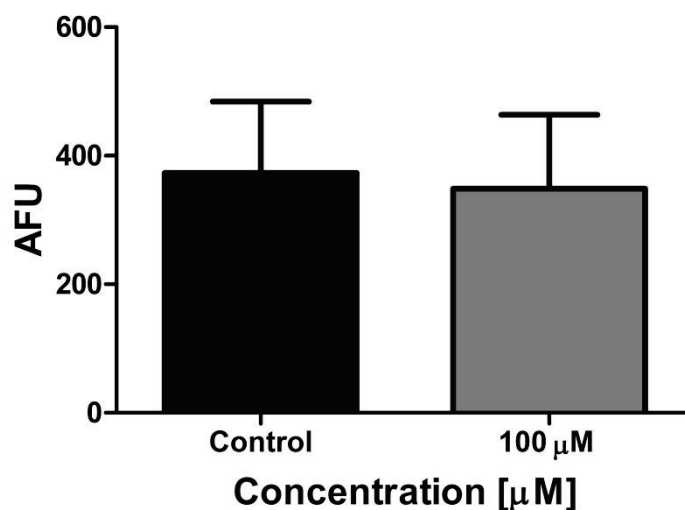


Figure 3.18. Inhibitory effect of TK126 on HDAC1 enzyme. Statistical analysis was performed with one-way ANOVA.

### 3.9. (*R*)-4'-methylklavuzon Upregulates H3K27 Trimethylation in Cells Sorted by FACS

Firstly, parental cells were examined to see any difference in methylation and acetylation status of H3K27 residue within 24 hours and 48 hours after drug candidate treatment. Unfortunately, no significant figures were obtained at the end of 24 and 48 hours of incubation (Figure 3.19). Afterwards, cells were treated with (*R*)-4'-methylklavuzon for 72 hours. To do this,  $5 \times 10^5$  HuH-7 cells/well were inoculated into tissue culture petri dishes and treated with the concentrations of 1.00 and 5.00  $\mu\text{M}$  of (*R*)-4'-methylklavuzon for 72 hours to analyse methylation profile and also treated with the concentrations of 0.25, 1.00 and 3.00  $\mu\text{M}$  of (*R*)-4'-methylklavuzon for 72 hours to analyse acetylation profile. Three cell populations were tested with same dose regimen for 72 hours. Histone extraction was performed after drug candidate treatment. Protein concentrations were determined by BCA Protein Assay (Pierce, 23227). Histone modification levels of H3K27 residue was analyzed by western blotting by using anti-H3K27me3 antibody (Figure 3.20) and anti-H3K27ac (Figure 3.21).

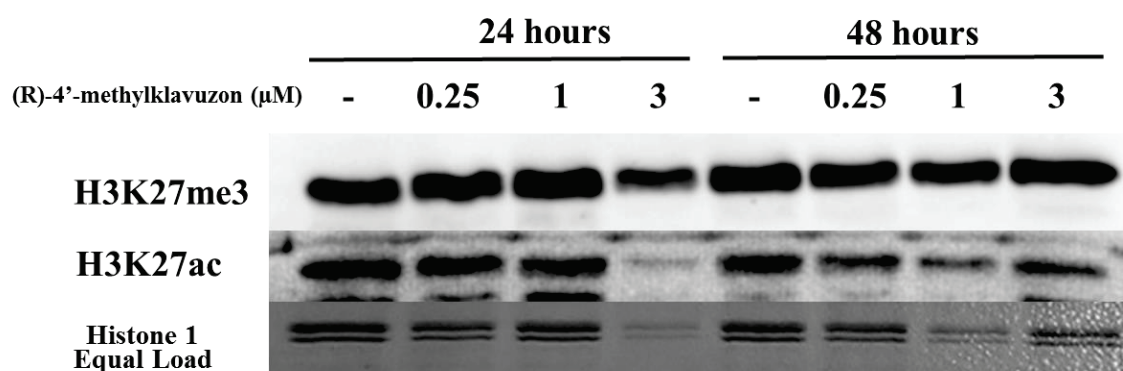


Figure 3.19. Effects of (*R*)-4'-methylklavuzon on methylation and acetylation status of H3K27 residue in HuH-7 parental cells at the end of 24 and 48 hour of incubation.

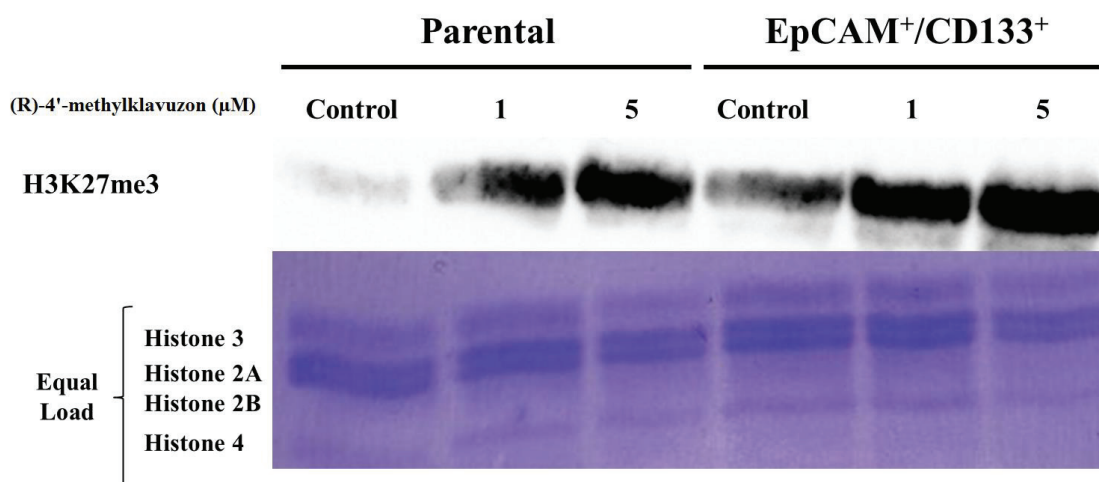


Figure 3.20. Effects of (R)-4'-methylklavuzon on methylation status of H3K27 residue in HuH-7 parental cells and EpCAM<sup>+</sup>/CD133<sup>+</sup> HuH-7 cells sorted by FACS after 72 hours of drug treatment.

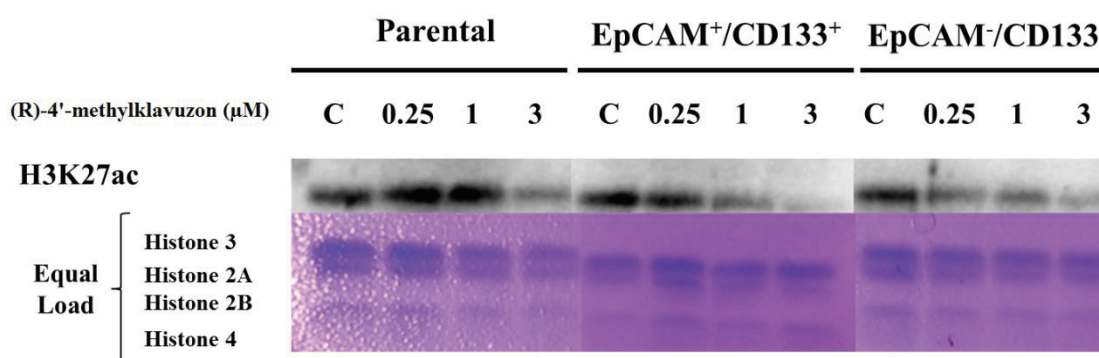


Figure 3.21. Effects of (R)-4'-methylklavuzon on acetylation status of H3K27 residue in HuH-7 cell populations sorted by MACS after 72 hours of drug treatment.

Methylation profile was analyzed for 72 hours and it was found that EpCAM<sup>+</sup>/CD133<sup>+</sup> cells together with parental cells revealed significant upregulation in their methylation status. EpCAM<sup>+</sup>/CD133<sup>+</sup> cells and other populations increased their methylation status with increasing concentrations (1.00 μM and 5.00 μM) of (R)-4'-methylklavuzon. The highest increment was obtained with the concentration of 5.00 μM among tested concentrations.

Any concentration dependent increase in acetylation of H3K27 residue could not be obtained after drug treatment. The possible reason of this might be that enzymes which can be inhibited by drug candidate are not responsible for the acetylation of



H3K27 residue. Hence, specific enzymes that can be inhibited by (*R*)-4'-methylklavuzon should be discovered and target histone proteins of these enzymes should be investigated in further studies.

### 3.10. (*R*)-4'-methylklavuzon Inhibits SIRT1 Enzyme Activity In Vitro

Inhibitory effect of (*R*)-4'-methylklavuzon on SIRT1 enzyme was tested by combining 1 unit/well enzyme with 50  $\mu$ M and 100  $\mu$ M of drug candidate. Concentration dependent decreases in the enzymatic activity after drug treatment are shown in Figure 3.22.

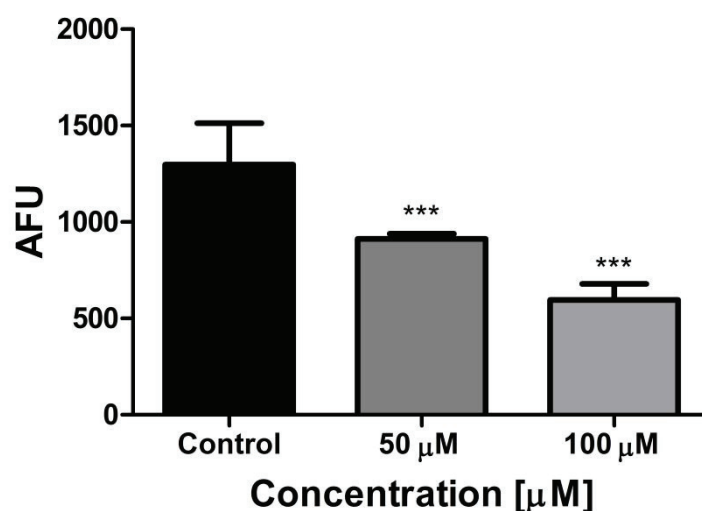


Figure 3.22. Inhibitory effect of (*R*)-4'-methylklavuzon on SIRT1 enzyme activity. Statistical analysis was performed with one-way ANOVA using Dunnett's multiple comparisons test and p values are  $< 0.001$  in \*\*\* indicating that results are statistically significant.

Inhibitory effect of TK126 on SIRT1 enzyme was tested as explained above. It was found that TK126 had higher inhibitory effect on SIRT1 compared to (*R*)-4'-methylklavuzon. Concentration dependent decreases in the enzymatic activity after TK126 treatment are shown in Figure 3.23.

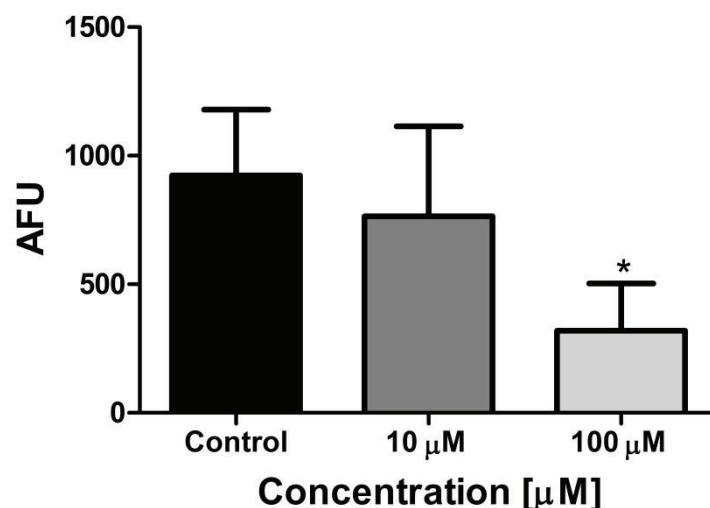


Figure 3.23. Inhibitory effect of TK126 on SIRT1 enzyme activity. Statistical analysis was performed with one-way ANOVA (Analysis of Variance).

### 3.11. (*R*)-4'-methylklavuzon Upregulates Intracellular SIRT1 Protein Levels

Effect of (*R*)-4'-methylklavuzon on intracellular SIRT1 levels was firstly tested by incubating HuH-7 cells at 1.00, 3.00 and 5.00 μM concentrations of the drug candidate for 24 hours. Cells were lysed by using the RIPA buffer provided with the kit to isolate total protein. Protein concentration was determined using BCA protein assay (Pierce, 23227). Then, 44 μg of total protein were used in each well of ELISA plate. Peroxidase activity was quantified by using the substrate 3,3',5,5'-tetramethylbenzidine (TMB) at 450 nm on a plate reader (Thermo, MultiSkan). Dose dependent increase in the SIRT1 levels are shown in the Figure 3.24. It was found that 1.00 μM, 3.00 μM and 5.00 μM of (*R*)-4'-methylklavuzon upregulates intracellular SIRT1 levels by 176%, 240% and 95%, respectively.

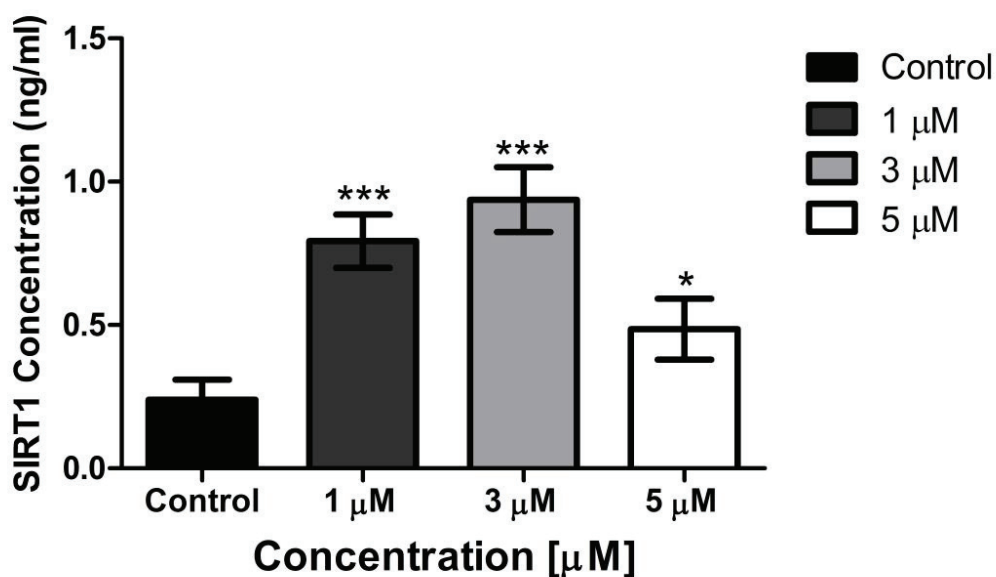


Figure 3.24. Effect of (*R*)-4'-methylklavuzon on SIRT1 enzyme levels within 24 hours. Statistical analysis was performed with one-way ANOVA using Dunnet's multiple comparisons test and p values are < 0.003 in \*\*\* and < 0.05 in \* indicating that results are statistically significant.

Comparative analysis of cell-based HDACs/sirtuins assay and intracellular SIRT1 ELISA revealed that SIRT1 protein levels were upregulated while HDACs/sirtuins activities were inhibited by drug candidate. It was assumed that if activities obtained by cell-based HDACs/sirtuins assay were dependent on SIRT1, the enzymatic activities should have been increased by upregulated SIRT1 levels. Contradictorily, enzymatic activities were dramatically decreased while SIRT1 protein levels were significantly increased as shown in the Figure 3.25 below. This data shows that (*R*)-4'-methylklavuzon inhibits SIRT1 rather than HDACs.

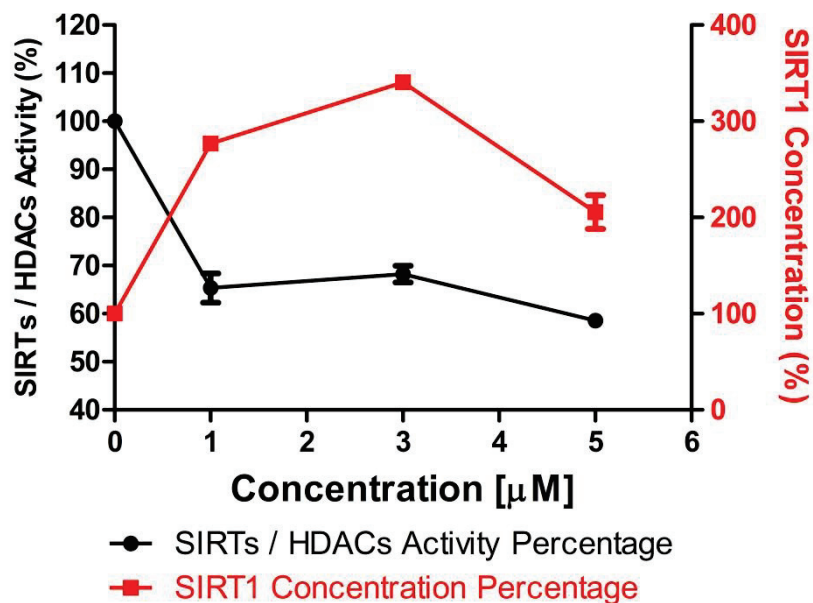


Figure 3.25. Comparative analysis of cell-based HDACs/sirtuins assay and intracellular SIRT1 ELISA.

### 3.12. (R)-4'-methylklavuzon Upregulates p21 and p27 Gene Expressions

Arrest in the G1 phase caused by (R)-4'-methylklavuzon might have been related to p21 and p27 expressions. Primers were optimized by conventional PCR before performing qPCR as shown in Figure 3.26.

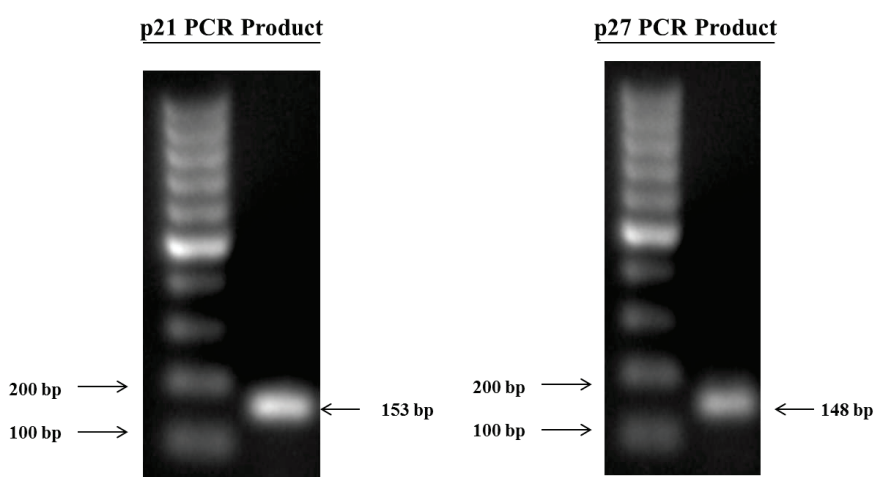


Figure 3.26. Agarose gel images of p21 and p27 PCR products

It was found that increasing concentrations of (*R*)-4'-methylklavuzon upregulates p21 expression by dose dependent manner. The highest upregulation of p21 gene expression was achieved with 3.00  $\mu$ M concentration for all the incubation times in parental HuH-7 cells. 3.00  $\mu$ M of (*R*)-4'-methylklavuzon upregulated p21 expression 1.9 times in parental cells for 24 hours; 3.3 times for 48 hours; 2.3 times for 72 hours as shown in Figure 3.27.

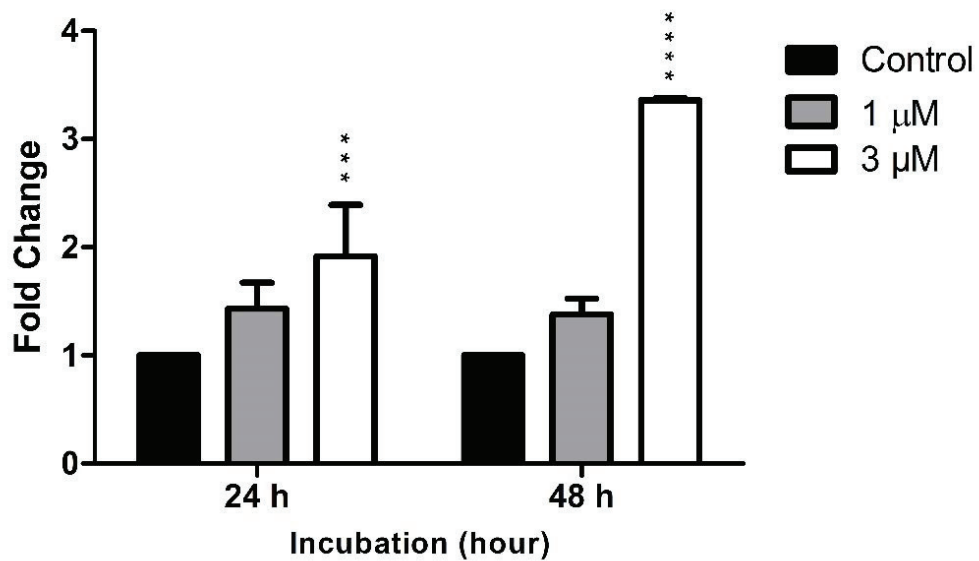


Figure 3.27. Time dependent fold changes of p21 expression in HuH-7 parental cells after incubation with (*R*)-4'-methylklavuzon treatment. Statistical analysis was performed by two-way ANOVA test and p values were obtained < 0.001 in \*\*\* and < 0.0001 in \*\*\*\* indicating that results are statistically significant.

It was found that 3.00  $\mu$ M of (*R*)-4'-methylklavuzon upregulates p27 significantly for 24 hours. 1.00  $\mu$ M of (*R*)-4'-methylklavuzon have milder effects compared to 3.00  $\mu$ M concentration. 3.00  $\mu$ M of (*R*)-4'-methylklavuzon upregulates p27 gene expression 2.8 times for 24 hours of incubation, 1.5 times for 48 hours and 1.2 times for 72 hours (Figure 3.28).

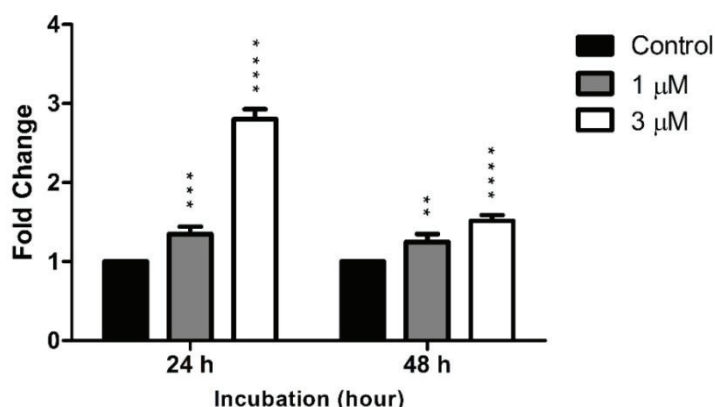


Figure 3.28. Time dependent fold changes of p27 expression in (*R*)-4'-methylklavuzon treated HuH-7 parental cells. Statistical analysis was performed by two-way ANOVA test and p values were obtained < 0.01 in \*\*, < 0.001 in \*\*\* and < 0.0001 in \*\*\*\* indicating that results are statistically significant.

3.00 μM of (*R*)-4'-methylklavuzon upregulated p21 expression more than other concentrations for all of the cell populations. 3.00 μM of (*R*)-4'-methylklavuzon upregulated p21 expression 2.3 times in parental cells; 1.7 times in EpCAM<sup>+</sup>/CD133<sup>+</sup> cells; 1.7 times in EpCAM<sup>-</sup>/CD133<sup>-</sup> cells. 1.00 μM of (*R*)-4'-methylklavuzon upregulated p21 expression 1.1 times in parental cells, 1.1 times in EpCAM<sup>+</sup>/CD133<sup>+</sup> cells, 1.5 times in EpCAM<sup>-</sup>/CD133<sup>-</sup> cells. The highest level of p21 expression on EpCAM<sup>-</sup>/CD133<sup>-</sup> cells was obtained with 1.00 μM of (*R*)-4'-methylklavuzon as shown in Figure 3.29.

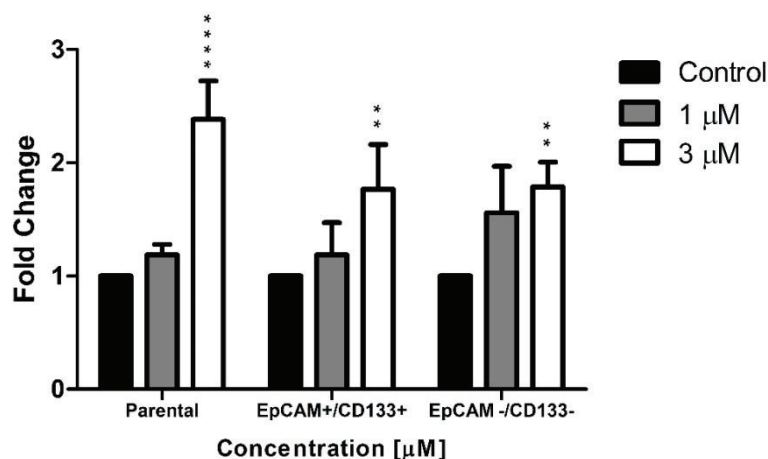


Figure 3.29. Concentration dependent p21 expression for 72 hours in (*R*)-4'-methylklavuzon treated HuH-7 cell populations (HuH-7 Parental, EpCAM<sup>+</sup>/CD133<sup>+</sup> and EpCAM<sup>-</sup>/CD133<sup>-</sup>). Statistical analysis was performed by two-way ANOVA test and p values were obtained < 0.01 in \*\* and < 0.0001 in \*\*\*\* indicating that results are statistically significant.

It was found that 3.00  $\mu\text{M}$  of (*R*)-4'-methylklavuzon upregulates p27 gene expression 1.2 times in parental cells. No significant upregulation were obtained for other cell populations. However, 1.00  $\mu\text{M}$  of (*R*)-4'-methylklavuzon downregulated p27 gene expression approximately 0.7 times for all of the cell populations as shown in Figure 3.30.

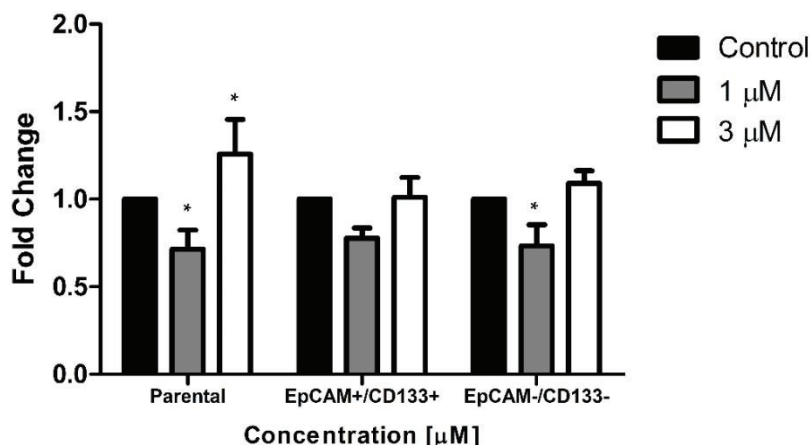


Figure 3.30. Concentration dependent p27 expression for 72 hours in (*R*)-4'-methylklavuzon treated HuH-7 cell populations (HuH-7 Parental, EpCAM<sup>+</sup>/CD133<sup>+</sup> and EpCAM<sup>-</sup>/CD133<sup>-</sup>). Statistical analysis was performed by two-way ANOVA test and p values were obtained < 0.05 in \* indicating that results are statistically significant.

### 3.13. (*R*)-4'-methylklavuzon Inhibits CRM1 Protein in HepG2 and HuH-7 Cells

HuH-7 cells were treated with various concentrations of (*R*)-4'-methylklavuzon. It was found that 0.10  $\mu\text{M}$  of drug candidate can inhibit CRM1 protein in 6 hours but it cannot inhibit CRM1 with same dosage at the end of 24 hours incubation. Concentrations of 1.00  $\mu\text{M}$  and 10  $\mu\text{M}$  can inhibit CRM1 in both 6 and 24 hours (Figure 3.31 and Figure 3.32).

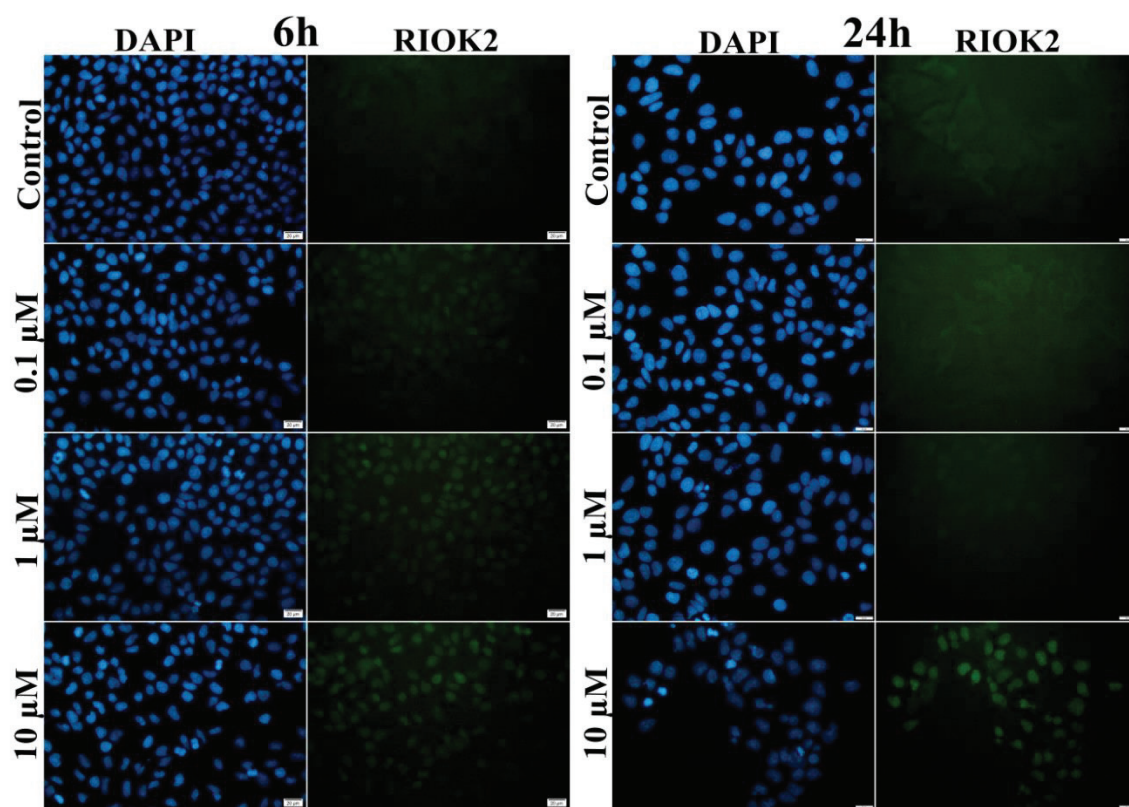


Figure 3.31. Immunofluorescence imaging of RIOK2 proteins in HuH-7 parental cells after (*R*)-4'-methylklavuzon treatment. Images were obtained by using 40X objective with 20 μm scale.



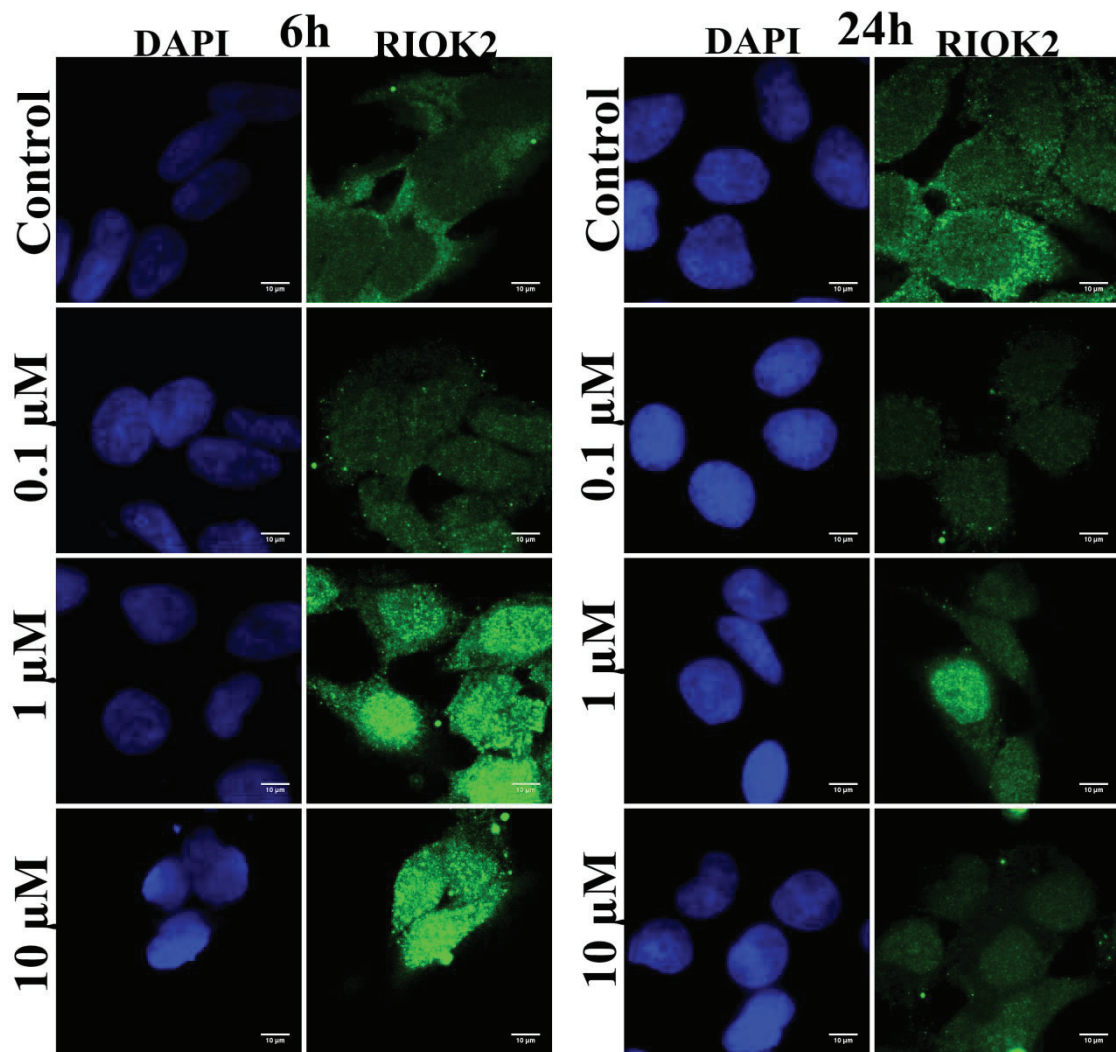


Figure 3.32. Spinning disc confocal microscopy imaging of RIOK2 proteins in HuH-7 parental cells after (*R*)-4'-methylklavuzon treatment by immunofluorescence staining. Images were obtained by using 100X objective with 10 μm scale.

In contradiction, CRM1 in HepG2 cells can be inhibited with especially 0.10  $\mu\text{M}$  and higher concentrations of drug candidate for both 6 and 24 hours (Figure 3.33 and Figure 3.34).

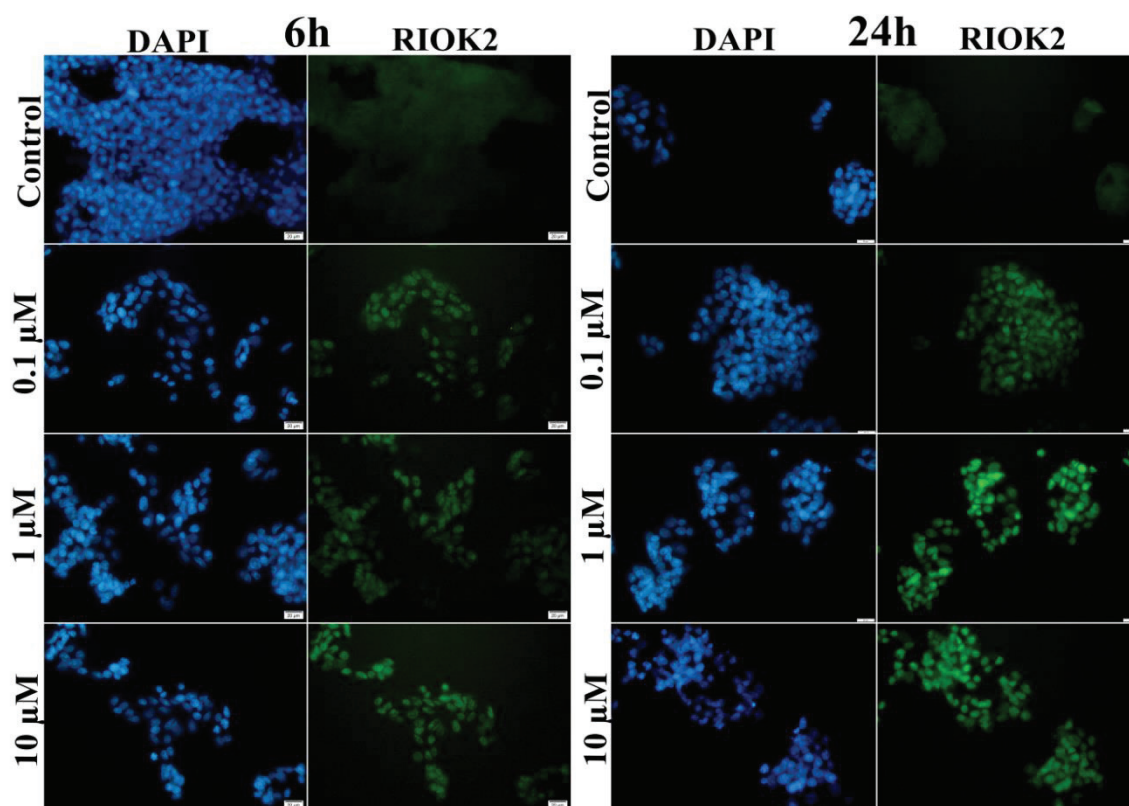


Figure 3.33. Immunofluorescence imaging of RIOK2 proteins in HepG2 cells after (*R*)-4'-methylklavuzon treatment. Images were obtained by using 40X objective with 20  $\mu\text{m}$  scale.

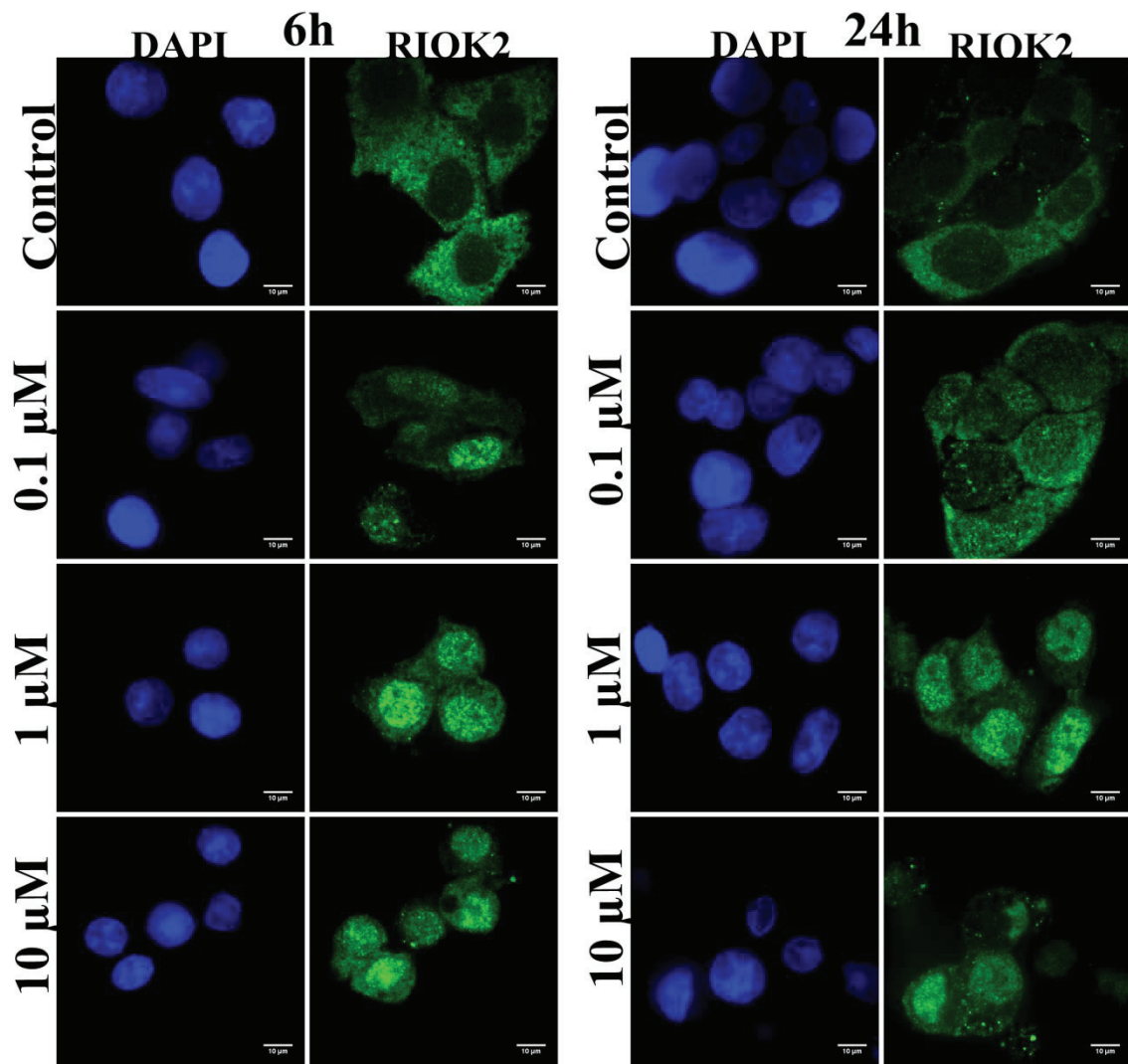


Figure 3.34. Spinning disc confocal microscopy imaging of RIOK2 proteins in HepG2 cells after (*R*)-4'-methylklavuzon treatment by immunofluorescence staining. Images were obtained by using 100X objective with 10 μm scale.

### 3.14. TK126 Inhibits CRM1 Proteins in HepG2 and HuH-7 Cells

HuH-7 and HepG2 cells were treated with various concentrations of TK126. It was found that 0.10  $\mu\text{M}$  of drug candidate can inhibit CRM1 protein in 6 hours but cannot inhibit with same dosage at the end of 24 hours of incubation for both of the cell lines. Concentrations of 0.50, 1.00 and 10  $\mu\text{M}$  can inhibit CRM1 in HuH-7 cells in both 6 and 24 hours of incubation (Figure 3.35).

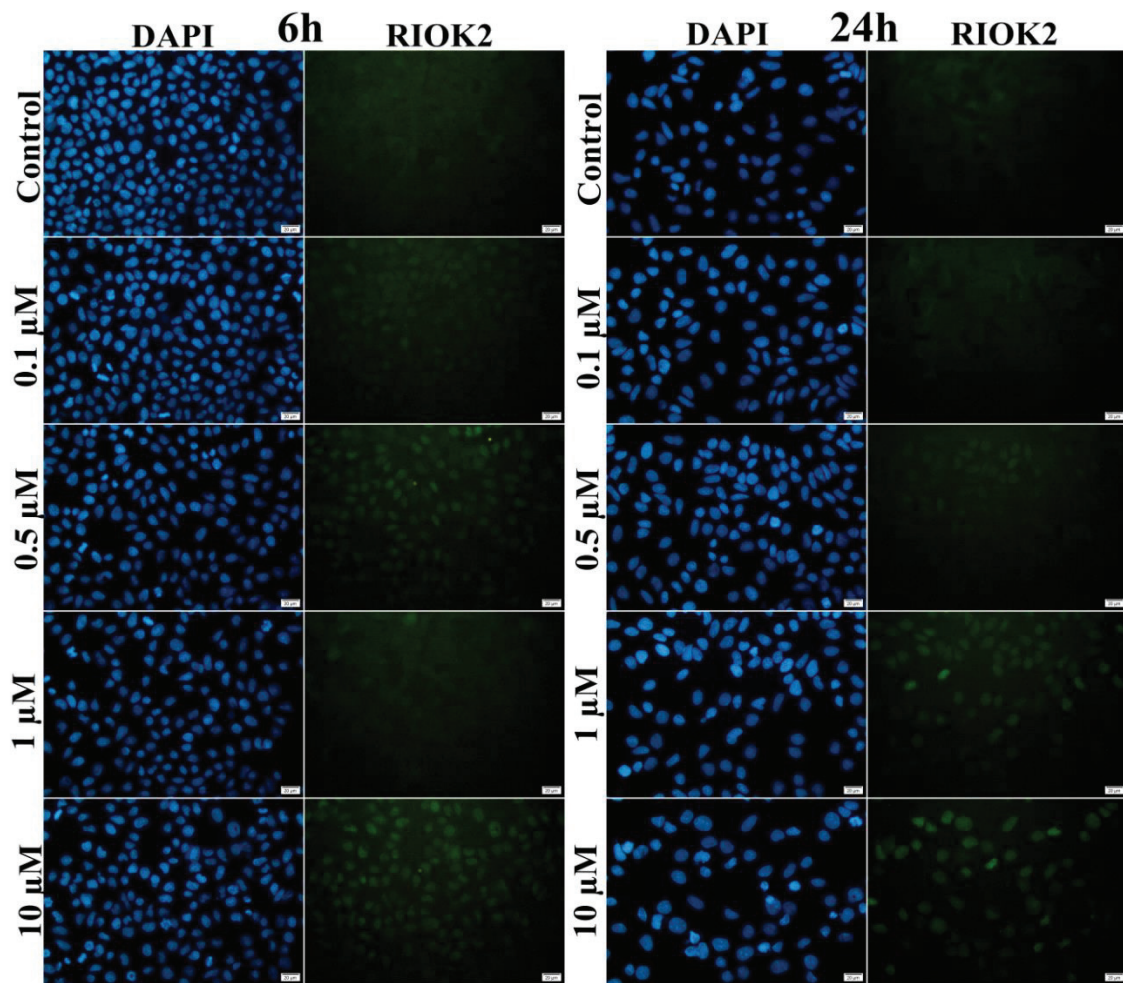


Figure 3.35. Immunofluorescence imaging of RIOK2 proteins in HuH-7 parental cells after TK126 treatment. Images were obtained by using 40X objective with 20  $\mu\text{m}$  scale.

CRM1 in HepG2 cells can be inhibited with especially 0.10  $\mu\text{M}$  and higher concentrations of drug candidate for both 6 and 24 hours (Figure 3.36).

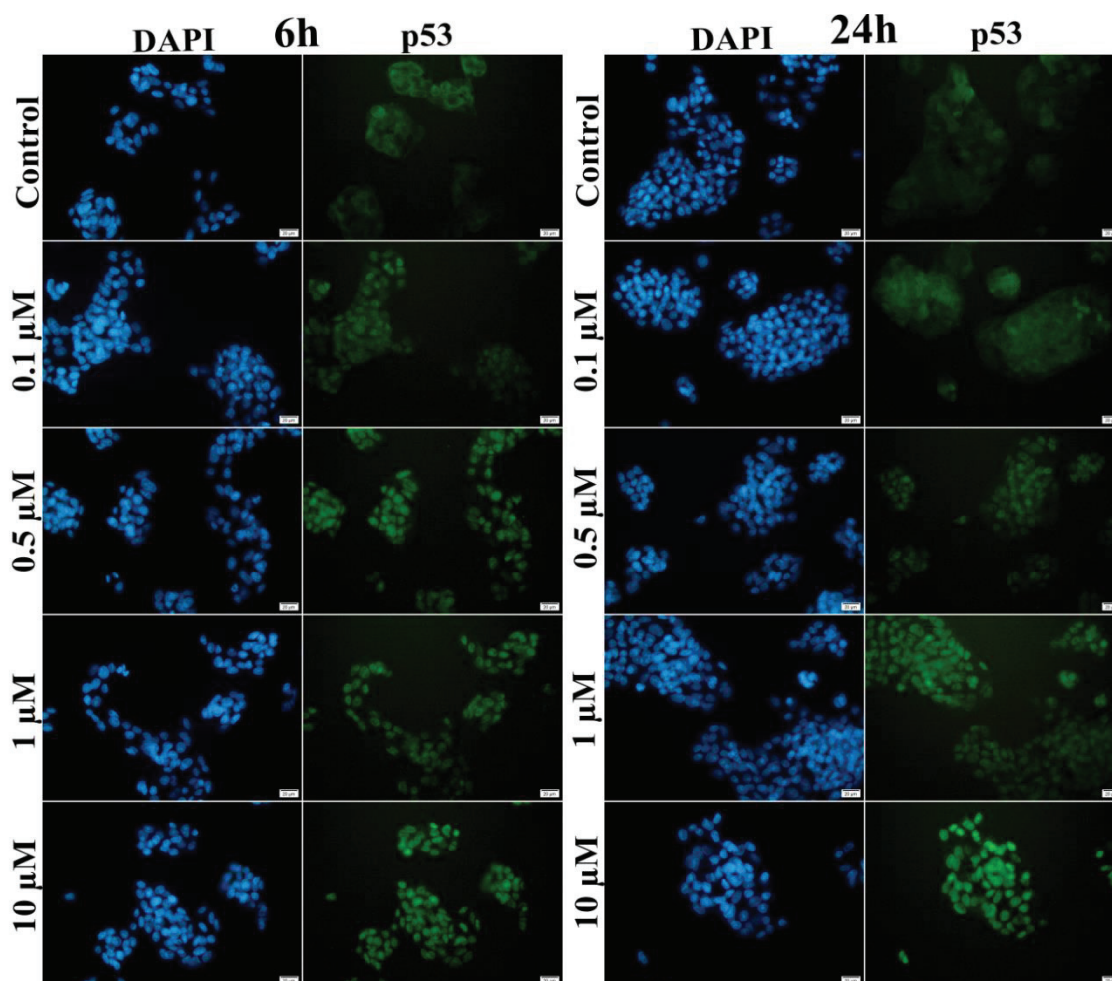


Figure 3.36. Immunofluorescence imaging of RIOK2 proteins in HepG2 cells after TK126 treatment. Images were obtained by using 40X objective with 20  $\mu\text{m}$  scale.

### 3.15. (*R*)-4'-methylklavuzon Upregulates p53 Protein Levels in HepG2 and HuH-7 Cells

Effect of (*R*)-4'-methylklavuzon on p53 protein expression levels in HepG2 cells (wild-type p53) and HuH-7 cells (p53 with a missense mutation) was analyzed using immunofluorescence microscopy. Control cells revealed that p53 was slightly expressed in HepG2 cells. When cells were treated with varying concentrations of drug candidate, p53 was significantly overexpressed within 6 and 24 hours in HepG2 cells. It was found

that low concentrations (0.10  $\mu\text{M}$  and 1.00  $\mu\text{M}$ ) upregulates p53 protein expression more than higher concentration (10  $\mu\text{M}$ ). Fluorescence intensities showed that drug candidate is more effective to upregulate p53 levels within 6 hours of incubation as seen in Figure 3.37. It was observed that overexpressed p53 protein was mainly accumulated in nucleus instead of cytoplasm. It might have been caused by CRM1 inhibition, formation of possible DNA breaks and induction of DNA repair mechanism of p53 in HuH-7 cells. Similar to HepG2 cells, p53 was slightly overexpressed in HuH-7 parental cells at 0.10  $\mu\text{M}$  and 0.50  $\mu\text{M}$  concentrations within 24 and 48 hours as seen in Figure 3.38.

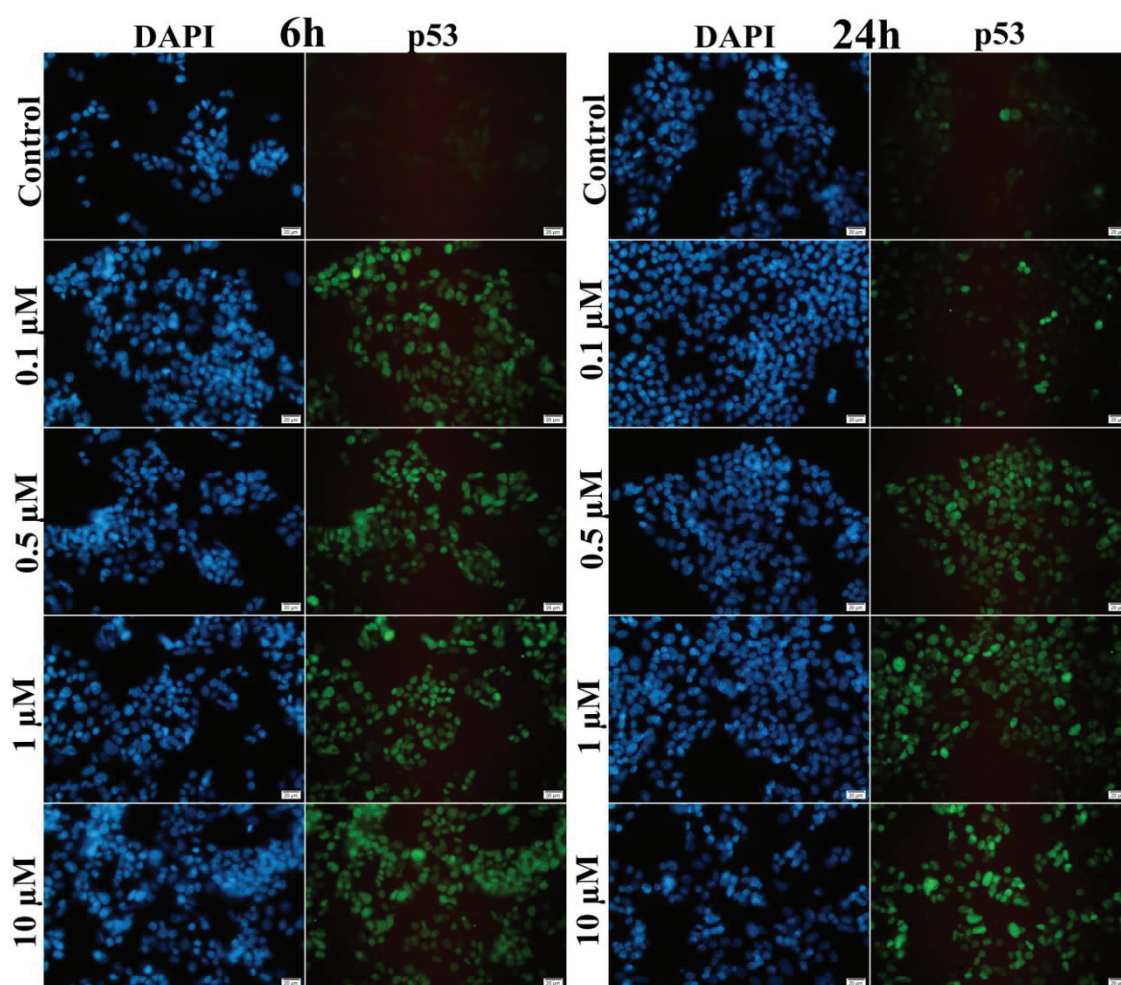


Figure 3.37. Immunofluorescence imaging of p53 upregulation in HepG2 cells after (R)-4'-methylklavuzon treatment. Images were obtained by using 40X objective with 20  $\mu\text{m}$  scale.

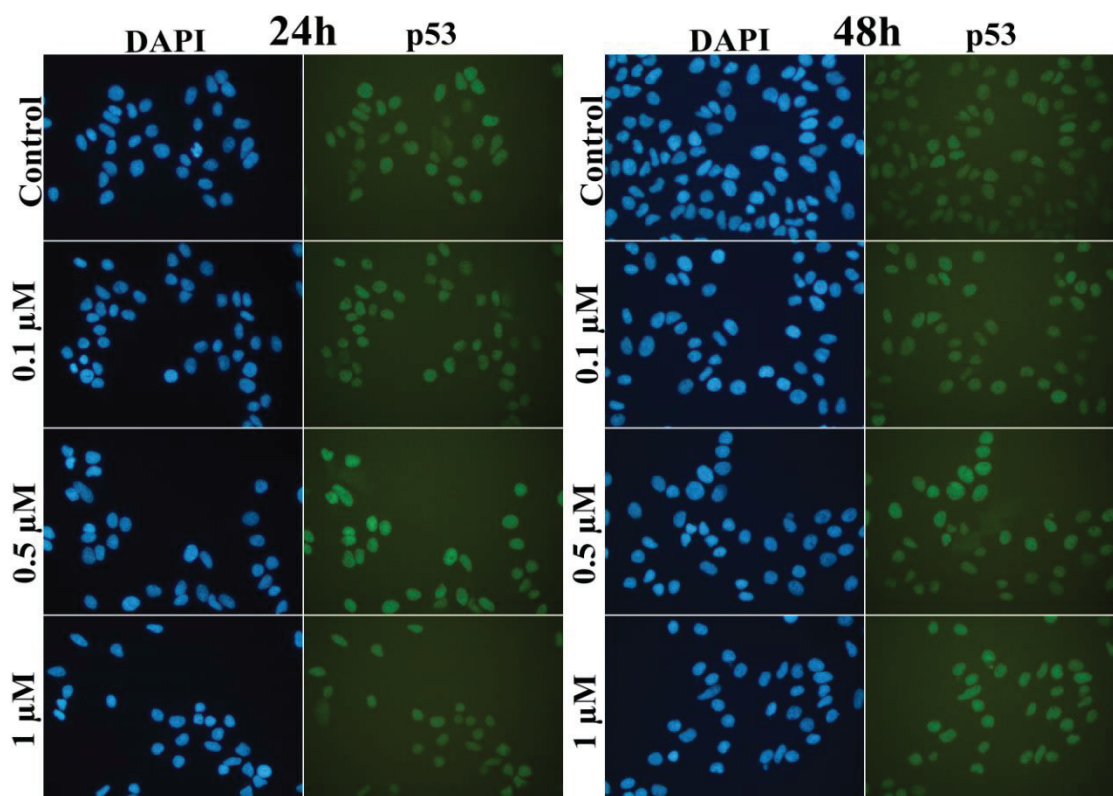


Figure 3.38. Immunofluorescence imaging of p53 upregulation in HuH-7 parental cells after (R)-4'-methylklavuzon treatment. Images were obtained by using 40X objective with 20 μm scale.

### 3.16. Immunofluorescence Visualization of p53 Protein Levels in HepG2 Cell Spheroids

It was found that p53 protein levels were upregulated in HepG2 spheroids with increasing concentrations of (*R*)-4'-methylklavuzon, 50  $\mu\text{M}$  of goniotalamin and 10  $\mu\text{M}$  of TK126 within 24 hours of incubation. Propidium Iodide staining indicated dying cells at the concentrations of 1.00, 10  $\mu\text{M}$  and 20  $\mu\text{M}$  of (*R*)-4'-methylklavuzon and 10  $\mu\text{M}$  of TK126 within 24 hours of incubation as shown in Figure 3.39.

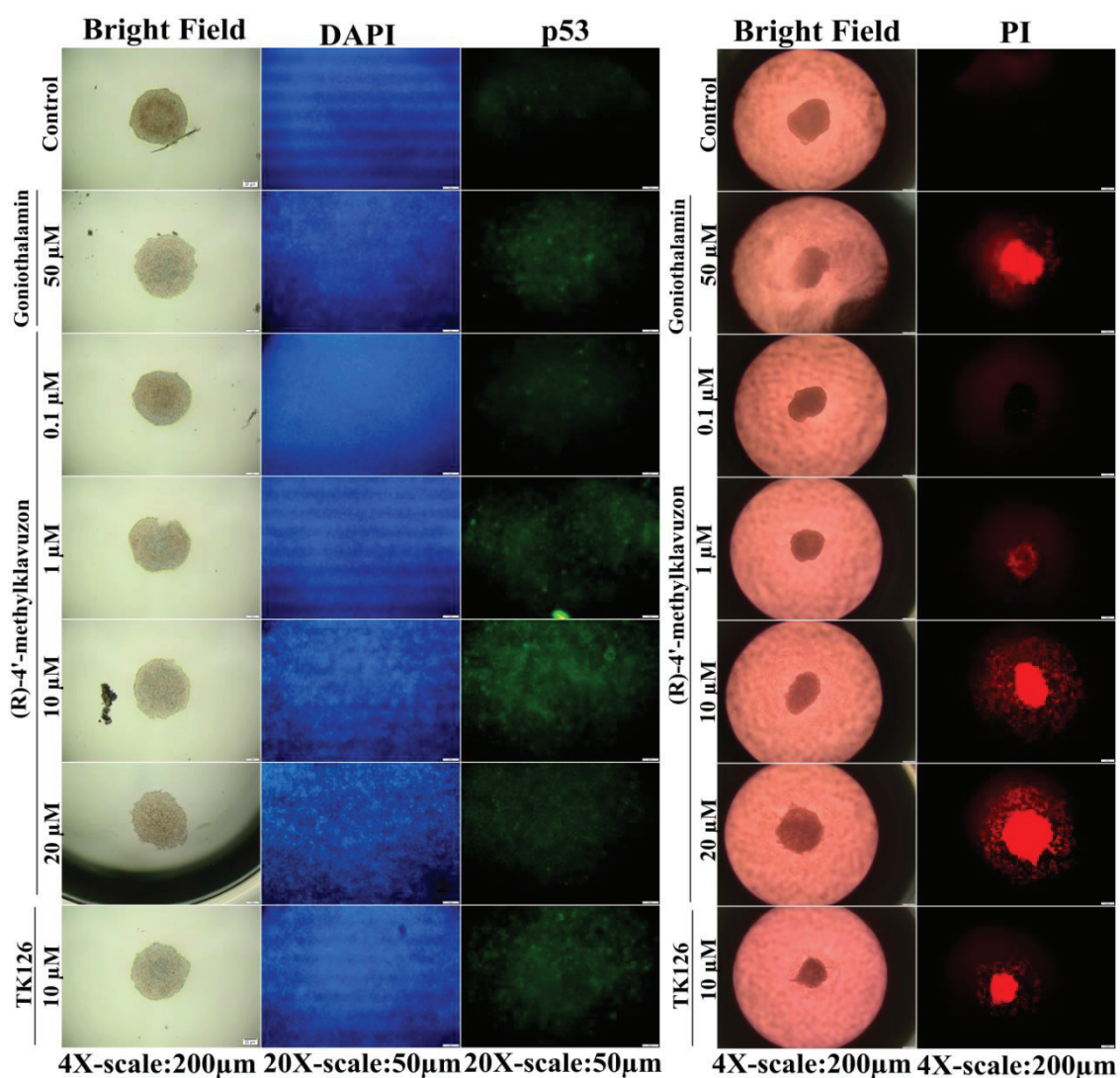


Figure 3.39. Microscope images of (*R*)-4'-methylklavuzon treated HepG2 spheroids stained with DAPI, PI and p53 antibody at the end of 24 hours of incubation.



### 3.17. Colorimetric Determination of p53/MDM2 Complex by ELISA

Prior to testing molecules, protein concentration to be used in each well was optimized in order to determine possible interference from cell matrix. To do this, total protein was isolated from HuH-7 cells by using RIPA buffer 2 (Enzo Life Science) and diluted 1:4, 1:8, 1:16 and 1:32 times with assay buffer (100 mM sodium phosphate, 150 mM NaCl, 1.0% BSA, 0.1% Tween-20, pH 7.4) as recommended in manufacturer's protocol. It was found that 1:32 times dilution is in the range of the p53/MDM2 complex standard curve. The total protein concentration isolated from HuH-7 cells was determined using BCA Assay Kit (Pierce, 23227) and found to be 1364.3  $\mu\text{g/ml}$  and the protein concentration of 1:32 times diluted protein is 42.6  $\mu\text{g/ml}$ . 4.2  $\mu\text{g}$  total protein in 100  $\mu\text{l}$  was used in each well for ELISA. The effect of 1.00  $\mu\text{M}$  of (*R*)-4'-methylklavuzon on different dilutions was also tested and it was found that somehow (*R*)-4'-methylklavuzon caused a slight decrease in p53/MDM2 complex formation at all dilution factors as shown Figure 3.40.

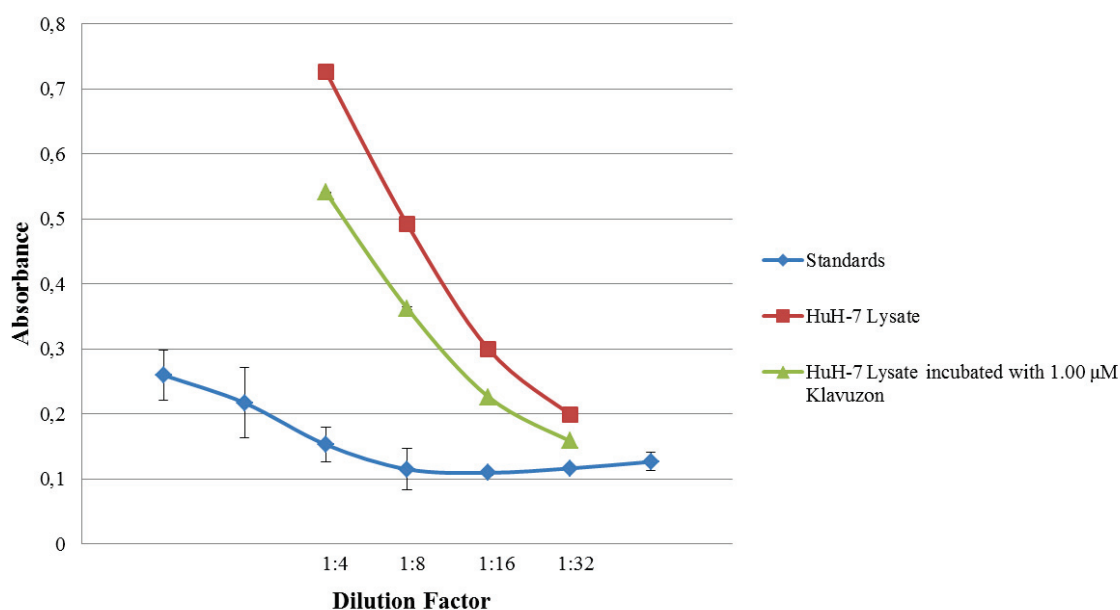


Figure 3.40. Total protein optimization of HuH-7 cell lysate

In the next step, effect of the drug candidate on pure p53/MDM2 complex was studied. To do this, pure p53 proteins were incubated with p53 capture antibody that is immobilized on microplate well for 1 hour and then unbound p53 proteins were removed by washing. After washing procedure, bound p53 proteins was treated with 1.00  $\mu\text{M}$  of (*R*)-4'-methylklavuzon dissolved in DMSO and assay buffer for 1 hour at room temperature and then washed with washing buffer. After washing, MDM2 proteins were incubated with p53 proteins for 1 hour at room temperature. Amount of decrease in p53/MDM2 complex formation was shown in the Table 3.2 and Figure 3.41 below.

Table 3.2. Amount of inhibition for p53/MDM2 complex formation by (*R*)-4'-methylklavuzon treated pure p53 and MDM2 proteins.

p53 Standard Concentrations (ng/ml)	MDM2 Standard Concentrations (ng/ml)	Untreated Standard Absorbance	1.00 $\mu\text{M}$ Drug Treated Absorbance	Inhibition (%)
50	16	0.3018	0.1639	45
25	8	0.2299	0.1606	30
12.50	4	0.2282	0.1466	36
6.25	2	0.1886	0.1484	21

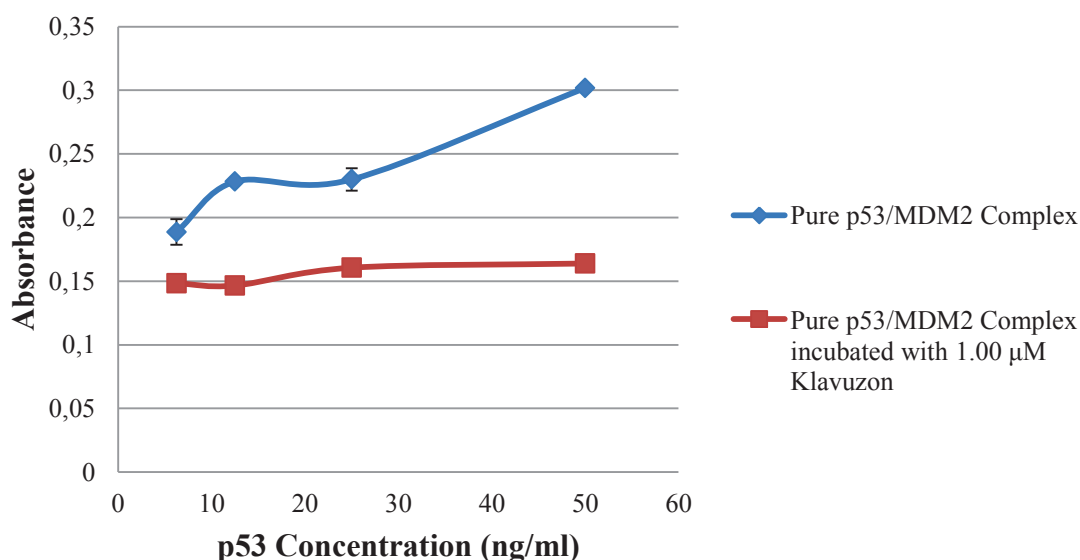


Figure 3.41. Effect of (*R*)-4'-methylklavuzon on pure p53/MDM2 complex

After in vitro protein-drug interaction assays, HuH-7 cells were treated with 0.30, 1.00 and 3.00  $\mu\text{M}$  of drug candidate for 6 hours and 24 hours. HuH-7 cells were also treated with 0.30, 1.00, 3.00 and 9.00  $\mu\text{M}$  of drug candidate for 48 hours. Then

total proteins were isolated from each treated cells using RIPA buffer 2 (Enzo Lifesciences) and protein concentrations were determined by BCA Assay Kit (Pierce, 23227). In order to determine p53/MDM2 complex, 4.2 µg total protein in 100 µl assay buffer was added into each well coated with p53 antibody. Results are summarized in Table 3.3 – 3.5 and Figures 3.42 – 3.44 as shown below.

Table 3.3. p53/MDM2 complex status in 6-hours drug treated HuH-7 cells

<b>Drug Concentration (µM)</b>	<b>Absorbance</b>	<b>Percentage Change (%)</b>
DMSO Control	0.2899	-
0.30	0.3627	+ 25
1.00	0.2871	- 1.00
3.00	0.2837	- 2.00

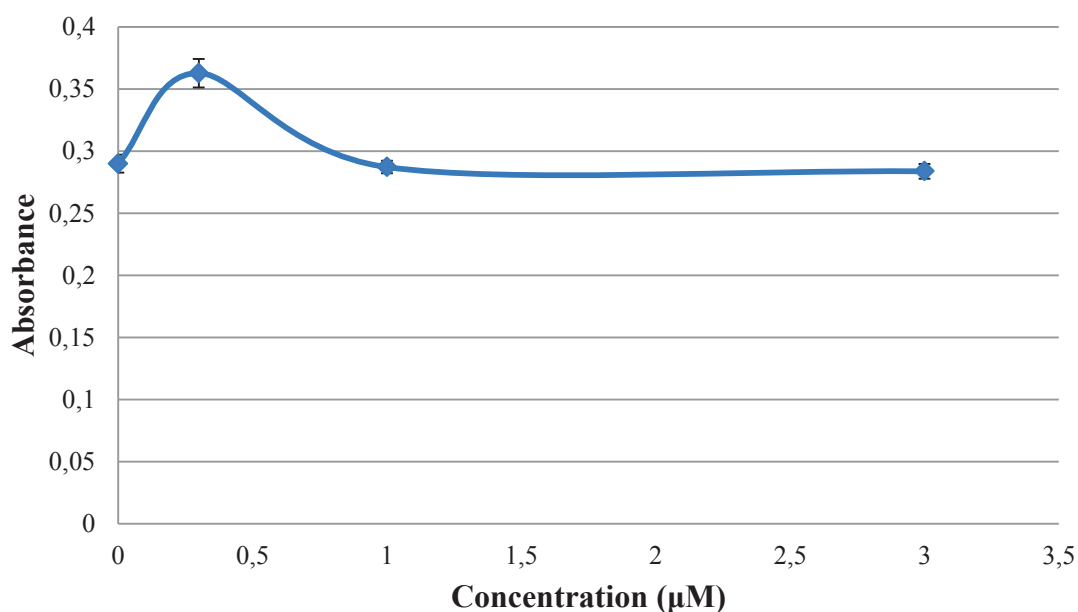


Figure 3.42. Levels of p53/MDM2 complex in HuH-7 cells incubated with various concentrations of (*R*)-4'-methylklavuzon for 6 hours

Table 3.4. p53/MDM2 complex status in 24-hours drug treated HuH-7 cells

Drug Concentration ( $\mu\text{M}$ )	Absorbance	Percentage Change (%)
DMSO Control	0.3543	-
0.30	0.3791	+ 7.00
1.00	0.4382	+ 23
3.00	0.4037	+ 14

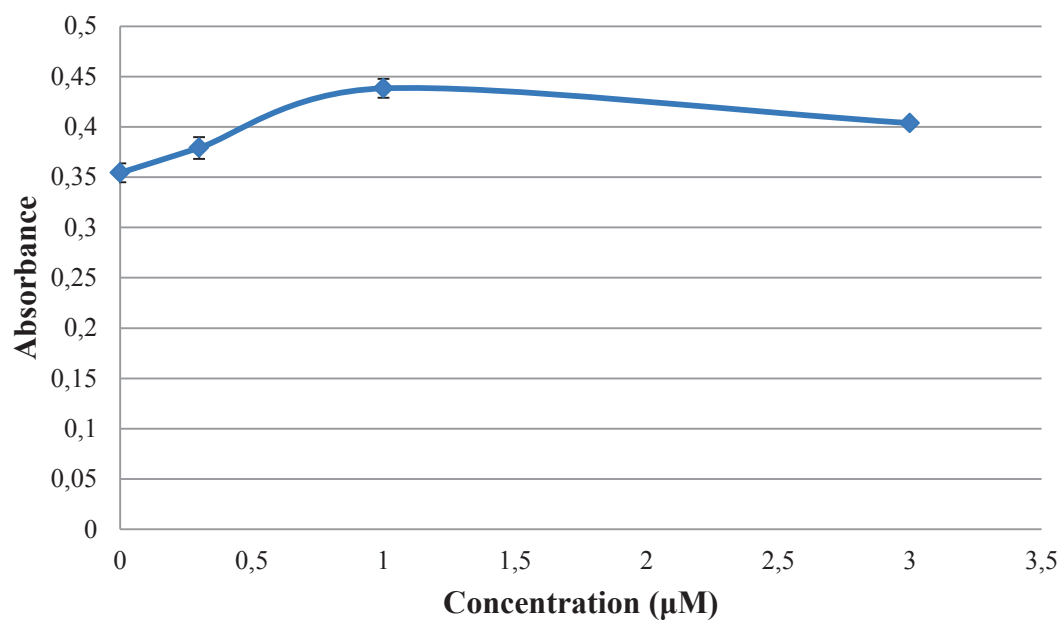


Figure 3.43. Levels of p53/MDM2 complex in HuH-7 cells incubated with various concentrations of (*R*)-4'-methylklavuzon for 24 hours

Table 3.5. p53/MDM2 complex status in 48-hours drug treated HuH-7 cells

Drug Concentration ( $\mu\text{M}$ )	Absorbance	Percentage Change (%)
DMSO Control	0.3146	-
0.30	0.3635	+15
1.00	0.2624	- 17
3.00	0.2664	- 15
9.00	0.2786	- 11

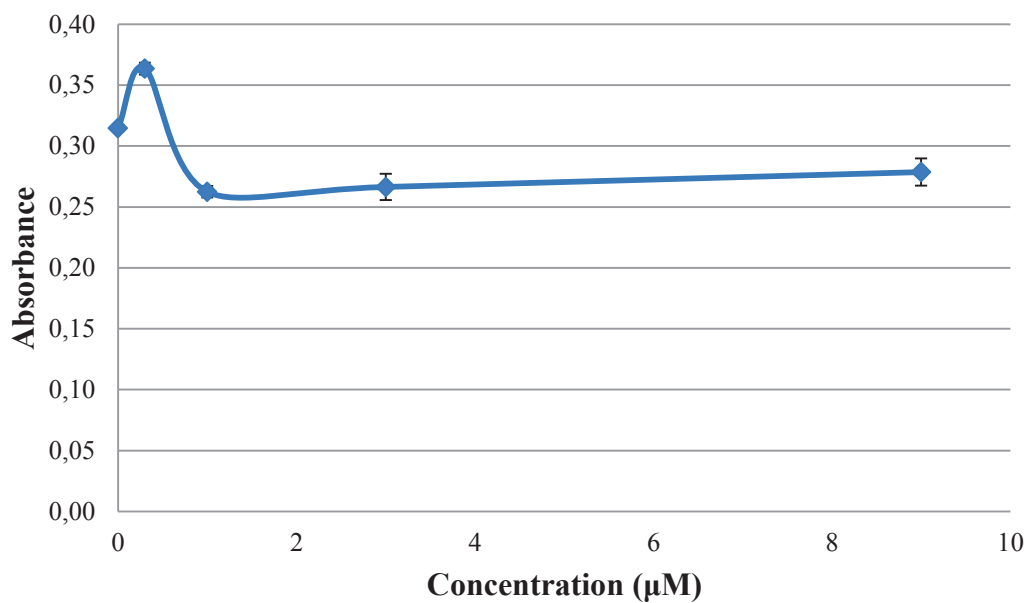


Figure 3.44. Levels of p53/MDM2 complex in HuH-7 cells incubated with various concentrations of (*R*)-4'-methylklavuzon for 48 hours

### 3.18. Effects of (*R*)-4'-methylklavuzon on HuH-7 Spheroids

Spheroids were analyzed with an alteration in their morphology by crumbling intact spheroid structures as illustrated in the Figures 3.45-3.49 below.

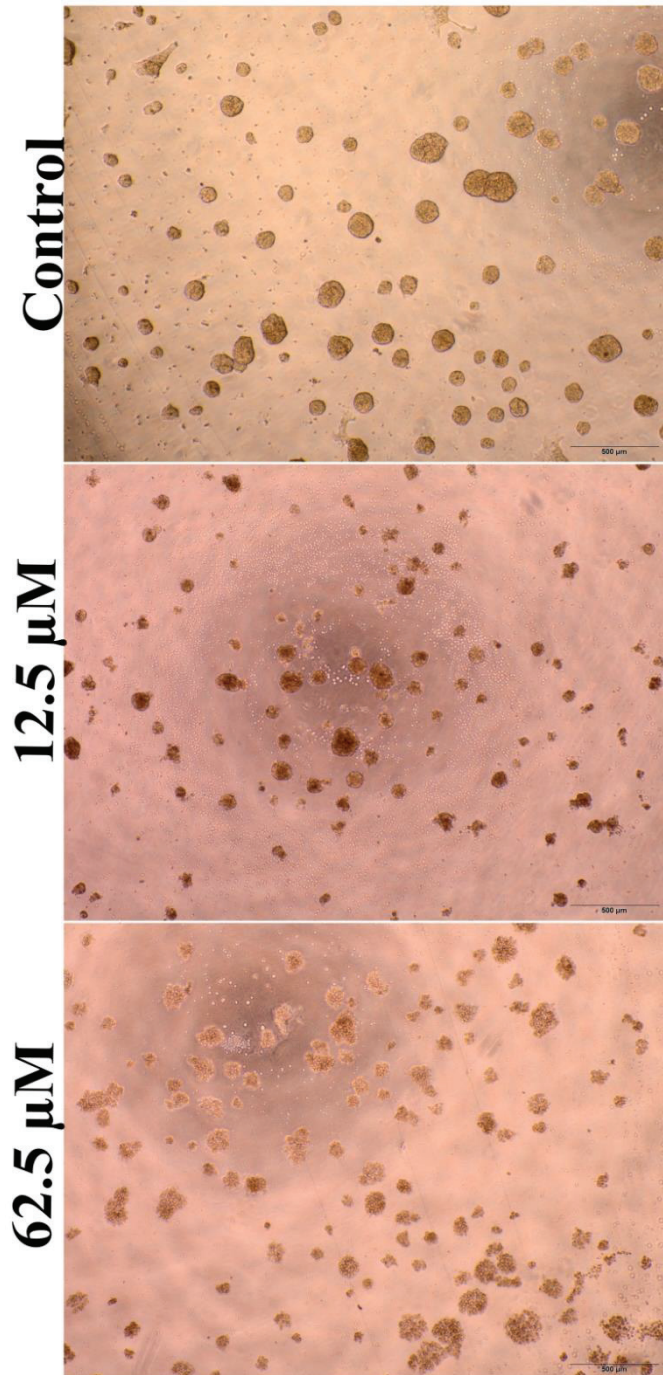


Figure 3.45. Microscope images (4X) of HuH-7 parental cell spheroids in matrigel at the end of 48 hours of incubation with (*R*)-4'-methylklavuzon. Images were obtained by using 4X objective with 500  $\mu\text{m}$  scale.

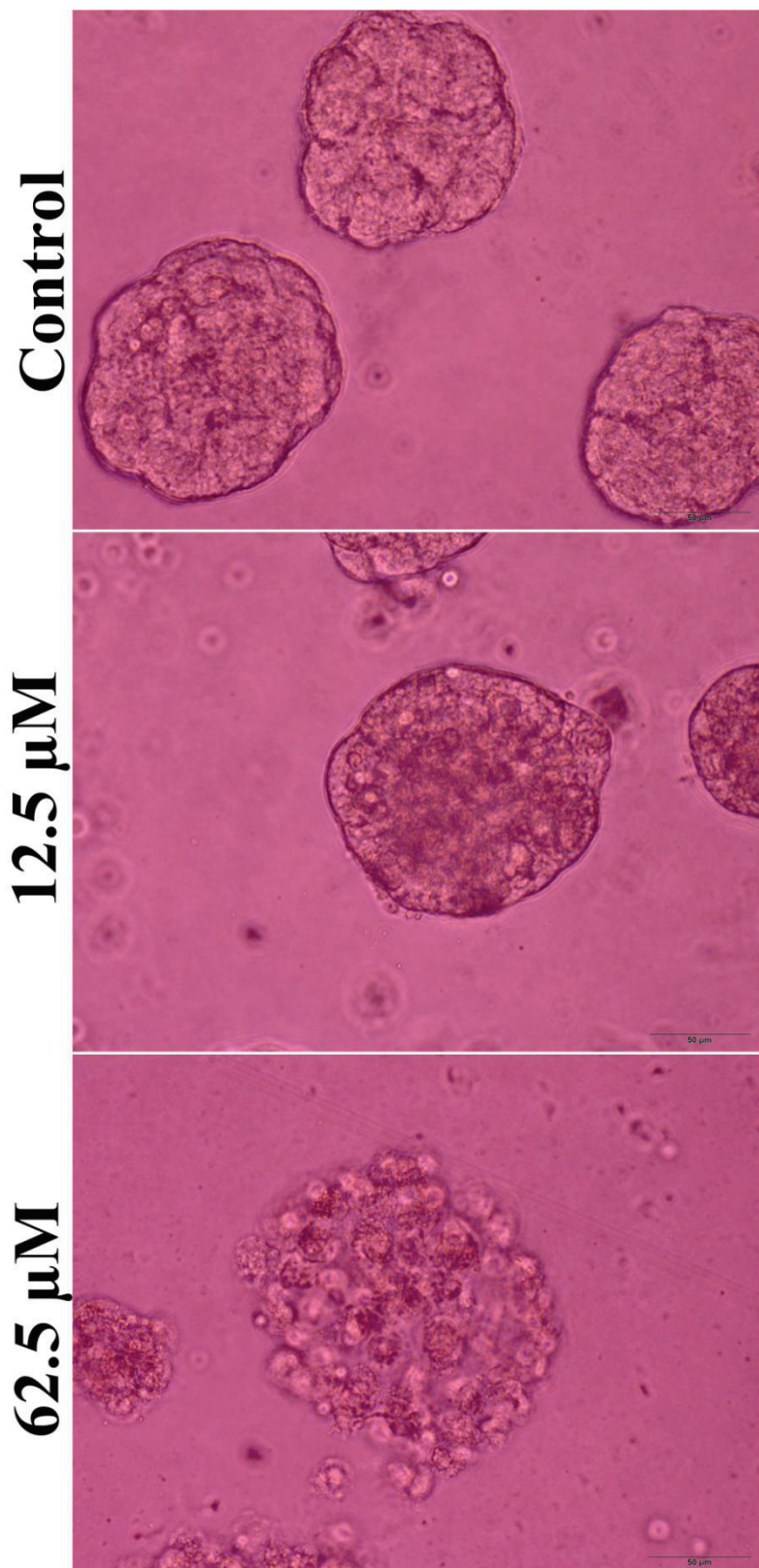


Figure 3.46. Microscope images (40X) of HuH-7 parental cell spheroids in matrigel at the end of 48 hours of incubation with (*R*)-4'-methylklavuzon. Images were obtained by using 4X objective with 50 μm scale.

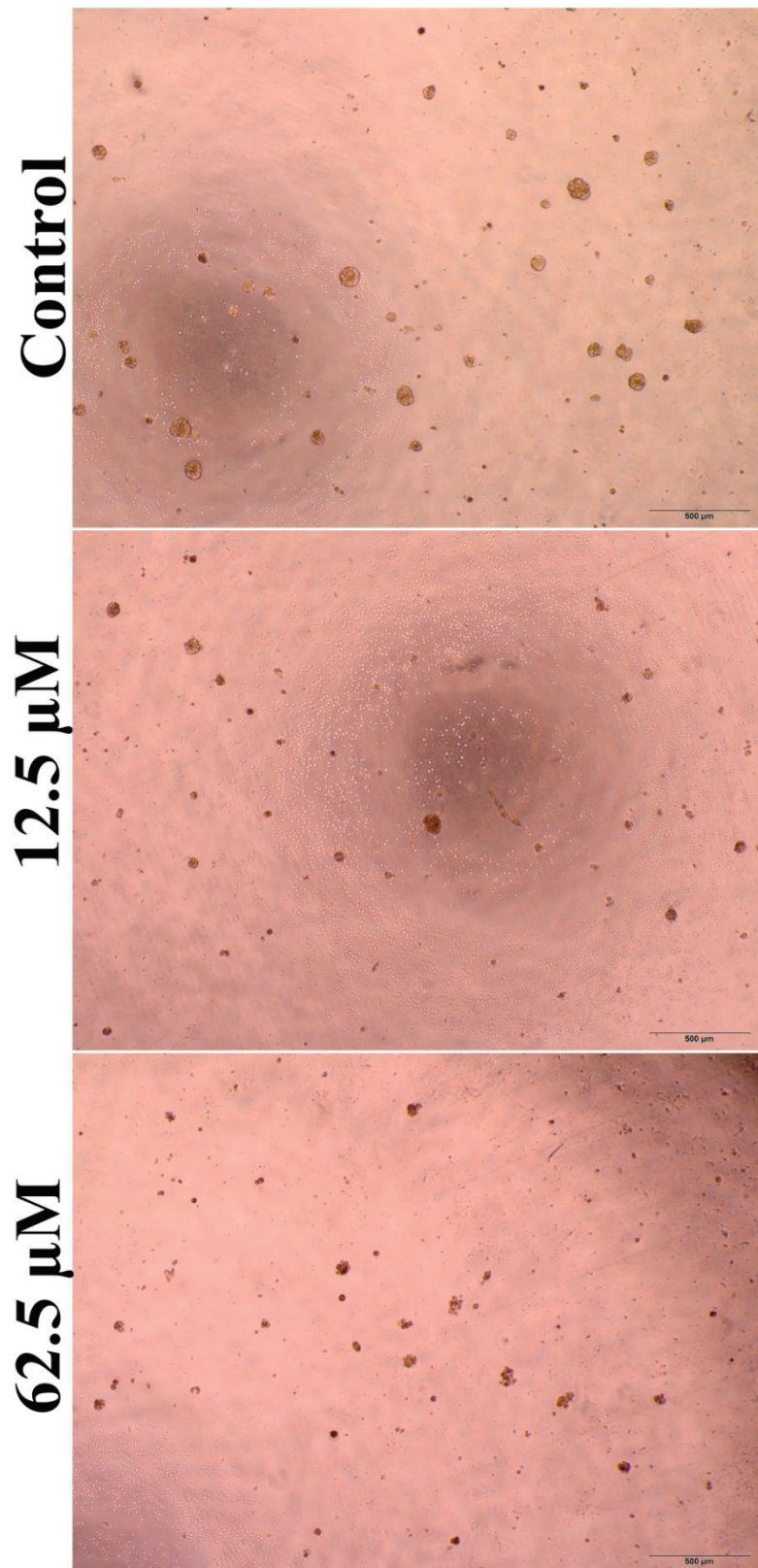


Figure 3.47. Microscope images (4X) of EpCAM<sup>+</sup>/CD133<sup>+</sup> HuH-7 cell spheroids in matrigel at the end of 48 hours of incubation with (*R*)-4'-methylklavuzon. Images were obtained by using 4X objective with 500 μm scale.



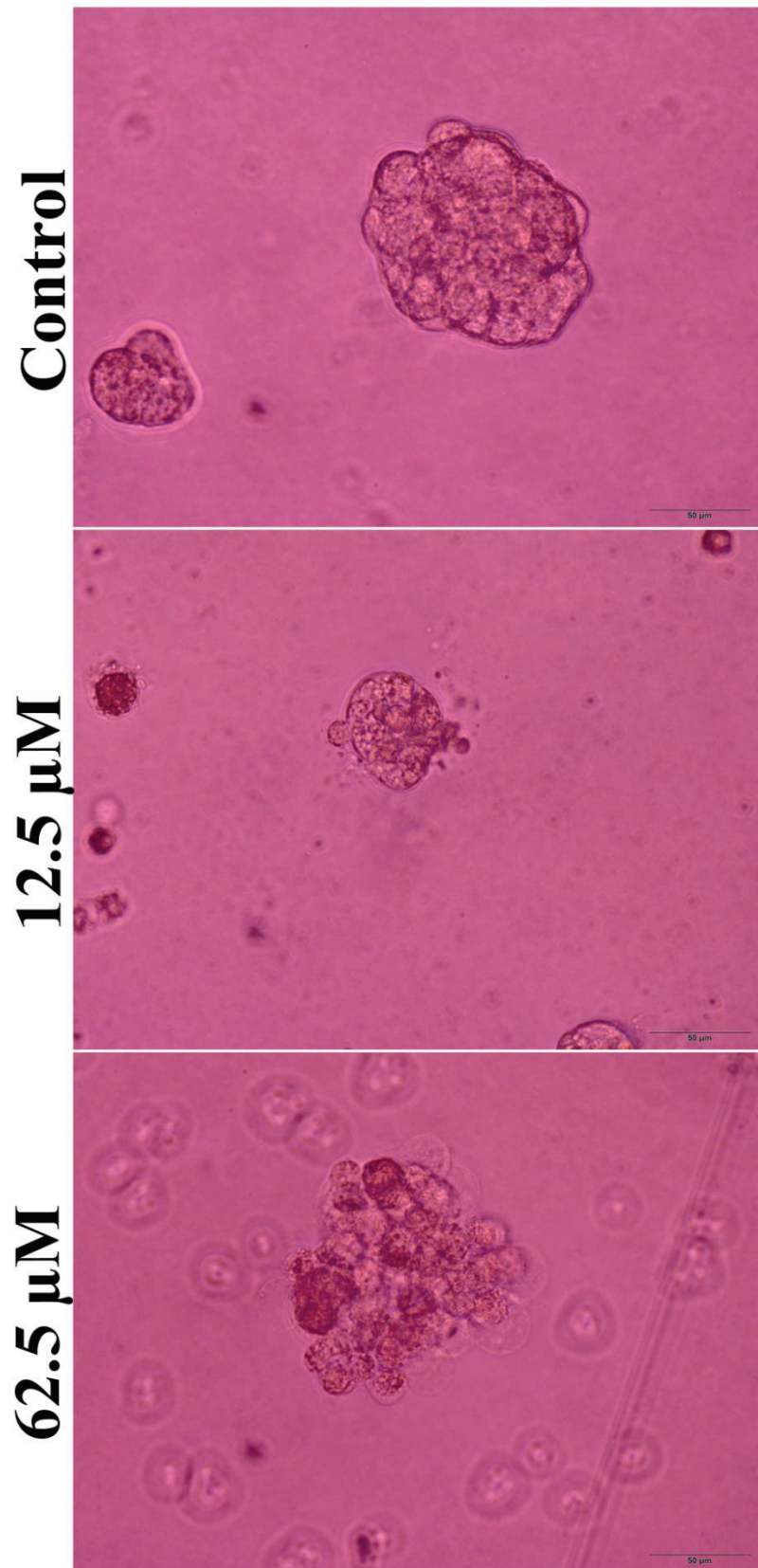


Figure 3.48. Microscope images (40X) of EpCAM<sup>+</sup>/CD133<sup>+</sup> HuH-7 cell spheroids in matrigel at the end of 48 hours of incubation with (*R*)-4'-methylklavuzon. Images were obtained by using 4X objective with 50 μm scale.

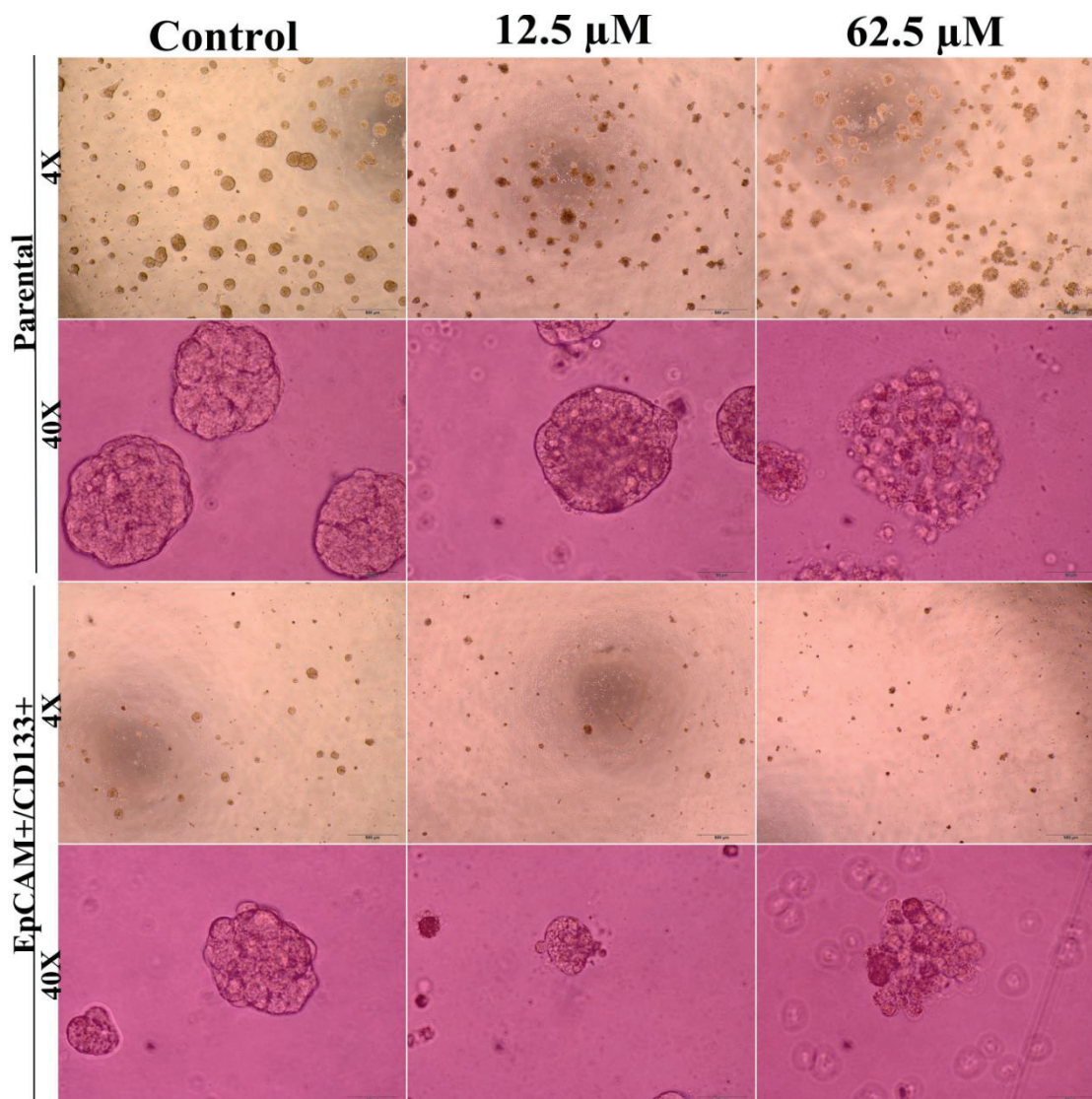


Figure 3.49. Microscope images (4X and 40X) of spheroids formed with HuH-7 parental and EpCAM<sup>+</sup>/CD133<sup>+</sup> HuH-7 cells at the end of 48 hours of incubation with (*R*)-4'-methylklavuzon. Images were obtained by using 4X objective with 500  $\mu\text{m}$  scale and 40X objective with 50  $\mu\text{m}$  scale.

## CHAPTER 4

### DISCUSSION

According to MTT cell viability assay,  $IC_{50}$  values of (*R*)-4'-methylklavuzon on HuH-7 parental cells were determined as 5.00  $\mu$ M for 24 hours, 1.25  $\mu$ M for 48 and 72 hours.  $IC_{50}$  values for EpCAM<sup>+</sup>/CD133<sup>+</sup> were determined as 10  $\mu$ M for 24 hours, 2.5  $\mu$ M for 48 hours and 1.25  $\mu$ M for 72 hours.  $IC_{50}$  values for EpCAM<sup>-</sup>/CD133<sup>-</sup> were determined as 10  $\mu$ M for 24 hours, 1.25  $\mu$ M for 48 and 72 hours.

EpCAM<sup>+</sup>/CD133<sup>+</sup> and EpCAM<sup>-</sup>/CD133<sup>-</sup> cells were determined as more resistant against the drug candidate especially for 24 hours of incubation compared to HuH-7 parental cells.  $IC_{50}$  values for 48 hours were obtained as 1.25  $\mu$ M for parental and EpCAM<sup>-</sup>/CD133<sup>-</sup> cells and 2.5  $\mu$ M for EpCAM<sup>+</sup>/CD133<sup>+</sup>. (*R*)-4'-methylklavuzon can inhibit 50% of EpCAM<sup>+</sup>/CD133<sup>+</sup> cell proliferation at 2.5  $\mu$ M concentration within 48 hours of incubation.  $IC_{50}$  values for 72 hours were 1.25  $\mu$ M for all the populations. The resistance of EpCAM<sup>+</sup>/CD133<sup>+</sup> cells against the drug candidate can be explained by possible overexpression of ABC-transport proteins in cell plasma membrane in cancer stem cells compared to HuH-7 parental cells.

It was found that (*R*)-4'-methylklavuzon acts on cell cycle at 1.00 and 10  $\mu$ M concentrations. Lower doses didn't have any influence. (*R*)-4'-methylklavuzon caused cell cycle arrests dose-dependently. It caused approximately 20% increment in G1 phase ratio in all of the three cell populations at 1.00  $\mu$ M, whereas it caused approximately 20% increment in G2 phase ratio in all of the three cell populations at 10  $\mu$ M concentration. Drug candidate works on cell cycle regulation with different mechanisms based on concentration. According to literature, G1 arrest was considered to be a possible result of sirtuin inhibition and upregulation of p21 gene expression. Increased ratio of G1 phase can also be explained that (*R*)-4'-methylklavuzon might act on proteins that are unique for G1 phase.

(*R*)-4'-methylklavuzon caused approximately 20% increase in late apoptosis within 48 and 72 hours at 10  $\mu$ M concentration regardless of cell populations. No significant results were obtained from treatments with (*R*)-4'-methylklavuzon at 1.00 and 0.10  $\mu$ M concentrations.

It was found that 4'-alkylklavuzon derivatives have similar cytotoxic effect on both MIA-PaCa2 (pancreatic cancer cells) and HPDEC (Human Pancreatic Duct Epithelial Cells) without any selective property. It was observed that TK126 which is a klavuzon derivative has a lower IC<sub>50</sub> compared to (R)-4'-methylklavuzon. HPDEC cells are immortalized by stable HPV E6 and E7 gene integration. E6 protein is an ubiquitin ligase which plays a role in degradation of p53 providing immortal property. Similarly, disruption of E6-p53 interaction by (R)-4'-methylklavuzon derivatives can cause death in HPDEC cells similar to HuH-7 and MIA PaCa-2 cells.

It was found that untreated EpCAM<sup>-</sup>/CD133<sup>-</sup> HuH-7 cells have approximately 2.5 times higher histone deacetylase enzyme activity compared to the other cells. It is known that EpCAM<sup>-</sup>/CD133<sup>-</sup> cells have an approximately 1.5 times higher proliferation rate which might be a consequence of this higher HDAC enzymatic activity.

(R)-4'-methylklavuzon has no inhibitory effects at all concentrations on histone deacetylase enzymes isolated from HuH-7 parental and EpCAM<sup>+</sup>/CD133<sup>+</sup> nucleus in vitro, whereas it has statistically significant inhibitory effects by approximately 20% at 27 and 81 μM concentrations on histone deacetylase enzymes isolated from EpCAM<sup>-</sup>/CD133<sup>-</sup> cells. Non-inhibitory effect of (R)-4'-methylklavuzon might be considered as a result of pH 8.0 of the reaction condition and better inhibitory effects might be achieved at lower pH values because it is believed that (R)-4'-methylklavuzon may inhibit proteins by acting as a Michael acceptor which is irreversible at pH 7.0.

It was found that (R)-4'-methylklavuzon does not have significant inhibitory effects on HDAC1 enzyme activity. It was found that 50 μM of (R)-4'-methylklavuzon inhibited HDAC1 activity by only 2.6% and 100 μM of (R)-4'-methylklavuzon inhibited HDAC1 activity by 9.2%. Data obtained from HDAC1 activity measurement was parallel to data obtained from in vitro histone deacetylase enzymatic activity measurement experiment.

It was also found that 50 μM of (R)-4'-methylklavuzon can inhibit SIRT1 enzyme activity by 29% and 100 μM of (R)-4'-methylklavuzon can inhibit SIRT1 enzyme activity by 46% in vitro. Moreover, 100 μM of TK126 can inhibit SIRT1 enzyme activity by 65%. Sirtuin enzymes catalyse NAD<sup>+</sup> dependent protein deacetylation that consumes a mole equivalent of NAD<sup>+</sup> per acetyl group removed.

Sirtuins contain highly conserved residues in their catalytic site or NAD<sup>+</sup> binding site which shows the possibility of (*R*)-4'-methylklavuzon to inhibit the other sirtuin enzymes (Figure 4.1).

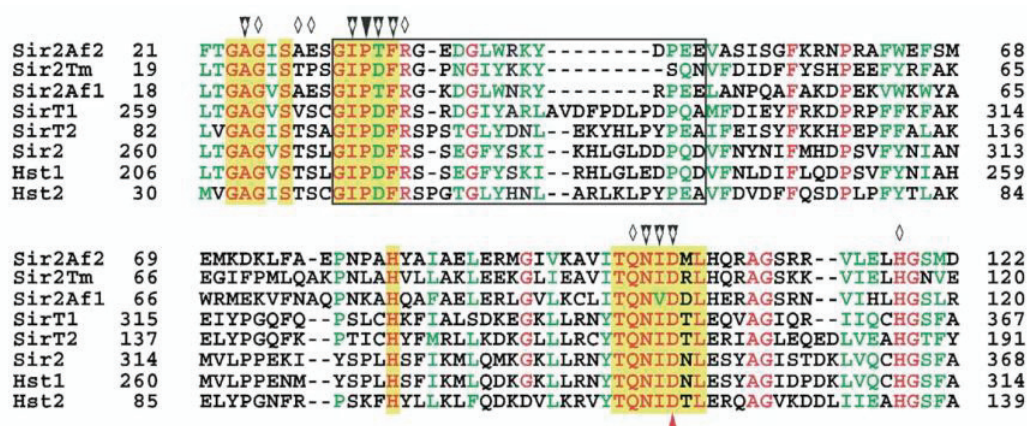


Figure 4.1. Multiple sequence alignment of different sirtuins indicating highly conserved residues (red) and conserved residues (green). Residues that are involved in the C pocket are highlighted in yellow, flexible loop is indicated by box. Residues that contact nicotinamide (black triangles) or contact NAD<sup>+</sup> bound in the productive conformation (white diamonds) are indicated above the alignment. The Asp that is responsible for NAAD-dependent deacetylation activity and nicotinic acid sensitivity when mutated to Asn is marked below (red triangle) (Avalos et al. 2005).

Docking studies were performed by using Autodock Vina software to better understand the nature of interactions between (*R*)-4'-methylklavuzon and TK126 with active site of SIRT1 enzyme. It was found that molecular docking and experimental results for binding to SIRT1 active site are parallel. According to Autodock Vina, binding of small molecules are spontaneous and TK126 has higher binding energy compared to (*R*)-4'-methylklavuzon. It was found that TK126 has higher inhibitory effect on SIRT1 enzyme than (*R*)-4'-methylklavuzon which means docking results and experimental results are consistent. Moreover, TK126 showed higher cytotoxic effect on MIA-PaCa2 (pancreatic cancer cells) and HPDEC (Human Pancreatic Duct Epithelial Cells) compared to (*R*)-4'-methylklavuzon. Higher cytotoxicity of TK126 compound might be related to higher SIRT1 inhibition compared to that of (*R*)-4'-methylklavuzon. Docking results of (*R*)-4'-methylklavuzon and TK126 to SIRT1 enzyme active site are illustrated in Figure 4.2.

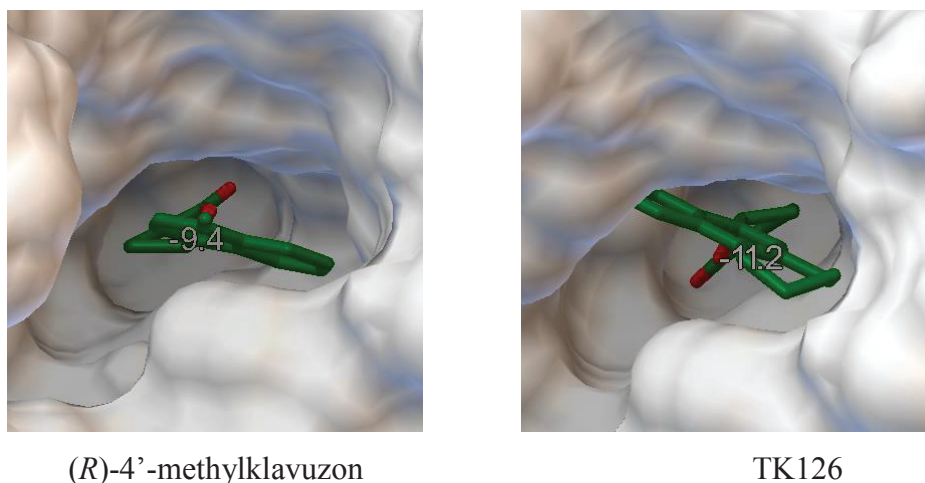


Figure 4.2. Docking studies of (R)-4'-methylklavuzon and TK126 to the active site of SIRT1.

Docking of (R)-4'-methylklavuzon in SIRT1 active site to determine proximity of cysteine amino acids which locate between 370th and 450th amino acids of SIRT1 protein to the drug candidate was performed and is illustrated in Figure 4.3.

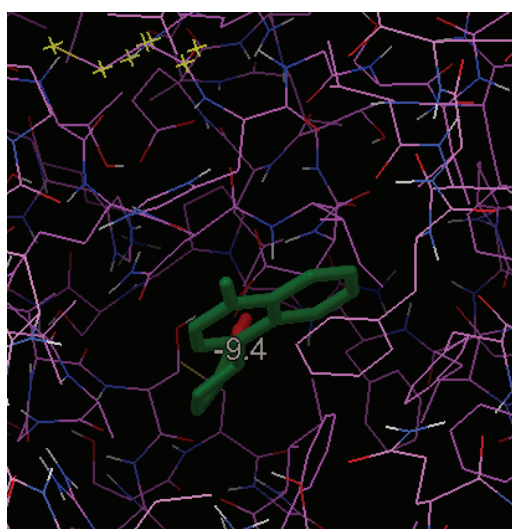


Figure 4.3. Proximity of cysteine amino acids to the (R)-4'-methylklavuzon. Yellow crosses are cysteine amino acids.

According to protein sequence and docking data, (R)-4'-methylklavuzon might bind to cysteine amino acids and blocks their roles in the catalysis reaction irreversibly or only blocks active site reversibly.

It was found that (*R*)-4'-methylklavuzon reduced histone deacetylase and/or sirtuin enzymatic activity almost by half for all of the cell populations when simultaneous cytotoxicity assays were ignored. The highest inhibition rate was obtained at 5.00  $\mu$ M concentration. The amount of inhibition slightly decreased at 3.00 and 1.00  $\mu$ M concentrations and it remained constant at 0.50, 0.25 and 0.10  $\mu$ M concentrations.

It was thought that  $\alpha,\beta$ -unsaturated carbonyl in the structure of (*R*)-4'-methylklavuzon may react with nucleophilic parts of the proteins inside the cells showing a biological activity. It was shown that this reaction is reversible at pH 8.0 but irreversible at pH 7.0. It is possible that the drug candidate might have reacted reversibly in the reaction buffer which has a pH of 8.0 causing a non-inhibitory effect. Inhibitory effects obtained from cell-based assay might have been achieved due to the intracellular compartments that have pH values lower than pH 8.0.

Additionally, in vitro HDAC assay examines only enzymes isolated from nucleus but cell-based assay can examine enzymes in nucleus, mitochondria and cytoplasm. (*R*)-4'-methylklavuzon might act on enzymes that locate in cytoplasm and mitochondria.

Cell-based HDAC enzyme measurement was performed also with cells isolated by fluorescence-activated cell sorting (FACS). It was found that cells isolated by MACS and FACS respond the drug in the same way in terms of cell-based HDACs/sirtuins activity. There were no significant differences between the data obtained from cell-based HDACs/sirtuins activity assays performed by using cells separated by MACS or FACS.

It was found that 1.00, 3.00 and 5.00  $\mu$ M of (*R*)-4'-methylklavuzon upregulates intracellular SIRT1 levels by 176%, 240% and 95%, respectively. Patients with high SIRT1 levels show chemoresistance to drugs. According to literature, SIRT1 inhibitors have a chance to reduce this resistance against chemotherapy and sensitize cancer cells for other chemotherapeutical combinations (Zhang et al. 2013, Li et al. 2015). It is reported that overexpression of SIRT1 attenuates p53-mediated apoptosis which is caused by DNA damage and oxidative stress. (*R*)-4'-methylklavuzon can inhibit overexpressed SIRT1 resulting a possible increment in p53-mediated apoptosis (Dai et al. 2007). E2F1 is known to provoke apoptosis as a consequence of DNA damage. E2F1 is downregulated via deacetylation by SIRT1 (Wang et al. 2006). Inductive effects of

the drug candidate on E2F1 protein expression levels should be investigated to better clarify the issue.

SIRT1 recruits DNA damage factors to the damaged sites after deacetylating histone H1 (Lys26) and H4 (Lys16). An interference to this repair mechanism by (*R*)-4'-methylklavuzon might lead cancer cells to apoptosis. Besides role of SIRT1 in DNA repair mechanism, topoisomerases are important factors in DNA repair. In house experiments showed that (*R*)-4'-methylklavuzon can form DNA breaks and can also inhibit topoisomerase I which means an interference in repair mechanism (Akçok et al. 2017). It was found that (*R*)-4'-methylklavuzon overexpresses SIRT1 protein levels to a maximum of 240% with concentration of 3.00  $\mu$ M. This overexpression might be a result of DNA break formation and topoisomerase I inhibition by (*R*)-4'-methylklavuzon. Inhibition of SIRT1 can also be a consequence of this overexpression. Lack of SIRT1 activity in the cell might have induced SIRT1 levels inside the cells. Moreover, interference in SIRT1 protein degradation pathway which is performed by MDM2 would be another explanation of increase in SIRT1 protein levels. It is reported that loss of SIRT1 shows cytotoxic effect on HCC cells as a result of G1 arrest (Portmann et al. 2013). It was also found that (*R*)-4'-methylklavuzon causes G1 arrest in both HCC tumor initiating cells and HCC parental cells which is consistent with previous literature data. Cytotoxic effect of (*R*)-4'-methylklavuzon on HCC tumor initiating cells might be a result of SIRT1 inhibition followed by increased p53 stability and activity.

SIRT1 is responsible in DNA repair mechanism by performing deacetylation of p53 together with HDAC1, directing cancer cells to survival. (*R*)-4'-methylklavuzon might have inhibited SIRT1 during DNA repair and provided increased stability of acetylated p53 which in turn overexpressed p21 gene expression.

Higher protein levels of SIRT1 compared to acetyl transferases can direct cancer cells to DNA repair, cell cycle arrest and survival. SIRT1 protein levels were increased by (*R*)-4'-methylklavuzon directing cells to apoptosis rather than survival.

The importance of SIRT1 can be listed as induction in p53-dependent apoptosis, decrease in cancer stem cell stemness and interference in DNA repair mechanism. Cell-based Histone Deacetylase Enzymatic Activity assay showed that (*R*)-4'-methylklavuzon can inhibit endogeneous Class I/II Histone deacetylase enzymes. But both in vitro class I/II HDAC enzyme activity assay and HDAC1 enzyme activity assay



showed that (*R*)-4'-methylklavuzon does not have significant inhibitory effects on histone deacetylase enzymes. It was thought that (*R*)-4'-methylklavuzon worked pH dependently inside the cells so that it could inhibit endogenous class I/II enzymes. But in vitro SIRT1 enzyme activity measurement showed that 100  $\mu$ M of (*R*)-4'-methylklavuzon can already inhibit SIRT1 by a maximum of 46% in vitro. This data supports that inhibition obtained from cell-based histone deacetylase enzymatic activity assay might have been achieved by sirtuin inhibition because substrate provided with the kit can be also deacetylated by sirtuins (Seidel et al. 2016, Dose et al. 2012, Borra et al. 2005). If sirtuins were inhibited by (*R*)-4'-methylklavuzon inside the cells, they could not have deacetylated the substrate after cell lysis. So decreased fluorescence intensity might have been achieved from inhibition of sirtuins.

Acetylation and methylation levels of histone 3 lysine 27 residue was investigated for an alteration after (*R*)-4'-methylklavuzon treatment for 24 and 48 hours of incubation. It has been observed that acetylation of H3K27 was not increased after drug treatment for both 24 and 48 hours. Additionally, methylation profile of H3K27 was investigated and no alteration was observed for both 24 and 48 hours.

The possible reason of this result might have been caused by insufficient dosing levels and timing of the drug treatment. The other reason might be that enzymes, which can be inhibited by drug candidate, may not be responsible for H3K27 residue. For this reason, specific HDACs/sirtuin enzymes that can be inhibited by (*R*)-4'-methylklavuzon should be identified and target histone proteins of these enzymes should be investigated. Effects of the drug candidate over deacetylation at the end of 72 hours of incubation were also investigated. In contrast to the expectations, acetylation levels were slightly increased in drug treated cell populations at 0.25  $\mu$ M and 1.00  $\mu$ M concentrations compared to the controls. Hyperacetylation of H3K27 residue were not obtained after drug treatment.

Methylation profile was analyzed at the end of 72 hours of incubation period with EpCAM<sup>+</sup>/CD133<sup>+</sup> cells sorted by FACS. EpCAM<sup>+</sup>/CD133<sup>+</sup> cells increased their methylation status with increasing concentrations of 1.00 and 5.00  $\mu$ M of (*R*)-4'-methylklavuzon. The highest increment were obtained at the concentration of 5.00  $\mu$ M. Upregulation of H3K27me3 residue was an unexpected result in the scope of this project. Possible reasons of the hypermethylation might be explained with two scenarios. First scenario is that when double strand breaks (DSB) occur in the promoter

of a gene, phosphorylation of H2AX and acetylation of H4K16 is increased and these events opens the chromatin. Then, repair proteins such as SIRT1, EZH2, DNMT1 and DNMT3B are recruited to the break site causing a decrease in H4K16ac and an increase in H3K27me3. This mechanism might prevent transcription of unrepaired DNA (O'Hagan et al. 2008). (*R*)-4'-methylklavuzon might have caused double strand breaks resulting in upregulation of H3K27me3 residue. Second scenario includes the acetylation of EZH2, which is the only known methyl transferase to H3K27 residue, at lysine 348 resulting in increased H3K27me3. Acetylation of EZH2 protein at lysine 348 stabilizes EZH2 to be recruited to H3K27 residue and trimethylate it. When EZH2 is deacetylated by SIRT1, methylation of H3K27 residue decreases. If (*R*)-4'-methylklavuzon inhibited SIRT1 and prevent deacetylation of lysine 348 residue of EZH2, trimethylation of H3K27 would have been increased. Investigation of increased acetylation of EZH2 at lysine 348 would be a significant supporting evidence of SIRT1 inhibitory property of the drug candidate as a future perspective.

It was found that (*R*)-4'-methylklavuzon upregulates p21 gene expression at all tested concentrations in all cell populations. The highest upregulation was achieved at 3.00  $\mu$ M concentration of drug candidate within 48 hours in parental cells. Upregulation of p21 gene may be a result of upregulation in p53 gene expression due to drug treatment. It is known that HDAC inhibitors cause G1/S arrest in cancer cells as a result of p21 gene upregulation. It was shown that drug candidate inhibits 40% of endogenous Class I/II HDAC and/or sirtuin enzymes and also 1.00  $\mu$ M of (*R*)-4'-methylklavuzon causes 8.6% and 20% increment in G1 phase for 24 and 48 hours of incubations, respectively. This increment may be as a result of increased p21 gene expressions. p21 functions by inhibiting cyclin-dependent kinase 4 and 6 which is responsible for phosphorylation of Retinoblastoma (Rb). When Retinoblastoma not phosphorylated, E2F cannot dissociate from Rb and enter into nucleus for transcription of necessary genes for S phase.

p27 expression was slightly increased at 3.00  $\mu$ M of (*R*)-4'-methylklavuzon but it was decreased at lower doses of (*R*)-4'-methylklavuzon. It is known that p27 levels are reduced during G1 and S phases. Drug candidate may have induced its proteolytic degradation with lower doses or interfered with its transcription mechanism. The other reason might be the upregulation of p21 cell cycle inhibitor.

Retaining tumor suppressive proteins in the nucleus is an effective strategy to induce apoptosis of cancer cells. (*R*)-4'-methylklavuzon can inhibit the most important exporter called CRM1 protein which exports over 230 proteins and RNAs from nucleus into cytoplasm. 0.10  $\mu$ M of drug candidate can inhibit CRM1 in 6 hours incubation time in HuH-7 cells revealing a distinct localisation of R1OK2 in the nucleus compared to controls which possess R1OK2 diffused both in nucleus and cytoplasm. Unfortunately, same dosage of drug candidate can not continue to inhibit CRM1 in 24 hours incubation time. It is considered as when cells are lack of CRM1 activity, they might increase protein levels of CRM1 to overcome this problem. Starting from 1.00  $\mu$ M of (*R*)-4'-methylklavuzon can inhibit CRM1 in both 6 hours and 24 hours incubation times in HuH-7 cells, which means concentration of drug molecule is still sufficient for already-existing or being-expressed CRM1 proteins. In contrast to HuH-7 cells, 0.10  $\mu$ M of drug candidate can inhibit CRM1 in both 6 hours and 24 hours incubation times maintaining nuclear R1OK2 localization in HepG2 cells. The other higher concentrations of (*R*)-4'-methylklavuzon provides CRM1 inhibition accompanied with increased R1OK2 protein levels in the nucleus of HepG2 cells, which is probably caused by complete inhibition of CRM1 more than the diluted concentrations of drug candidate.

The other data which was obtained by Ali Çağır's group is that drug candidate can inhibit CRM1 mediated nuclear export of R1OK2 (Serine/threonine-protein kinase Rio2) in HeLa cells. Data revealed that drug candidate started to inhibit CRM1 at 0.20  $\mu$ M concentration even at the end of the 90 minutes of incubation (87%) whereas goniotalamin inhibited at 1.00  $\mu$ M concentration at the end of the 90 minutes of incubation. It was found that (*R*)-4'-methylklavuzon started to inhibit CRM1 at 20 nM concentration and it almost inhibited CRM1 completely in all cells at 50 nM concentration (Kanbur et. al. 2017).

Overexpression and stabilization of p53 in cancer patients are the most leading therapeutical targets due to their strong tumor suppressive ability. (*R*)-4'-methylklavuzon can slightly trigger p53 overexpression in HuH-7 parental cells at only 0.50  $\mu$ M concentration within 24 and 48 hours.

(*R*)-4'-methylklavuzon can start to trigger p53 overexpression mainly in the nucleus of HepG2 cells at 0.10  $\mu$ M concentration within 6 hours significantly. It was also found that p53 protein is upregulated in HepG2 spheroids by drug candidate. Upregulation of p53 in HepG2 spheroids were parallel to increased propidium iodide

staining of spheroids indicating cell death. This data proves penetration and apoptotic effects of (*R*)-4'-methylklavuzon in spheroids. This data might have been achieved due to a possible DNA damage caused by drug candidate or CRM1 inhibition at the end of the incubation. It was previously showed by Ali Çağır's group that (*R*)-4'-methylklavuzon can form comet (DNA breaks) in Mia-PaCa2 cells according to comet assay as an indication of double strand DNA breaks (Kanbur et al. 2017, Akçok et al. 2017).

It was found that transcriptional activity of p53 was silenced via deacetylation by SIRT1 (Lou et al. 2000, Juan et al. 2000, Lou et al. 2001). In addition to p53-regulatory property of HDAC1, SIRT1 is considered to play a crucial role in deacetylation of p53 in cytoplasm whereas HDAC1 deacetylates it mostly in nucleus (Lou et al. 2001, Vaziri et al. 2001). According to the data in this study, SIRT1 enzyme was inhibited and SIRT1 protein levels were significantly upregulated by (*R*)-4'-methylklavuzon. In addition to possible DNA damage in HepG2 cells, p53 levels might have been increased or stabilized due to both SIRT1 enzymatic activity inhibition. When SIRT1 is inhibited, p53 can't be deacetylated by SIRT1 and can't be ubiquitinated by MDM2 ligase. As a result of blockage in ubiquitination, p53 can not be directed to proteasomal degradation and maintained in the nucleus of the cell.

It was previously found by Ali Çağır's group that drug candidate can inhibit topoisomerase I enzyme in 30 minutes at even 1.00  $\mu$ M concentration. 100  $\mu$ M of drug candidate was found to be sufficient for topoisomerase I inhibition within only 5 and 10 minutes of preincubation (Akçok et al. 2017). When topoisomerase I is inhibited, DNA can not be repaired after any DNA damage.

It was found that (*R*)-4'-methylklavuzon caused an inhibition of p53/MDM2 complex formation by 46% when 50 ng/ml of pure p53 protein present. Percentage of this inhibition declined with decreasing concentrations of p53 standard.

Effect of (*R*)-4'-methylklavuzon over the amount of p53/MDM2 complex in HuH-7 cells was also studied at cellular level. There was 25% increase in p53/MDM2 complex when HuH-7 cells treated with 0.30  $\mu$ M concentration of drug candidate within 6 hours. Higher doses of (*R*)-4'-methylklavuzon does not have any effect over this complex for 6 hours. At the end of 24 hours of incubation 0.30, 1.00 and 3.00  $\mu$ M concentration of drug candidate caused an increase in p53/MDM2 complex levels by 7.00, 23.7 and 13.9%, respectively. On the other hand, at the end of 48 hours of

incubation, p53/MDM2 complex level was decreased by 15.5% at 3.00  $\mu$ M concentration. The decrement by 15.5% at 3.00  $\mu$ M concentration for 48 hours can be linked to the highest upregulation of p21 gene expression. If (*R*)-4'-methylklavuzon might have disrupted p53/MDM2 complex inside the cells, p53 could have bound to promoter of p21 gene and upregulated its expression. p53 might have been isolated free from MDM2 in total protein. When ELISA assay was performed, only free p53 was captured by antibody on the plate without MDM2. It is known that ELISA assay measures signals that are only coming from MDM2 protein. The decrease by 15.5% could have been caused by absence of MDM2 bound to p53 protein in ELISA plate due to disruption of p53/MDM2 complex inside the cells.

Drug candidate was tested in order to see whether it can penetrate into the core of a spheroid or not. It was found that it can crumble and disrupt spheroids formed with parental cells and EpCAM<sup>+</sup>/CD133<sup>+</sup> cells at 62.5  $\mu$ M concentration. Morphology of the spheroids changed from intact to crumbled individual cells. Any significant crumbling in spheroids treated at 12.5  $\mu$ M concentration couldn't be achieved. Spheroids could not be destroyed with the drug within short incubation times like 24, 48 and 72 hours but there was a little decrement in the spheroid volume. Longer incubation times should be tested as a future direction. It is thought that drug candidate decreases spheroid viability significantly but doesn't destroy spheroids completely because cell debris could not be digested by remaining healthy cells.

## CHAPTER 5

### CONCLUSION

Epigenetic changes in histone proteins located in chromatin may cause cancer in humans. Histone Deacetylases (HDAC) and sirtuins which are responsible for the removal of acetyl groups from histone proteins are overexpressed in various types of cancer followed by the downregulation of tumor suppressor genes. Re-acetylation of the chromatin and upregulation of the tumor suppressor genes by inhibiting overexpressed HDAC and sirtuin activity are one of the main therapeutic strategies against cancer.

(*R*)-4'-methylklavuzon was tested on HuH-7 parental cells, HuH-7 EpCAM<sup>+</sup>/CD133<sup>+</sup> cancer stem cells and EpCAM<sup>-</sup>/CD133<sup>-</sup> HuH-7 cells for the first time in this study. Cytotoxic activity analysis revealed that drug candidate reduced HuH-7 parental cell population by half in 48 hours at 1.25  $\mu$ M concentration whereas it reduced EpCAM<sup>+</sup>/CD133<sup>+</sup> HuH-7 and EpCAM<sup>-</sup>/CD133<sup>-</sup> HuH-7 population by half at 2.50  $\mu$ M concentration which is the twice the concentration required for HuH-7 parental cells in 48 hours. EpCAM<sup>+</sup>/CD133<sup>+</sup> and EpCAM<sup>-</sup>/CD133<sup>-</sup> cells showed twice fold resistance to (*R*)-4'-methylklavuzon compared to HuH-7 parental cells. Possible reason of this situation might be that ABC-transport proteins in cell plasma membrane are overexpressed in cancer stem cells compared to HuH-7 parental cells.

In vitro HDAC assays revealed that drug candidate doesn't inhibit HDAC enzymes isolated from nucleus of HuH-7 cell populations. In contradiction, cell-based HDACs/sirtuins activity assays revealed that even at the concentration of 0.10  $\mu$ M (*R*)-4'-methylklavuzon can inhibit 50% of HDACs/sirtuins activity in the cells. Possible reasons of this contradiction may arise from pH of the kit buffer which has a pH of 8.0 limiting the interaction between the molecule and enzymes. But in cell-based assay, molecule might have functioned in cell compartments with different pH levels rather than pH 8.0. Additionally, in cell-based assay, enzymes in the cytoplasm may have been affected by the molecule.

In vitro HDAC1 and SIRT1 enzyme activity measurements revealed that (*R*)-4'-methylklavuzon tends to inhibit sirtuins rather than HDACs. 100  $\mu$ M of (*R*)-4'-methylklavuzon inhibited 46% of SIRT1 enzyme activity in vitro. The substrate used in

cell-based HDAC assay kit can also be deacetylated by sirtuins. According to cell-based HDAC enzyme activity assay, inhibition obtained by drug treatment seems like achieved by sirtuin inhibition rather than HDACs inhibition.

It was shown that (*R*)-4'-methylklavuzon can inhibit proliferation of EpCAM<sup>+</sup>/CD133<sup>+</sup> hepatocellular carcinoma cancer stem cells enriched from HuH-7 parental cells providing a novel drug candidate for the treatment of hepatocellular carcinoma for literature.

It was shown that (*R*)-4'-methylklavuzon upregulates p21 expression which may be the reason of G1 arrest in HuH-7 cells. Drug candidate inhibited pure p53/MDM2 complex in vitro whereas generally increased p53/MDM2 levels with 0.30  $\mu$ M concentration. It only decreases p53/MDM2 complex levels at higher concentrations for 48 hours of incubation. Spheroid assay showed that drug candidate can penetrate into the core of a spheroid formed with HuH-7 cells and crumbles cells individually separating from the main spheroid.

All data obtained in this thesis indicate that (*R*)-4'-methylklavuzon might damage DNA in HuH-7 cells resulting in p53 protein upregulation and simultaneously could inhibit topoisomerase I preventing DNA repair mechanism. It also could inhibit both SIRT1 and CRM1 preventing deacetylation of p53 and nuclear export of p53, respectively. In conclusion, p53 was upregulated due to DNA damage and it was not deacetylated by SIRT1 resulting in blockage of proteasomal degradation and maintained in nucleus as a result of CRM1 inhibition. These inhibitory effects of (*R*)-4'-methylklavuzon can prevent cancer cells and cancer stem cells escape from apoptosis and it can open a door to cure tumor in future studies.

## REFERENCES

- Abou-Alfa, Ghassan K., Dino Amadori, Armando Santoro, Arie Figier, Jacques de Greve, Chetan Lathia, Dimitris Voliotis, Sibyl Anderson, Marius Moscovici, and Sergio Ricci. 2011. "Safety and Efficacy of Sorafenib in Patients with Hepatocellular Carcinoma (HCC) and Child-Pugh A versus B Cirrhosis." *Gastrointestinal Cancer Research* 4 (2):40–44.
- Abukhdeir, Abde M., and Ben Ho Park. 2008. "p21 and p27: Roles in Carcinogenesis and Drug Resistance." *Expert Reviews in Molecular Medicine*.
- Ahuja, Nidhi, Bjoern Schwer, Stefania Carobbio, David Waltregny, Brian J. North, Vincenzo Castronovo, Pierre Maechler, and Eric Verdin. 2007. "Regulation of Insulin Secretion by SIRT4, a Mitochondrial ADP-Ribosyltransferase." *Journal of Biological Chemistry* 282 (46):33583–92.
- Akçok, İsmail, Derya Mete, Ayhan Şen, Pınar Kasaplar, Kemal S. Korkmaz, and Ali Çağır. 2017. "Synthesis and Topoisomerase I Inhibitory Properties of Klavuzon Derivatives." *Bioorganic Chemistry* 71:275–84.
- Ambrosini, G., E. B. Sambol, D. Carvajal, L. T. Vassilev, S. Singer, and G. K. Schwartz. 2007. "Mouse Double Minute Antagonist Nutlin-3a Enhances Chemotherapy-Induced Apoptosis in Cancer Cells with Mutant p53 by Activating E2F1." *Oncogene* 26 (24):3473–81.
- Asher, Gad, David Gatfield, Markus Stratmann, Hans Reinke, Charna Dibner, Florian Kreppel, Raul Mostoslavsky, Frederick W. Alt, and Ueli Schibler. 2008. "SIRT1 Regulates Circadian Clock Gene Expression through PER2 Deacetylation." *Cell* 134 (2):317–28.
- Avalos, José L., Katherine M. Bever, and Cynthia Wolberger. 2005. "Mechanism of Sirtuin Inhibition by Nicotinamide: Altering the NAD<sup>+</sup> cosubstrate Specificity of a Sir2 Enzyme." *Molecular Cell* 17 (6):855–68.
- Bae, H. J., J. H. Noh, J. K. Kim, J. W. Eun, K. H. Jung, M. G. Kim, Y. G. Chang, et al. 2014. "MicroRNA-29c Functions as a Tumor Suppressor by Direct Targeting Oncogenic SIRT1 in Hepatocellular Carcinoma." *Oncogene* 33 (20):2557–67.
- Bao, Xiucong, Yi Wang, Xin Li, Xiao Meng Li, Zheng Liu, Tangpo Yang, Chi F.at Wong, Jiangwen Zhang, Quan Hao, and Xiang D.avid Li. 2014. "Identification of 'Erasers' for Lysine Crotonylated Histone Marks Using a Chemical Proteomics Approach." *eLife* 3.
- Bellet, Marina M., Yasukazu Nakahata, Mohamed Boudjelal, Emma Watts, Danuta E. Mossakowska, Kenneth A. Edwards, Marlene Cervantes, et al. 2013. "Pharmacological Modulation of Circadian Rhythms by Synthetic Activators of the Deacetylase SIRT1." *Proceedings of the National Academy of Sciences* 110 (9):3333–38.
- Bhaskara, Srividya, Sarah K. Knutson, Guochun Jiang, Mahesh B. Chandrasekharan, Andrew J. Wilson, Siyuan Zheng, Ashwini Yenamandra, et al. 2010. "Hdac3 Is Essential for the Maintenance of Chromatin Structure and Genome Stability." *Cancer Cell* 18 (5):436–47.



- Bitterman, Kevin J., Rozalyn M. Anderson, Haim Y. Cohen, Magda Latorre-Esteves, and David A. Sinclair. 2002. "Inhibition of Silencing and Accelerated Aging by Nicotinamide, a Putative Negative Regulator of Yeast Sir2 and Human SIRT1." *Journal of Biological Chemistry* 277 (47):45099–107.
- Bond, Gareth L, Wenwei Hu, and Arnold J Levine. 2005. "MDM2 Is a Central Node in the p53 Pathway: 12 Years and Counting." *Current Cancer Drug Targets* 5 (1):3–8.
- Bond, Gareth L., Wenwei Hu, Elisabeth E. Bond, Harlan Robins, Stuart G. Lutzker, Nicoleta C. Arva, Jill Bargonetti, et al. 2004. "A Single Nucleotide Polymorphism in the MDM2 Promoter Attenuates the p53 Tumor Suppressor Pathway and Accelerates Tumor Formation in Humans." *Cell* 119 (5):591–602.
- Borra, Margie T., Brian C. Smith, and John M. Denu. 2005. "Mechanism of Human SIRT1 Activation by Resveratrol." *Journal of Biological Chemistry* 280 (17): 17187–95
- Brooks, Christopher L., and Wei Gu. 2009. "How Does SIRT1 Affect Metabolism, Senescence and Cancer?" *Nature Reviews Cancer*.
- Byles, V., L. Zhu, J. D. Lovaas, L. K. Chmielewski, J. Wang, D. V. Faller, and Y. Dai. 2012. "SIRT1 Induces EMT by Cooperating with EMT Transcription Factors and Enhances Prostate Cancer Cell Migration and Metastasis." *Oncogene* 31 (43):4619–29.
- Calvanese, Vincenzo, Ester Lara, Beatriz Suárez-Alvarez, Raed Abu Dawud, Mercedes Vázquez-Chantada, Maria Luz Martínez-Chantar, Nieves Embade, et al. 2010. "Sirtuin 1 Regulation of Developmental Genes during Differentiation of Stem Cells." *Proceedings of the National Academy of Sciences of the United States of America* 107 (31):13736–41.
- Capoulade, C, B Bressac-de Paillerets, I Lefrère, M Ronsin, J Feunteun, T Tursz, and J Wiels. 1998. "Overexpression of MDM2, due to Enhanced Translation, Results in Inactivation of Wild-Type p53 in Burkitt's Lymphoma Cells." *Oncogene* 16:1603–10.
- Carlisi, D., B. Vassallo, M. Lauricella, S. Emanuele, A. D'Anneo, E. Di Leonardo, P. Di Fazio, R. Vento, and Giovanni Tesoriere. 2008. "Histone Deacetylase Inhibitors Induce in Human Hepatoma HepG2 Cells Acetylation of p53 and Histones in Correlation with Apoptotic Effects." *International Journal of Oncology* 32 (1):177–84.
- Champoux, J J. 2001. "DNA Topoisomerases: Structure, Function, and Mechanism." *Annu Rev Biochem* 70:369–413.
- Chang, Hung Chun, and Leonard Guarente. 2014. "SIRT1 and Other Sirtuins in Metabolism." *Trends in Endocrinology and Metabolism*.
- Chang, Charn Jung, Chuan Chih Hsu, Ming Chi Yung, Kai Yun Chen, Ching Tzao, Wei Fong Wu, Hsiang Yun Chou, et al. 2009. "Enhanced Radiosensitivity and Radiation-Induced Apoptosis in Glioma CD133-Positive Cells by Knockdown of SirT1 Expression." *Biochemical and Biophysical Research Communications* 380 (2):236–42.

- Chen, Hsieh-Cheng, Yung-Ming Jeng, Ray-Hwang Yuan, Hey-Chi Hsu, and Yu-Ling Chen. 2012. "SIRT1 Promotes Tumorigenesis and Resistance to Chemotherapy in Hepatocellular Carcinoma and Its Expression Predicts Poor Prognosis." *Annals of Surgical Oncology* 19 (6):2011–19.
- Chen, I-Chieh, Wei-Fan Chiang, Hsin-Hsiu Huang, Pei-Fen Chen, Ying-Ying Shen, and Hung-Che Chiang. 2014a. "Role of SIRT1 in Regulation of Epithelial-to-Mesenchymal Transition in Oral Squamous Cell Carcinoma Metastasis." *Molecular Cancer* 13 (1):254.
- Chen, Xiaojing, Kai Sun, Shufan Jiao, Ning Cai, Xue Zhao, Hanbing Zou, Yuexia Xie, Zhengshi Wang, Ming Zhong, and Lixin Wei. 2014. "High Levels of SIRT1 Expression Enhance Tumorigenesis and Associate with a Poor Prognosis of Colorectal Carcinoma Patients." *Scientific Reports* 4.
- Chen, J, V Marechal, and a J Levine. 1993. "Mapping of the p53 and Mdm-2 Interaction Domains." *Molecular and Cellular Biology* 13 (7):4107–14.
- Cheng, Alfred S.L., Suki S. Lau, Yangchao Chen, Yutaka Kondo, May S. Li, Hai Feng, Arthur K. Ching, et al. 2011. "EZH2-Mediated Concordant Repression of Wnt Antagonists Promotes  $\beta$ -Catenin-Dependent Hepatocarcinogenesis." *Cancer Research* 71 (11):4028–39.
- Cheng, H.-L., R. Mostoslavsky, S. Saito, J. P. Manis, Y. Gu, P. Patel, R. Bronson, E. Appella, F. W. Alt, and K. F. Chua. 2003. "Developmental defects and p53 hyperacetylation in Sir2 homolog (SIRT1)-Deficient mice." *Proceedings of the National Academy of Sciences* 100 (19): 10794–99.
- Chiba, Tetsuhiro, Kaoru Kita, Yun Wen Zheng, Osamu Yokosuka, Hiromitsu Saisho, Atsushi Iwama, Hiromitsu Nakauchi, and Hideki Taniguchi. 2006. "Side Population Purified from Hepatocellular Carcinoma Cells Harbors Cancer Stem Cell-like Properties." *Hepatology* 44 (1):240–51.
- Choi, Ha Na, Jun Sang Bae, Urangoo Jamiyandorj, Sang Jae Noh, Ho Sung Park, Kyu Yun Jang, Myoung Ja Chung, Myoung Jae Kang, Dong Geun Lee, and Woo Sung Moon. 2011. "Expression and Role of SIRT1 in Hepatocellular Carcinoma." *Oncology Reports* 26 (2):503–10.
- Cohen, Haim Y., Siva Lavu, Kevin J. Bitterman, Brian Hekking, Thomas A. Imahiyerobo, Christine Miller, Roy Frye, Hidde Ploegh, Benedikt M. Kessler, and David A. Sinclair. 2004. "Acetylation of the C Terminus of Ku70 by CBP and PCAF Controls Bax-Mediated Apoptosis." *Molecular Cell* 13 (5):627–38.
- Colaluca, Ivan N., Daniela Tosoni, Paolo Nuciforo, Francesca Senic-Matuglia, Viviana Galimberti, Giuseppe Viale, Salvatore Pece, and Pier Paolo Di Fiore. 2008. "NUMB Controls p53 Tumour Suppressor Activity." *Nature* 451 (7174):76–80.
- Dai, Wei, Jingfeng Zhou, Bei Jin, and Jingxuan Pan. 2016. "Class III-Specific HDAC Inhibitor Tenovin-6 Induces Apoptosis, Suppresses Migration and Eliminates Cancer Stem Cells in Uveal Melanoma." *Scientific Reports* 6.
- Das, Chandrima, M. Scott Lucia, Kirk C. Hansen, and Jessica K. Tyler. 2009. "Erratum: CBP/p300-Mediated acetylation of histone H3 on lysine 56." *Nature* 460 (7259): 1164–64.

- Deng, Chu Xia. 2009. "SIRT1, Is It a Tumor Promoter or Tumor Suppressor?" *International Journal of Biological Sciences*.
- Deng, Shichang, Shuai Zhu, Bo Wang, Xiang Li, Yang Liu, Qi Qin, Qiong Gong, et al. 2014. "Chronic Pancreatitis and Pancreatic Cancer Demonstrate Active Epithelial-Mesenchymal Transition Profile, Regulated by miR-217-SIRT1 Pathway." *Cancer Letters* 355 (2):184–91.
- Dioum, Elhadji M., Rui Chen, Matthew S. Alexander, Quiyang Zhang, Richard T. Hogg, Robert D. Gerard, and Joseph A. Garcia. 2009. "Regulation of Hypoxia-Inducible Factor 2 $\alpha$  Signaling by the Stress-Responsive Deacetylase Sirtuin 1." *Science* 324 (5932):1289–93.
- Donmez, G., A. Arun, C.-Y. Chung, P. J. McLean, S. Lindquist, and L. Guarente. 2012. "SIRT1 Protects against  $\alpha$ -Synuclein Aggregation by Activating Molecular Chaperones." *Journal of Neuroscience* 32 (1):124–32.
- Dose, Alexander, Jan Oliver Jost, Antje C. Spieß, Petra Henklein, Michael Beyermann, and Dirk Schwarzer. 2012. "Facile synthesis of colorimetric histone deacetylase substrates." *Chemical Communications* 48 (76): 9525.
- Du, Jintang, Yeyun Zhou, Xiaoyang Su, Jiu Jiu Yu, Saba Khan, Hong Jiang, Jungwoo Kim, et al. 2011. "Sirt5 Is a NAD-Dependent Protein Lysine Demalonylase and Desuccinylase." *Science* 334 (6057):806–9.
- Efroni, Sol, Radharani Duttgupta, Jill Cheng, Hesam Dehghani, Daniel J. Hoepfner, Chandravanu Dash, David P. Bazett-Jones, et al. 2008. "Global Transcription in Pluripotent Embryonic Stem Cells." *Cell Stem Cell* 2 (5):437–47.
- El-Tanani, Mohamed, El-Habib Dakir, Bethany Raynor, and Richard Morgan. 2016. "Mechanisms of Nuclear Export in Cancer and Resistance to Chemotherapy." *Cancers* 8 (3):35.
- Erster, Susan, Motohiro Mihara, Roger H Kim, Oleksi Petrenko, and Ute M Moll. 2004. "In Vivo Mitochondrial p53 Translocation Triggers a Rapid First Wave of Cell Death in Response to DNA Damage That Can Precede p53 Target Gene Activation." *Molecular and Cellular Biology* 24 (15):6728–41.
- Etchin, Julia, Takaomi Sanda, Marc R. Mansour, Alex Kentsis, Joan Montero, Bonnie T. Le, Amanda L. Christie, et al. 2013a. "KPT-330 inhibitor of CRM1 (XPO1)-Mediated nuclear export has selective anti-Leukaemic activity in preclinical models of T-Cell acute lymphoblastic leukaemia and acute myeloid leukaemia." *British Journal of Haematology* 161 (1): 117–27.
- Etchin, J., Q. Sun, A. Kentsis, A. Farmer, Z. C. Zhang, T. Sanda, M. R. Mansour, et al. 2013b. "Antileukemic Activity of Nuclear Export Inhibitors That Spare Normal Hematopoietic Cells." *Leukemia* 27 (1):66–74.
- Fakharzadeh, Steven S., Lynne Rosenblum-Vos, Maureen Murphy, Eric K. Hoffman, and Donna L. George. 1993. "Structure and Organization of Amplified DNA on Double Minutes Containing the mdm2 Oncogene." *Genomics* 15 (2):283–90.
- Fakharzadeh, S S, S P Trusko, and D L George. 1991. "Tumorigenic Potential Associated with Enhanced Expression of a Gene That Is Amplified in a Mouse Tumor Cell Line." *The EMBO Journal* 10 (6):1565–69.

- Falenczyk, C., M. Schiedel, B. Karaman, T. Rumpf, N. Kuzmanovic, M. Grötli, W. Sippl, M. Jung, and B. König. 2014. “Chromo-Pharmacophores: Photochromic Diarylmaleimide Inhibitors for Sirtuins.” *Chem. Sci.* 5 (12):4794–99.
- Feki, Anis, and Irmgard Irminger-Finger. 2004. “Mutational Spectrum of p53 Mutations in Primary Breast and Ovarian Tumors.” *Critical Reviews in Oncology/Hematology*.
- Feldman, Jessica L., Josue Baeza, and John M. Denu. 2013. “Activation of the Protein Deacetylase SIRT6 by Long-Chain Fatty Acids and Widespread Deacylation by Mammalian Sirtuins.” *Journal of Biological Chemistry* 288 (43):31350–56.
- Feng, Guijuan, Ke Zheng, Donghui Song, Ke Xu, Dan Huang, Ye Zhang, Peipei Cao, et al. 2016. “SIRT1 was involved in TNF- $\alpha$ -Promoted osteogenic differentiation of human DPSCs through Wnt/ $\beta$ -Catenin signal.” *In Vitro Cellular & Developmental Biology - Animal* 52 (10): 1001–11.
- Fornierod, Maarten, Mutsuhito Ohno, Minoru Yoshida, and Iain W. Mattaj. 1997. “CRM1 Is an Export Receptor for Leucine-Rich Nuclear Export Signals.” *Cell* 90 (6):1051–60.
- Freedman, D. A., L. Wu, and A. J. Levine. 1999. “Functions of the MDM2 Oncoprotein.” *Cellular and Molecular Life Sciences*.
- Fridman, Jordan S., and Scott W. Lowe. 2003. “Control of Apoptosis by p53.” *Oncogene*.
- Frye, Roy A. 2000. “Phylogenetic Classification of Prokaryotic and Eukaryotic Sir2-like Proteins.” *Biochemical and Biophysical Research Communications* 273 (2):793–98.
- Fukuda, Makoto, Shiro Asano, Takahiro Nakamura, Makoto Adachi, Minoru Yoshida, Mitsuhiro Yanagida, and Eisuke Nishida. 1997. “CRM1 Is Responsible for Intracellular Transport Mediated by the Nuclear Export Signal.” *Nature* 390 (6657):308–11.
- Gademann, Karl. 2011. “Controlling Protein Transport by Small Molecules.” *Current Drug Targets* 12 (11): 1574–80.
- Gan, Li, and Lennart Mucke. 2008. “Paths of Convergence: Sirtuins in Aging and Neurodegeneration.” *Neuron*.
- Gao, Yijie, David O. Ferguson, Wei Xie, John P. Manis, Jo Ann Sekiguchi, Karen M. Frank, Jayanta Chaudhuri, James Horner, Ronald A. DePinho, and Frederick W. Alt. 2000. “Interplay of p53 and DNA-Repair Protein XRCC4 in Tumorigenesis, Genomic Stability and Development.” *Nature* 404 (6780):897–900.
- Golomb, Lior, Debora Rosa Bublik, Sylvia Wilder, Reinat Nevo, Vladimir Kiss, Kristina Grabusic, Sinisa Volarevic, and Moshe Oren. 2012. “Importin 7 and Exportin 1 Link c-Myc and p53 to Regulation of Ribosomal Biogenesis.” *Molecular Cell* 45 (2):222–32.
- Gores, Gregory J. 2014. “HCC—subtypes, stratification and sorafenib.” *Nature Reviews Gastroenterology & Hepatology* 11 (11): 645–47.
- Grant, Steven, Chris Easley, and Peter Kirkpatrick. 2007. “Vorinostat.” *Nature Reviews Drug Discovery*.

- Gu, Wei, and Robert G. Roeder. 1997. "Activation of p53 Sequence-Specific DNA Binding by Acetylation of the p53 C-Terminal Domain." *Cell* 90 (4):595–606.
- Günther, T, R Schneider-Stock, C Häckel, H U Kasper, M Pross, A Hackelsberger, H Lippert, and A Roessner. 2000. "Mdm2 Gene Amplification in Gastric Cancer Correlation with Expression of Mdm2 Protein and p53 Alterations." *Modern Pathology: An Official Journal of the United States and Canadian Academy of Pathology, Inc* 13 (6):621–26.
- Haigis, Marcia C., and Leonard P. Guarente. 2006. "Mammalian Sirtuins - Emerging Roles in Physiology, Aging, and Calorie Restriction." *Genes and Development*.
- Han, Myung Kwan, Eun Kyung Song, Ying Guo, Xuan Ou, Charlie Mantel, and Hal E. Broxmeyer. 2008. "SIRT1 Regulates Apoptosis and Nanog Expression in Mouse Embryonic Stem Cells by Controlling p53 Subcellular Localization." *Cell Stem Cell* 2 (3):241–51.
- Hao, Chong, Peng Xi Zhu, Xue Yang, Zhi Peng Han, Jing Hua Jiang, Chen Zong, Xu Guang Zhang, et al. 2014. "Overexpression of SIRT1 Promotes Metastasis through Epithelial-Mesenchymal Transition in Hepatocellular Carcinoma." *BMC Cancer* 14 (1).
- Heltweg, Birgit, Tonibelle Gatbonton, Aaron D. Schuler, Jeff Posakony, Hongzhe Li, Sondra Goehle, Ramya Kollipara, et al. 2006. "Antitumor Activity of a Small-Molecule Inhibitor of Human Silent Information Regulator 2 Enzymes." *Cancer Research* 66 (8):4368–77.
- Hill, Richard, Bastien Cautain, Nuria de Pedro, and Wolfgang Link. 2014. "Targeting Nucleocytoplasmic Transport in Cancer Therapy." *Oncotarget* 5 (1):11–28.
- Houtkooper, Riekelt H., Eija Pirinen, and Johan Auwerx. 2012. "Sirtuins as Regulators of Metabolism and Healthspan." *Nature Reviews Molecular Cell Biology*.
- Howitz, Konrad T., Kevin J. Bitterman, Halm Y. Cohen, Dudley W. Lamming, Siva Lavu, Jason G. Wood, Robert E. Zipkin, et al. 2003. "Small Molecule Activators of Sirtuins Extend *Saccharomyces Cerevisiae* Lifespan." *Nature* 425 (6954):191–96.
- Hu, Bin, Ye Guo, Chunyuan Chen, Qing Li, Xin Niu, Shangchun Guo, Aijun Zhang, Yang Wang, and Zhifeng Deng. 2014. "Repression of SIRT1 Promotes the Differentiation of Mouse Induced Pluripotent Stem Cells into Neural Stem Cells." *Cellular and Molecular Neurobiology* 34 (6):905–12.
- Huang, Chuanshu, Wei Ya Ma, Angela Goranson, and Zigang Dong. 1999. "Resveratrol Suppresses Cell Transformation and Induces Apoptosis through a p53-Dependent Pathway." *Carcinogenesis* 20 (2):237–42.
- Huang, Wei-yi, Lu Yue, Wen-shen Qiu, Li-Wei Wang, Xiao-han Zhou, and Yuan-jue Sun. 2009. "Prognostic Value of CRM1 in Pancreas Cancer." *Clinical and Investigative Medicine. Médecine Clinique et Experimentale* 32 (6):E315.
- Inoue, Hiromi, Michael Kauffman, Sharon Shacham, Yosef Landesman, Joy Yang, Christopher P. Evans, and Robert H. Weiss. 2013. "CRM1 Blockade by Selective Inhibitors of Nuclear Export Attenuates Kidney Cancer Growth." *Journal of Urology* 189 (6):2317–26.

- Ito, Akihiro, Chun-Hsiang Lai, Xuan Zhao, Shinichi Saito, Maria H. Hamilton, Ettore Appella, and Tso-Pang Yao. 2001. "p300/CBP-Mediated p53 acetylation is commonly induced by p53-Activating agents and inhibited by MDM2." *The EMBO Journal* 20 (6): 1331–40.
- Jang, Kyu Yun, Sang Jae Noh, Nadja Lehwald, Guo-Zhong Tao, David I. Bellovin, Ho Sung Park, Woo Sung Moon, Dean W. Felsher, and Karl G. Sylvester. 2012. "SIRT1 and c-Myc Promote Liver Tumor Cell Survival and Predict Poor Survival of Human Hepatocellular Carcinomas." *PLoS ONE* 7 (9):e45119.
- Jeong, Hyunkyung, Dena E. Cohen, Libin Cui, Andrea Supinski, Jeffrey N. Savas, Joseph R. Mazzulli, John R. Yates, Laura Bordone, Leonard Guarente, and Dimitri Krainc. 2012. "Sirt1 Mediates Neuroprotection from Mutant Huntingtin by Activation of the TORC1 and CREB Transcriptional Pathway." *Nature Medicine* 18 (1):159–65.
- Jeong, Jaemin, Kyungmi Juhn, Hansoo Lee, Sang-Hoon Kim, Bon-Hong Min, Kyung-Mi Lee, Myung-Haeng Cho, Gil-Hong Park, and Kee-Ho Lee. 2007. "SIRT1 Promotes DNA Repair Activity and Deacetylation of Ku70." *Experimental & Molecular Medicine* 39 (1):8–13.
- Jewers, K., Miss M.B. Burbage, G. Blunden, and W. J. Griffin. 1974. "Brisbagenin and Brisbenone, Two New Spirostanes from Cordyline Species." *Steroids* 24 (2):203–8.
- Jiang, Hong, Saba Khan, Yi Wang, Guillaume Charron, Bin He, Carlos Sebastian, Jintang Du, et al. 2013. "SIRT6 Regulates TNF- $\alpha$  Secretion through Hydrolysis of Long-Chain Fatty Acyl Lysine." *Nature* 496 (7443):110–13.
- Jiang, Mali, Jiawei Wang, Jinrong Fu, Lin Du, Hyunkyung Jeong, Tim West, Lan Xiang, et al. 2012. "Neuroprotective Role of Sirt1 in Mammalian Models of Huntington's Disease through Activation of Multiple Sirt1 Targets." *Nature Medicine* 18 (1):153–58.
- Jin, Qihuang, Tingting Yan, Xinjian Ge, Cheng Sun, Xianglin Shi, and Qiwei Zhai. 2007. "Cytoplasm-Localized SIRT1 Enhances Apoptosis." *Journal of Cellular Physiology* 213 (1):89–97.
- Jin, Yanli, Qi Cao, Chun Chen, Xin Du, Bei Jin, and Jingxuan Pan. 2015. "Tenovin-6-Mediated Inhibition of SIRT1/2 Induces Apoptosis in Acute Lymphoblastic Leukemia (ALL) Cells and Eliminates ALL Stem/progenitor Cells." *BMC Cancer* 15 (1).
- Juven-Gershon T., Oren M. 1999. "Mdm2: the ups and downs." *Molecular Medicine*, 5(12), 71–83.
- Kanbur, Tuğçe, Murat Kara, Meltem Kutluer, Ayhan Şen, Murat Delman, Aylin Alkan, Hasan Ozan Otaş, İsmail Akçok, and Ali Çağır. 2017. "CRM1 Inhibitory and Antiproliferative Activities of Novel 4'-Alkyl Substituted Klavuzon Derivatives." *Bioorganic and Medicinal Chemistry* 25 (16):4444–51.
- Kasaplar, Pinar, Özgür Yilmazer, and Ali Çağır. 2009. "6-Bicycloaryl Substituted (S)- and (R)-5,6-Dihydro-2H-Pyran-2-Ones: Asymmetric Synthesis, and Anti-Proliferative Properties." *Bioorganic and Medicinal Chemistry* 17 (1):311–18.

- Kau, Tweeny R., Jeffrey C. Way, and Pamela A. Silver. 2004. "Nuclear Transport and Cancer: From Mechanism to Intervention." *Nature Reviews Cancer* 4 (2):106–17.
- Kauppinen, Anu, Tiina Suuronen, Johanna Ojala, Kai Kaarniranta, and Antero Salminen. 2013. "Antagonistic Crosstalk between NF- $\kappa$ B and SIRT1 in the Regulation of Inflammation and Metabolic Disorders." *Cellular Signalling*.
- Kawahara, Tiara L A, Eriko Michishita, Adam S Adler, Mara Damian, Elisabeth Berber, Meihong Lin, Ron A McCord, et al. 2009. "SIRT6 Links Histone H3 Lysine 9 Deacetylation to NF-kappaB-Dependent Gene Expression and Organismal Life Span." *Cell* 136 (1):62–74.
- Kojima, Kensuke, Steven M. Kornblau, Vivian Ruvolo, Archana Dilip, Seshagiri Duvvuri, R. Eric Davis, Min Zhang, et al. 2013. "Prognostic Impact and Targeting of CRM1 in Acute Myeloid Leukemia." *Blood* 121 (20):4166–74.
- Kuo, Po Lin, Lien Chai Chiang, and Chun Ching Lin. 2002. "Resveratrol- Induced Apoptosis Is Mediated by p53-Dependent Pathway in Hep G2 Cells." *Life Sciences* 72 (1):23–34.
- Kuzmichev, A., R. Margueron, A. Vaquero, T. S. Preissner, M. Scher, A. Kirmizis, X. Ouyang, et al. 2005. "Composition and Histone Substrates of Polycomb Repressive Group Complexes Change during Cellular Differentiation." *Proceedings of the National Academy of Sciences* 102 (6):1859–64.
- Lackey, Karen, Michael Cory, Ronda Davis, Stephen V. Frye, Philip A. Harris, Robert N. Hunter, David K. Jung, et al. 2000. "The Discovery of Potent cRaf1 Kinase Inhibitors." *Bioorganic and Medicinal Chemistry Letters* 10 (3):223–26.
- Lagger, Gerda, Donal O'Carroll, Martina Rembold, Harald Khier, Julia Tischler, Georg Weitzer, Bernd Schuettengruber, et al. 2002. "Essential Function of Histone Deacetylase 1 in Proliferation Control and CDK Inhibitor Repression." *EMBO Journal* 21 (11):2672–81.
- Lain, Sonia, Jonathan J. Hollick, Johanna Campbell, Oliver D. Staples, Maureen Higgins, Mustapha Aoubala, Anna McCarthy, et al. 2008. "Discovery, In Vivo Activity, and Mechanism of Action of a Small-Molecule p53 Activator." *Cancer Cell* 13 (5):454–63.
- Lapalombella, R., Q. Sun, K. Williams, L. Tangeman, S. Jha, Y. Zhong, V. Goettl, et al. 2012. "Selective Inhibitors of Nuclear Export (SINE) Show That CRM1/XPO1 Is a Target in Chronic Lymphocytic Leukemia." *Blood* 120 (23):4621–34.
- Lara, E., A. Mai, V. Calvanese, L. Altucci, P. Lopez-Nieva, M. L. Martinez-Chantar, M. Varela-Rey, et al. 2009. "Salermide, a Sirtuin Inhibitor with a Strong Cancer-Specific Proapoptotic Effect." *Oncogene* 28 (6):781–91.
- LaRusch, Gretchen a, Mark W Jackson, James D Dunbar, Robert S Warren, David B Donner, and Lindsey D Mayo. 2007. "Nutlin3 Blocks Vascular Endothelial Growth Factor Induction by Preventing the Interaction between Hypoxia Inducible Factor 1alpha and Hdm2." *Cancer Research* 67 (2):450–54.
- Lau, L. M S, J. K. Nugent, X. Zhao, and M. S. Irwin. 2008. "HDM2 Antagonist Nutlin-3 Disrupts p73-HDM2 Binding and Enhances p73 Function." *Oncogene* 27 (7):997–1003.

- Lee, Chi Wai, Leo Lap Yan Wong, Edith Yuk Ting Tse, Heong Fai Liu, Veronica Yee Law Leong, Joyce Man Fong Lee, D. Grahame Hardie, Irene Oi Lin Ng, and Yick Pang Ching. 2012. "AMPK Promotes p53 Acetylation via Phosphorylation and Inactivation of SIRT1 in Liver Cancer Cells." *Cancer Research* 72 (17):4394–4404.
- Lee, J-H, M L Choy, L Ngo, S S Foster, and Paul a Marks. 2010. "Histone Deacetylase Inhibitor Induces DNA Damage, Which Normal but Not Transformed Cells Can Repair." *Proceedings of the National Academy of Sciences of the United States of America* 107 (33):14639–44.
- Lee, Ji Seon, Jeong Rak Park, Ok Seon Kwon, Tae Hee Lee, Ichiro Nakano, Hiroyuki Miyoshi, Kwang Hoon Chun, et al. 2015. "SIRT1 Is Required for Oncogenic Transformation of Neural Stem Cells and for the Survival Of 'cancer Cells with Neural Stemness' in a p53-Dependent Manner." *Neuro-Oncology* 17 (1):95–106.
- Lee, Y L, Q Peng, S W Fong, A C Chen, K F Lee, E H Ng, A Nagy, and W S Yeung. 2012. "Sirtuin 1 Facilitates Generation of Induced Pluripotent Stem Cells from Mouse Embryonic Fibroblasts through the miR-34a and p53 Pathways." *PLoS One* 7 (9):e45633.
- Lei, W-W, K-H Zhang, X-C Pan, D-M Wang, Y Hu, Y-N Yang, and J-G Song. 2010. "Histone deacetylase 1 and 2 differentially regulate apoptosis by opposing effects on extracellular signal-Regulated kinase 1/2." *Cell Death & Disease* 1 (5).
- Li, Kai, Alex Casta, Rui Wang, Enerlyn Lozada, Wei Fan, Susan Kane, Qingyuan Ge, Wei Gu, David Orren, and Jianyuan Luo. 2008. "Regulation of WRN Protein Cellular Localization and Enzymatic Activities by SIRT1-Mediated Deacetylation." *Journal of Biological Chemistry* 283 (12):7590–98.
- Li, Ling, Tereza Osdal, Yinwei Ho, Sookhee Chun, Tinisha McDonald, Puneet Agarwal, Allen Lin, et al. 2014. "SIRT1 Activation by a c-MYC Oncogenic Network Promotes the Maintenance and Drug Resistance of Human FLT3-ITD Acute Myeloid Leukemia Stem Cells." *Cell Stem Cell* 15 (4):431–46.
- Li, Ling, Lisheng Wang, Liang Li, Zhiqiang Wang, Yinwei Ho, Tinisha McDonald, Tessa L. Holyoake, Wen Yong Chen, and Ravi Bhatia. 2012. "Activation of p53 by SIRT1 Inhibition Enhances Elimination of CML Leukemia Stem Cells in Combination with Imatinib." *Cancer Cell* 21 (2):266–81.
- Lim, Ji-Hong, Yoon-Mi Lee, Yang-Sook Chun, Junjie Chen, Ja-Eun Kim, and Jong-Wan Park. 2010. "Sirtuin 1 Modulates Cellular Responses to Hypoxia by Deacetylating Hypoxia-Inducible Factor 1alpha." *Molecular Cell* 38 (6):864–78.
- Lin, Yi Hui, Jian Yuan, Huadong Pei, Tongzheng Liu, David K. Ann, and Zhenkun Lou. 2015. "KAP1 Deacetylation by SIRT1 Promotes Non-Homologous End-Joining Repair." *PLoS ONE* 10 (4).
- Liu, Limei, Chungang Liu, Qianzhen Zhang, Junjie Shen, Heng Zhang, Juanjuan Shan, Guangjie Duan, et al. 2016. "SIRT1-Mediated Transcriptional Regulation of SOX2 Is Important for Self-Renewal of Liver Cancer Stem Cells." *Hepatology* 64 (3):814–27.



- Llovet, J M, S Ricci, V Mazzaferro, P Hilgard, E Gane, J F Blanc, A C de Oliveira, et al. 2008. "Sorafenib in Advanced Hepatocellular Carcinoma." *N Engl J Med* 359 (4):378–90.
- Lombard, D. B., B. Schwer, F. W. Alt, and R. Mostoslavsky. 2008. "SIRT6 in DNA Repair, Metabolism and Ageing." In *Journal of Internal Medicine*, 263:128–41.
- Lowinger, T.B., B. Riedl, J. Dumas, and R.A. Smith. 2002. "Design and Discovery of Small Molecules Targeting Raf-1 Kinase." *Current Pharmaceutical Design* 8 (25):2269–78.
- Luo, Jianyuan, Anatoly Y Nikolaev, Shin-ichiro Imai, Delin Chen, Fei Su, Ariel Shiloh, Leonard Guarente, and Wei Gu. 2001. "Negative Control of p53 by Sir2alpha Promotes Cell Survival under Stress." *Cell* 107 (2):137–48.
- Luo, Jianyuan, Fei Su, Delin Chen, Ariel Shiloh, and Wei Gu. 2000. "Deacetylation of p53 Modulates Its Effect on Cell Growth and Apoptosis." *Nature* 408 (6810):377–81.
- Ma, Stephanie, Kwok Wah Chan, Terence Kin-Wah Lee, Kwan Ho Tang, Jana Yim-Hung Wo, Bo-Jian Zheng, and Xin-Yuan Guan. 2008b. "Aldehyde Dehydrogenase Discriminates the CD133 Liver Cancer Stem Cell Populations." *Molecular Cancer Research : MCR* 6 (7):1146–53.
- Ma, Wei, Gary Guishan Xiao, Jun Mao, Ying Lu, Bo Song, Lihui Wang, Shujun Fan, et al. 2015. "Dysregulation of the miR-34a-SIRT1 Axis Inhibits Breast Cancer Stemness." *Oncotarget* 6 (12):10432–44.
- Mani, Sendurai A., Wenjun Guo, Mai Jing Liao, Elinor Ng Eaton, Ayyakkannu Ayyanan, Alicia Y. Zhou, Mary Brooks, et al. 2008. "The Epithelial-Mesenchymal Transition Generates Cells with Properties of Stem Cells." *Cell* 133 (4):704–15.
- Mann, Amrit, Kai Breuhahn, Peter Schirmacher, Arnd Wilhelmi, Carsten Beyer, Andrea Rosenau, Suat Özbek, Stefan Rose-John, and Manfred Blessing. 2001. "Up- and Down-Regulation of Granulocyte/Macrophage-Colony Stimulating Factor Activity in Murine Skin Increase Susceptibility to Skin Carcinogenesis by Independent Mechanisms." *Cancer Research* 61 (5):2311.
- Mao, Beibei, Guowei Zhao, Xiang Lv, Hou-Zao Chen, Zheng Xue, Ben Yang, De-Pei Liu, and Chih-Chuan Liang. 2011. "Sirt1 deacetylates c-Myc and promotes c-Myc/Max association." *The International Journal of Biochemistry & Cell Biology* 43 (11): 1573–81.
- Matsui, Keiko, Sachiko Ezoe, Kenji Oritani, Masaru Shibata, Masahiro Tokunaga, Natsuko Fujita, Akira Tanimura, et al. 2012. "NAD-Dependent Histone Deacetylase, SIRT1, Plays Essential Roles in the Maintenance of Hematopoietic Stem Cells." *Biochemical and Biophysical Research Communications* 418 (4):811–17.
- Medda, Federico, Rupert J.M. Russell, Maureen Higgins, Anna R. McCarthy, Johanna Campbell, Alexandra M.Z. Slawin, David P. Lane, Sonia Lain, and Nicholas J. Westwood. 2009. "Novel Cambinol Analogs as Sirtuin Inhibitors: Synthesis, Biological Evaluation, and Rationalization of Activity." *Journal of Medicinal Chemistry* 52 (9):2673–82.

- Menssen, A., P. Hydbring, K. Kapelle, J. Vervoorts, J. Diebold, B. Luscher, L.-G. Larsson, and H. Hermeking. 2012. "The c-MYC Oncoprotein, the NAMPT Enzyme, the SIRT1-Inhibitor DBC1, and the SIRT1 Deacetylase Form a Positive Feedback Loop." *Proceedings of the National Academy of Sciences* 109 (4):E187–96.
- Momand, Jamil, David Jung, Sharon Wilczynski, and Joyce Niland. 1998. "The MDM2 Gene Amplification Database." *Nucleic Acids Research*.
- Momand, J, H H Wu, and G Dasgupta. 2000. "MDM2--Master Regulator of the p53 Tumor Suppressor Protein." *Gene* 242 (1–2):15–29.
- Mottamal, Madhusoodanan, Shilong Zheng, Tien L. Huang, and Guangdi Wang. 2015. "Histone Deacetylase Inhibitors in Clinical Studies as Templates for New Anticancer Agents." *Molecules*.
- Nakagawa, Takashi, David J. Lomb, Marcia C. Haigis, and Leonard Guarente. 2009. "SIRT5 Deacetylates Carbamoyl Phosphate Synthetase 1 and Regulates the Urea Cycle." *Cell* 137 (3):560–70.
- Nakahata, Yasukazu, Milota Kaluzova, Benedetto Grimaldi, Saurabh Sahar, Jun Hirayama, Danica Chen, Leonard P. Guarente, and Paolo Sassone-Corsi. 2008. "The NAD<sup>+</sup>-Dependent Deacetylase SIRT1 Modulates CLOCK-Mediated Chromatin Remodeling and Circadian Control." *Cell* 134 (2):329–40.
- Newell, Pippa, Augusto Villanueva, and Josep M. Llovet. 2008. "Molecular targeted therapies in hepatocellular carcinoma: From pre-Clinical models to clinical trials." *Journal of Hepatology* 49 (1): 1–5.
- North, Brian J., and Eric Verdin. 2007. "Interphase Nucleo-Cytoplasmic Shuttling and Localization of SIRT2 during Mitosis." *PLoS ONE* 2 (8).
- North, Brian J., and Eric Verdin. 2004. "Sirtuins: Sir2-Related NAD-Dependent Protein Deacetylases." *Genome Biology*.
- Noske, Aurelia, Wilko Weichert, Silvia Niesporek, Annika Röske, Ann Christin Buckendahl, Ines Koch, Jalid Sehoul, Manfred Dietel, and Carsten Denkert. 2008. "Expression of the Nuclear Export Protein Chromosomal Region Maintenance/exportin 1/Xpo1 Is a Prognostic Factor in Human Ovarian Cancer." *Cancer* 112 (8):1733–43.
- O'Callaghan, Carol, and Athanassios Vassilopoulos. 2017. "Sirtuins at the Crossroads of Stemness, Aging, and Cancer." *Aging Cell*.
- O'Hagan, Heather M., Helai P. Mohammad, and Stephen B. Baylin. 2008. "Double Strand Breaks Can Initiate Gene Silencing and SIRT1-Dependent Onset of DNA Methylation in an Exogenous Promoter CpG Island." *PLoS Genetics* 4 (8).
- Oliner, J.D., KW Kinzler, P.S. Meltzer, D.L. George, and B. Vogelstein. 1992. "Amplification of a Gene Encoding a p53-Associated Protein in Human Sacromas." *Nature* 358 (6381):80–83.
- Ossareh-Nazari, Batool, Françoise Bachelerie, and Catherine Dargemont. 1997. "Evidence for a Role of CRM1 in Signal-Mediated Nuclear Protein Export." *Science* 278 (5335):141–44.

- Ota, H., E. Tokunaga, K. Chang, M. Hikasa, K. Iijima, M. Eto, K. Kozaki, M. Akishita, Y. Ouchi, and M. Kaneki. 2006. "Sirt1 Inhibitor, Sirtinol, Induces Senescence-like Growth Arrest with Attenuated Ras-MAPK Signaling in Human Cancer Cells." *Oncogene* 25 (2):176–85.
- Pagans, Sara, Angelika Pedal, Brian J. North, Katrin Kaehlcke, Brett L. Marshall, Alexander Dorr, Claudia Hetzer-Egger, et al. 2005. "SIRT1 Regulates HIV Transcription via Tat Deacetylation." *PLoS Biology* 3 (2):0210–20.
- Picksley, S M, B Vojtesek, A Sparks, and D P Lane. 1994. "Immunochemical Analysis of the Interaction of p53 with MDM2;--Fine Mapping of the MDM2 Binding Site on p53 Using Synthetic Peptides." *Oncogene* 9 (9):2523.
- Portmann, S., R. Fahrner, A. Lechleiter, A. Keogh, S. Overney, A. Laemmle, K. Mikami, et al. 2013. "Antitumor Effect of SIRT1 Inhibition in Human HCC Tumor Models In Vitro and In Vivo." *Molecular Cancer Therapeutics* 12 (4):499–508.
- Pruitt, Kevin, Rebekah L. Zinn, Joyce E. Ohm, Kelly M. McGarvey, Sung Hae L Kang, D. Neil Watkins, James G. Herman, and Stephen B. Baylin. 2006. "Inhibition of SIRT1 Reactivates Silenced Cancer Genes without Loss of Promoter DNA Hypermethylation." *PLoS Genetics* 2 (3):0344–52.
- Psyri, Amanda, Nikolaos Arkadopoulos, Maria Vassilakopoulou, Vassilios Smyrniotis, and George Dimitriadis. 2012. "Pathways and Targets in Hepatocellular Carcinoma." *Expert Review of Anticancer Therapy*.
- Qin, Weiping, Tianle Yang, Lap Ho, Zhong Zhao, Jun Wang, Linghong Chen, Wei Zhao, et al. 2006. "Neuronal SIRT1 Activation as a Novel Mechanism Underlying the Prevention of Alzheimer Disease Amyloid Neuropathology by Calorie Restriction." *Journal of Biological Chemistry* 281 (31):21745–54.
- Quint, Karl, Abbas Agaimy, Pietro Di Fazio, Roberta Montalbano, Claudia Steindorf, Rudolf Jung, Claus Hellerbrand, et al. 2011. "Clinical Significance of Histone Deacetylases 1, 2, 3, and 7: HDAC2 Is an Independent Predictor of Survival in HCC." *Virchows Archiv: An International Journal of Pathology* 459 (2):129–39.
- Ranganathan, Parvathi, Xueyan Yu, Caroline Na, Ramasamy Santhanam, Sharon Shacham, Michael Kauffman, Alison Walker, et al. 2012. "Preclinical Activity of a Novel CRM1 Inhibitor in Acute Myeloid Leukemia." *Blood* 120 (9):1765–73.
- Rayburn, Elizabeth, Ruiwen Zhang, Jie He, and Hui Wang. 2005. "MDM2 and Human Malignancies: Expression, Clinical Pathology, Prognostic Markers, and Implications for Chemotherapy." *Current Cancer Drug Targets* 5:27–41.
- Reilmann, R., F. Squitieri, J. Priller, C. Saft, C. Mariotti, S. Sussmuth, A. Nemeth, et al. 2014. "N02 Safety And Tolerability Of Selisistat For The Treatment Of Huntingtons Disease: Results From A Randomised, Double-Blind, Placebo-Controlled Phase Ii Trial." *Journal of Neurology, Neurosurgery & Psychiatry* 85 (Suppl 1).
- Rodriguez, M. S., J M Desterro, S. Lain, D. P. Lane, and R. T. Hay. 2000. "Multiple C-Terminal Lysine Residues Target p53 for Ubiquitin-Proteasome-Mediated Degradation." *Molecular and Cellular Biology* 20 (22):8458–67.

- Rotili, Dante, Domenico Tarantino, Angela Nebbioso, Chantal Paolini, Covadonga Huidobro, Ester Lara, Paolo Mellini, et al. 2012. "Discovery of Salermide-Related Sirtuin Inhibitors: Binding Mode Studies and Antiproliferative Effects in Cancer Cells Including Cancer Stem Cells." *Journal of Medicinal Chemistry* 55 (24):10937–47.
- Rumpf, Tobias, Matthias Schiedel, Berin Karaman, Claudia Roessler, Brian J. North, Attila Lehotzky, Judit Oláh, et al. 2015. "Selective Sirt2 Inhibition by Ligand-Induced Rearrangement of the Active Site." *Nature Communications* 6.
- Sakakibara, Keiichi, Naoya Saito, Takuji Sato, Atsushi Suzuki, Yoko Hasegawa, Jonathan M. Friedman, Donald W. Kufe, Daniel D. VonHoff, Tadahiko Iwami, and Takumi Kawabe. 2011. "CBS9106 Is a Novel Reversible Oral CRM1 Inhibitor with CRM1 Degrading Activity." *Blood* 118 (14):3922–31.
- Saunders, Laura R., Amar Deep Sharma, Jaime Tawney, Masato Nakagawa, Keisuke Okita, Shinya Yamanaka, Holger Willenbring, and Eric Verdin. 2010. "miRNAs Regulate SIRT1 Expression during Mouse Embryonic Stem Cell Differentiation and in Adult Mouse Tissues." *Aging* 2 (7):415–31.
- Saunders, L. R., and E. Verdin. 2007. "Sirtuins: Critical Regulators at the Crossroads between Cancer and Aging." *Oncogene*.
- Sauve, Anthony A., and Dou Yeon Youn. 2012. "Sirtuins: NAD<sup>+</sup>-Dependent Deacetylase Mechanism and Regulation." *Current Opinion in Chemical Biology*.
- Sauve, Anthony A., Cynthia Wolberger, Vern L. Schramm, and Jef D. Boeke. 2006. "The Biochemistry of Sirtuins." *Annual Review of Biochemistry* 75 (1):435–65.
- Schmidt, J., E. Braggio, K. M. Kortuem, J. B. Egan, Y. X. Zhu, C. S. Xin, R. E. Tiedemann, et al. 2013. "Genome-Wide Studies in Multiple Myeloma Identify XPO1/CRM1 as a Critical Target Validated Using the Selective Nuclear Export Inhibitor KPT-276." *Leukemia* 27 (12):2357–65.
- Schuetz, Anja, Jinrong Min, Tatiana Antoshenko, Chia L. Wang, Abdellah Allali-Hassani, Aiping Dong, Peter Loppnau, et al. 2007. "Structural Basis of Inhibition of the Human NAD<sup>+</sup>-Dependent Deacetylase SIRT5 by Suramin." *Structure* 15 (3):377–89.
- Schwer, Bjoern, and Eric Verdin. 2008. "Conserved Metabolic Regulatory Functions of Sirtuins." *Cell Metabolism*.
- Seidel, Julian, Cordula Klockenbusch, and Dirk Schwarzer. 2016. "Investigating Deformylase and Deacylase Activity of Mammalian and Bacterial Sirtuins." *ChemBioChem* 17 (5):398–402.
- Schiedel, Matthias, Dina Robaa, Tobias Rumpf, Wolfgang Sippl, and Manfred Jung. 2017. "The Current State of NAD<sup>+</sup>-Dependent Histone Deacetylases (Sirtuins) as Novel Therapeutic Targets." *Medicinal Research Reviews* 38 (1): 147–200.
- Shangary, Sanjeev, Dongguang Qin, Donna McEachern, Meilan Liu, Rebecca S Miller, Su Qiu, Zaneta Nikolovska-Coleska, et al. 2008. "Temporal Activation of p53 by a Specific MDM2 Inhibitor Is Selectively Toxic to Tumors and Leads to Complete Tumor Growth Inhibition." *Proceedings of the National Academy of Sciences of the United States of America* 105 (10):3933–38.

- Shen, Aiguo, Yuchan Wang, Yueming Zhao, Lin Zou, Linlin Sun, and Chun Cheng. 2009. "Expression of CRM1 in Human Gliomas and Its Significance in p27 Expression and Clinical Prognosis." *Neurosurgery* 65 (1):153–59.
- Shih, Ai, Faith B. Davis, Hung-Yun Lin, and Paul J. Davis. 2002. "Resveratrol Induces Apoptosis in Thyroid Cancer Cell Lines via a MAPK- and p53-Dependent Mechanism." *The Journal of Clinical Endocrinology & Metabolism* 87 (3): 1223–32.
- Signore, Michele, Lucia Ricci-Vitiani, and Ruggero De Maria. 2011. "Targeting Apoptosis Pathways in Cancer Stem Cells." *Cancer Letters*, 1–9.
- Simic, Petra, Eric O. Williams, Eric L. Bell, Jing Jing Gong, Michael Bonkowski, and Leonard Guarente. 2013. "SIRT1 Suppresses the Epithelial-to-Mesenchymal Transition in Cancer Metastasis and Organ Fibrosis." *Cell Reports* 3 (4):1175–86.
- Chen, Juan, Bin Zhang, Nathalie Wong, Anthony W.I. Lo, Ka Fai To, Anthony W.H. Chan, Margaret H.L. Ng, et al. 2011. "Sirtuin 1 Is Upregulated in a Subset of Hepatocellular Carcinomas Where It Is Essential for Telomere Maintenance and Tumor Cell Growth." *Cancer Research* 71 (12):4138–49.
- Song, Shijun, Min Luo, Yan Song, Tianji Liu, Haishan Zhang, and Zhongshi Xie. 2014. "Prognostic Role of SIRT1 in Hepatocellular Carcinoma." *Journal of the College of Physicians and Surgeons Pakistan* 24 (11):849–54.
- Spiegel, S., S. Milstien, and S. Grant. 2012. "Endogenous Modulators and Pharmacological Inhibitors of Histone Deacetylases in Cancer Therapy." *Oncogene*.
- Sun, Lina, H. Li, Junliang Chen, Vanessa Dehennaut, Yuhao Zhao, Yuyu Yang, Yasumasa Iwasaki, et al. 2013a. "A SUMOylation-Dependent Pathway Regulates SIRT1 Transcription and Lung Cancer Metastasis." *Journal of the National Cancer Institute* 105 (12):887–98.
- Sun, L., H. Li, J. Chen, Y. Iwasaki, T. Kubota, M. Matsuoka, A. Shen, Q. Chen, and Y. Xu. 2013b. "PIASy Mediates Hypoxia-Induced SIRT1 Transcriptional Repression and Epithelial-to-Mesenchymal Transition in Ovarian Cancer Cells." *Journal of Cell Science* 126 (17):3939–47.
- Süssmuth, Sigurd D., Salman Haider, G. Bernhard Landwehrmeyer, Ruth Farmer, Chris Frost, Giovanna Tripepi, Claus A. Andersen, et al. 2015. "An Exploratory Double-Blind, Randomized Clinical Trial with Selisistat, a Sirt1 Inhibitor, in Patients with Huntington's Disease." *British Journal of Clinical Pharmacology* 79 (3):465–76.
- Suter, Melissa A., Aishe Chen, Marie S. Burdine, Mahua Choudhury, R. Alan Harris, Robert H. Lane, Jacob E. Friedman, Kevin L. Grove, Alan J. Tackett, and Kjersti M. Aagaard. 2012. "A Maternal High-Fat Diet Modulates Fetal SIRT1 Histone and Protein Deacetylase Activity in Nonhuman Primates." *FASEB Journal* 26 (12):5106–14.
- Tai, Y-T, Y Landesman, C Acharya, Y Calle, M Y Zhong, M Cea, D Tannenbaum, et al. 2014. "CRM1 Inhibition Induces Tumor Cell Cytotoxicity and Impairs Osteoclastogenesis in Multiple Myeloma: Molecular Mechanisms and Therapeutic Implications." *Leukemia* 28 (1):155–65.

- Tan, Minjia, Chao Peng, Kristin A. Anderson, Peter Chhoy, Zhongyu Xie, Lunzhi Dai, Jeongsoon Park, et al. 2014. "Lysine Glutarylation Is a Protein Posttranslational Modification Regulated by SIRT5." *Cell Metabolism* 19 (4):605–17.
- Tang, Yi, Wenhui Zhao, Yue Chen, Yingming Zhao, and Wei Gu. 2008. "Acetylation Is Indispensable for p53 Activation." *Cell* 133 (4):612–26.
- Tanno, Masaya, Jun Sakamoto, Tetsuji Miura, Kazuaki Shimamoto, and Yoshiyuki Horio. 2007. "Nucleocytoplasmic Shuttling of the NAD<sup>+</sup>-Dependent Histone Deacetylase SIRT1." *Journal of Biological Chemistry* 282 (9):6823–32.
- Teodoro, Jose G., Sara K. Evans, and Michael R. Green. 2007. "Inhibition of Tumor Angiogenesis by p53: A New Role for the Guardian of the Genome." *Journal of Molecular Medicine*.
- Tiberi, Luca, Jérôme Bonnefont, Jelle vandenAmeele, Serge Daniel LeBon, Adèle Herpoel, Angéline Bilheu, Beverly W. Baron, and Pierre Vanderhaeghen. 2014. "A BCL6/BCOR/SIRT1 Complex Triggers Neurogenesis and Suppresses Medulloblastoma by Repressing Sonic Hedgehog Signaling." *Cancer Cell* 26 (6):797–812.
- Tissenbaum, H. A., and L. Guarente. 2001. "Increased Dosage of a Sir-2 Gene Extends Lifespan in *Caenorhabditis Elegans*." *Nature* 410 (6825):227–30.
- Toh, Tan Boon, Jhin Jieh Lim, and Edward Kai-Hua Chow. 2017. "Epigenetics in Cancer Stem Cells." *Molecular Cancer* 16 (1):29.
- Trapp, Johannes, Anne Jochum, Rene Meier, Laura Saunders, Brett Marshall, Conrad Kunick, Eric Verdin, Peter Goekjian, Wolfgang Sippl, and Manfred Jung. 2006. "Adenosine Mimetics as Inhibitors of NAD<sup>+</sup>-Dependent Histone Deacetylases, from Kinase to Sirtuin Inhibition." *Journal of Medicinal Chemistry* 49 (25): 7307–16.
- Trapp, Johannes, Rene Meier, Darunee Hongwiset, Matthias U. Kassack, Wolfgang Sippl, and Manfred Jung. 2007. "Structure–Activity Studies on Suramin Analogues as Inhibitors of NAD<sup>+</sup>-Dependent Histone Deacetylases (Sirtuins)." *ChemMedChem* 2 (10): 1419–31.
- Turner, Joel G., Jana Dawson, and Daniel M. Sullivan. 2012. "Nuclear Export of Proteins and Drug Resistance in Cancer." *Biochemical Pharmacology*.
- Horst, Armando Van Der, Leon G J Tertoolen, Lydia M M De Vries-Smits, Roy A. Frye, René H. Medema, and Boudewijn M T Burgering. 2004. "FOXO4 Is Acetylated upon Peroxide Stress and Deacetylated by the Longevity Protein hSir2/SIRT1." *Journal of Biological Chemistry* 279 (28):28873–79.
- Watt, Pauline J. Van Der, Christopher P. Maske, Denver T. Hendricks, M. Iqbal Parker, Lynette Denny, Dharendra Govender, Michael J. Birrer, and Virna D. Leaner. 2009. "The Karyopherin Proteins, Crm1 and Karyopherin  $\beta$ 1, Are Overexpressed in Cervical Cancer and Are Critical for Cancer Cell Survival and Proliferation." *International Journal of Cancer* 124 (8):1829–40.
- Vaquero, Alejandro, Michael Scher, Donghoon Lee, Hediye Erdjument-Bromage, Paul Tempst, and Danny Reinberg. 2004. "Human SirT1 Interacts with Histone H1 and Promotes Formation of Facultative Heterochromatin." *Molecular Cell* 16 (1):93–105.

- Vaquero, A., R. Sternglanz, and D. Reinberg. 2007. "NAD<sup>+</sup>-Dependent Deacetylation of H4 Lysine 16 by Class III HDACs." *Oncogene*.
- Vassilev, Lyubomir T., Binh T. Vu, Bradford Graves, Daisy Carvajal, Frank Podlaski, Zoran Filipovic, Norman Kong, et al. 2004. "In Vivo Activation of the p53 Pathway by Small-Molecule Antagonists of MDM2." *Science* 303 (5659):844–48.
- Vaziri, Homayoun, Scott K. Dessain, Elinor Ng Eaton, Shin Ichiro Imai, Roy A. Frye, Tej K. Pandita, Leonard Guarente, and Robert A. Weinberg. 2001. "hSIR2/SIRT1 functions as an NAD-Dependent p53 Deacetylase." *Cell* 107 (2):149–59.
- Vousden, Karen H., and Xin Lu. 2002. "Live or Let Die: The Cell's Response to p53." *Nature Reviews Cancer*.
- Wach, Jean Yves, Stephan Güttinger, Ulrike Kutay, and Karl Gademann. 2010. "The Cytotoxic Styryl Lactone Goniotalamin Is an Inhibitor of Nucleocytoplasmic Transport." *Bioorganic and Medicinal Chemistry Letters* 20 (9):2843–46.
- Walker, Christopher J., Joshua J. Oaks, Ramasamy Santhanam, Paolo Neviani, Jason G. Harb, Gregory Ferencak, Justin J. Ellis, et al. 2013. "Preclinical and Clinical Efficacy of XPO1/CRM1 Inhibition by the Karyopherin Inhibitor KPT-330 in Ph+leukemias." *Blood* 122 (17):3034–44.
- Wang, Hanning, Hao Liu, Kaiyun Chen, Jinfeng Xiao, Ke He, Jinqian Zhang, and Guoan Xiang. 2012. "SIRT1 Promotes Tumorigenesis of Hepatocellular Carcinoma through PI3K/PTEN/AKT Signaling." *Oncology Reports* 28 (1):311–18.
- Wang, Rui Hong, Kundan Sengupta, Cuiling Li, Hyun Seok Kim, Liu Cao, Cuiying Xiao, Sangsoo Kim, et al. 2008. "Impaired DNA Damage Response, Genome Instability, and Tumorigenesis in SIRT1 Mutant Mice." *Cancer Cell* 14 (4):312–23.
- Wang, Chuangui, Lihong Chen, Xinghua Hou, Zhenyu Li, Neha Kabra, Yihong Ma, Shino Nemoto, et al. 2006. "Interactions between E2F1 and SirT1 Regulate Apoptotic Response to DNA Damage." *Nature Cell Biology* 8 (9):1025–31.
- Westerberg, Goran, Joseph A. Chiesa, Claus A. Andersen, Daniela Diamanti, Letizia Magnoni, Giuseppe Pollio, Borje Darpo, and Meijian Zhou. 2015. "Safety, Pharmacokinetics, Pharmacogenomics and QT Concentration-Effect Modelling of the SirT1 Inhibitor Selisistat in Healthy Volunteers." *British Journal of Clinical Pharmacology* 79 (3):477–91.
- Wilhelm, Scott, Christopher Carter, Mark Lynch, Timothy Lowinger, Jacques Dumas, Roger A. Smith, Brian Schwartz, Ronit Simantov, and Susan Kelley. 2006. "Discovery and Development of Sorafenib: A Multikinase Inhibitor for Treating Cancer." *Nature Reviews Drug Discovery*.
- Wood, Jazon G., Blanka Regina, Siva Lavu, Konrad Hewitz, Stephen L. Helfand, Marc Tatar, and David Sinclair. 2004. "Sirtuin Activators Mimic Caloric Restriction and Delay Ageing in Metazoans." *Nature* 430 (7000):686–89.
- Wu, Xiangwei, J. Henri Bayle, David Olson, and Arnold J. Levine. 1993. "The p53-Mdm-2 Autoregulatory Feedback Loop." *Genes and Development* 7 (7):1126–32.

- Xu, J, W Zhu, W Xu, W Yao, B Zhang, Y Xu, S Ji, et al. 2013. "Up-Regulation of MBD1 Promotes Pancreatic Cancer Cell Epithelial-Mesenchymal Transition and Invasion by Epigenetic down-Regulation of E-Cadherin." *Curr Mol Med* 13 (3):387–400.
- Wu, Yuting, Xiaoming Meng, Cheng Huang, and Jun Li. 2015. "Emerging Role of Silent Information Regulator 1 (SIRT1) in Hepatocellular Carcinoma: A Potential Therapeutic Target." *Tumor Biology*.
- Xu, D., N. V. Grishin, and Y. M. Chook. 2012. "NESdb: A Database of NES-Containing CRM1 Cargoes." *Molecular Biology of the Cell* 23 (18):3673–76.
- Yamashita, Taro, Marshonna Forgues, Wei Wang, Woo Kim Jin, Qinghai Ye, Huliang Jia, Anuradha Budhu, et al. 2008. "EpCAM and Alpha-Fetoprotein Expression Defines Novel Prognostic Subtypes of Hepatocellular Carcinoma." *Cancer Research* 68 (5):1451–61.
- Yang, L., G. Xie, Q. Fan, and J. Xie. 2010. "Activation of the Hedgehog-Signaling Pathway in Human Cancer and the Clinical Implications." *Oncogene*.
- Yang, Yonghua, Huayan Hou, Edward M. Haller, Santo V. Nicosia, and Wenlong Bai. 2005. "Suppression of FOXO1 Activity by FHL2 through SIRT1-Mediated Deacetylation." *EMBO Journal* 24 (5):1021–32.
- Yao, Y, Y Yang, and W G Zhu. 2014. "Sirtuins: Nodes Connecting Aging, Metabolism and Tumorigenesis." *Current Pharmaceutical Design* 20 (11):1614–24.
- Yao, Yang, Yang Dong, Feng Lin, Hui Zhao, Zan Shen, Ping Chen, Yuan Jue Sun, Li Na Tang, and Shui Er Zheng. 2009. "The Expression of CRM1 Is Associated with Prognosis in Human Osteosarcoma." *Oncology Reports* 21 (1):229–35.
- Yau, Thomas, Pierre Chan, Kelvin K Ng, Sin Ho Chok, Tan To Cheung, Sheung Tat Fan, and Ronnie T Poon. 2009. "Phase 2 Open-Label Study of Single-Agent Sorafenib in Treating Advanced Hepatocellular Carcinoma in a Hepatitis B-Endemic Asian Population: Presence of Lung Metastasis Predicts Poor Response." *Cancer* 115 (2):428–36.
- Yee, Andrew J., Peter M. Voorhees, William Bensinger, Jesus G. Berdeja, Jeffrey G. Supko, Paul G. Richardson, David Tamang, Simon S. Jones, Gretchen Patrick, Catherine Wheeler, and Noopur Raje. 2014. "Ricolinostat (ACY-1215), a Selective HDAC6 Inhibitor, in Combination with Lenalidomide and Dexamethasone: Results of a Phase 1b Trial in Relapsed and Relapsed Refractory Multiple Myeloma." *Blood* 124 (21):4772.
- Yeung, Fan, Jamie E. Hoberg, Catherine S. Ramsey, Michael D. Keller, David R. Jones, Roy A. Frye, and Marty W. Mayo. 2004. "Modulation of NF- $\kappa$ B-Dependent Transcription and Cell Survival by the SIRT1 Deacetylase." *EMBO Journal* 23 (12):2369–80.
- Yi, Jingjie, and Jianyuan Luo. 2010. "SIRT1 and p53, Effect on Cancer, Senescence and beyond." *Biochimica et Biophysica Acta - Proteins and Proteomics*.
- Yoshimura, Mariko, Jo Ishizawa, Vivian Ruvolo, Archana Dilip, Alfonso Quintás-Cardama, Timothy J. McDonnell, Sattva S. Neelapu, et al. 2014. "Induction of p53-Mediated Transcription and Apoptosis by Exportin-1 (XPO1) Inhibition in Mantle Cell Lymphoma." *Cancer Science* 105 (7):795–801.



- Yu, Qiang, Shelagh E.L. Mirski, Kathryn E. Sparks, and Susan P.C. Cole. 1997. "Two COOH-Terminal Truncated Cytoplasmic Forms of Topoisomerase II $\alpha$  in a VP-16-Selected Lung Cancer Cell Line Result from Partial Gene Deletion and Alternative Splicing." *Biochemistry* 36 (19):5868–77.
- Yuan, Zhigang, and Edward Seto. 2007. "A Functional Link between SIRT1 Deacetylase and NBS1 in DNA Damage Response." *Cell Cycle*.
- Yuan, Zhigang, Xiaohong Zhang, Nilanjan Sengupta, William S. Lane, and Edward Seto. 2007. "SIRT1 Regulates the Function of the Nijmegen Breakage Syndrome Protein." *Molecular Cell* 27 (1):149–62.
- Zhang, Zheng Yun, Doopyo Hong, Seung Hoon Nam, Jong Man Kim, Yong Han Paik, Jae Won Joh, Choon Hyuck David Kwon, et al. 2015. "SIRT1 Regulates Oncogenesis via a Mutant p53-Dependent Pathway in Hepatocellular Carcinoma." *Journal of Hepatology* 62 (1):121–30.
- Zhang, Kejie, Michael Wang, Archito T. Tamayo, Sharon Shacham, Michael Kauffman, John Lee, Liang Zhang, et al. 2013. "Novel Selective Inhibitors of Nuclear Export CRM1 Antagonists for Therapy in Mantle Cell Lymphoma." *Experimental Hematology* 41 (1).
- Zhou, Yuanfei, Tongxing Song, Jie Peng, Zheng Zhou, Hongkui Wei, Rui Zhou, Siwen Jiang, and Jian Peng. 2016. "SIRT1 suppresses adipogenesis by activating Wnt/ $\beta$ -Catenin signaling in vivo and in vitro." *Oncotarget*.
- Zhou, M, L Gu, T C Abshire, A Homans, A L Billett, A M Yeager, and H W Findley. 2000. "Incidence and Prognostic Significance of MDM2 Oncoprotein Overexpression in Relapsed Childhood Acute Lymphoblastic Leukemia." *Leukemia* 14 (1):61–67.

# VITA

**Murat DELMAN**

**Date and Place of Birth:** 1987 İzmir/TURKEY

**E-mail :** murat.delman@gmail.com

## **Education**

### **Ph.D. Bioengineering**

2012-2018 Izmir Institute of Technology,  
PhD Degree Program of the Department of Bioengineering, Izmir, Turkey

### **MSc. Biotechnology**

2009-2012 Izmir Institute of Technology,  
Biotechnology and Bioengineering Master's Program, Izmir, Turkey

### **BSc. Biochemistry**

2005 – 2009 Ege University,  
Biochemistry Department, Izmir, Turkey

## **Teaching and Professional Experience**

Research assistant

2011-2018 Izmir Institute of Technology,  
Biotechnology and Bioengineering Interdisciplinary Program, serviced in Molecular  
Biology and Genetics Department and Department of Chemistry, Izmir, Turkey

## **Publications**

Kanbur, Tuğçe, Murat Kara, Meltem Kutluer, Ayhan Şen, Murat Delman, Aylin Alkan, Hasan Ozan Otaş, İsmail Akçok, and Ali Çağır. 2017. "CRM1 Inhibitory and Antiproliferative Activities of Novel 4'-Alkyl Substituted Klavuzon Derivatives." *Bioorganic and Medicinal Chemistry* 25 (16):4444–51.

Seyrantepe, Volkan, and Murat Delman. 2014. "Characterization of the Human Sialidase Neu4 Gene Promoter." *Turkish Journal of Biology* 38 (5):574–80.